

PERSONALIZED ENDOVASCULAR STENT GRAFTS

Re-inventing the personalized stent graft and its production process;
a finite element analysis.



Master thesis – Technical Medicine – Tim Boers
University of Twente
Meander Medical Centre

CONTENTS

- Graduation committee..... 2
- Summary 3
- 1. Introduction 4
 - Clinical background 4
 - Technical background 6
- 2. Exploration 9
- 3. Analysis..... 12
 - Design requirements 19
- 4. Concept Phase..... 22
- 5. Embodiment Phase 25
- 6. Evaluation and Recommendations 38
- 7. Outlook..... 53
- 8. Acknowledgement 54
- 9. References..... 55
- 10.1 Appendix 1 – Research line 61
 - Clinical background 61
 - Technical background..... 61
 - Production method 63
 - Research line 66
- 10.2 Appendix 2 – Additional results 70
- 10.3 Appendix 3 – Clinical studies hybrid operating room 78
 - Ergonomics study 78
 - DISCOVER trial 79
 - iFlow study 79

GRADUATION COMMITTEE

Chairmen: prof.dr.ir. C.H. Slump

Medical supervisor: dr. V. van Weel

Technical supervisor: prof.dr.ir. C.H. Slump

Process supervisor: drs. B.J.C.C. Hessink-Sweep

Outside member: dr. ir. Javad Hazrati

SUMMARY

This master thesis focusses on the development of personalized endovascular stent grafts and its production process. These stent grafts are used in endovascular aneurysm repair (EVAR). EVAR is a form of minimally invasive surgery and is the therapy of choice in 78% of all abdominal aneurysm repairs. Showing superior short-term outcomes when compared to open repair, it is still similar or inferior to open repair for long-term outcome especially in re-intervention rates due to endoleaks or migration of the implanted device.

EVAR excludes the aneurysmal sac from blood circulation using a stent graft. This stent graft is often a self-expanding straight tubular construct which accommodates to the anatomy of the patient creating a zone of sealing with the vascular wall. However, the anatomy of the patient is not straight therefore one diameter causes variations in stress induced in the vascular wall. This might cause unnecessary overstressing of the wall when large diameter differences are present. Producing a personalized stent graft might solve this problem and thereby reduce adverse clinical outcome especially on the long-term.

Based upon literature and personal experience a list of requirements was created as well as two straight and personalized stent graft designs; both designs in two variations: a fishmouth and a z-shape version. To test the effects of these design a finite element analysis was performed. This analysis simulated the designs and inserted them in three vascular models: a straight tube, an anatomical straight neck, and an anatomical conical neck. For the stents, an elastoplastic formulation was created and for the vascular wall a 3rd order polynomial was chosen, both based upon literature with experimental validation.

Results show stent behaviour similar to real-life cases. Maximum principal elastic strain and equivalent (von-Mises) stress were measured and showed a reduction in both variables for the personalized stent, indicating a positive effect on reducing vascular wall stress. These simulations offer insight as to the effects of personalized stent grafts on the vascular wall, future research should expand on these results by investigating the effects of various stent designs, grafts, bridging between stents, and include more realistic stent and vascular material formulations.

1. INTRODUCTION

CLINICAL BACKGROUND

Aortic abdominal aneurysms (AAA) are dilations of the lower aortic vessel wall, which are located below the renal arteries in 85% of the cases.¹ A representation of a healthy abdominal aorta can be seen Figure 1. An example of an aneurysm can be seen in Figure 2. Most patients with AAA are asymptomatic, however, lower back pain and abdominal pain may occur. Aneurysms may rupture resulting in a life-threatening situation. Patients with a ruptured AAA, who make it to the hospital have a 75-79% chance of survival.² The chance of rupture increases with an increase in diameter of the aneurysm, which is the primary prognostic factor.^{3,4} This ranges from a diameter of 5.5 cm with a yearly incidence of 5-10% to larger than 7.0 cm with a yearly incidence of 32.5%.⁴⁻⁶ Treatment is beneficial when the aortic diameter is equal to or greater than 5 cm for women and 5.5 cm for men,⁷⁻⁹ or when the AAA is symptomatic or its expansion rate is larger than 10 mm per year.¹⁰

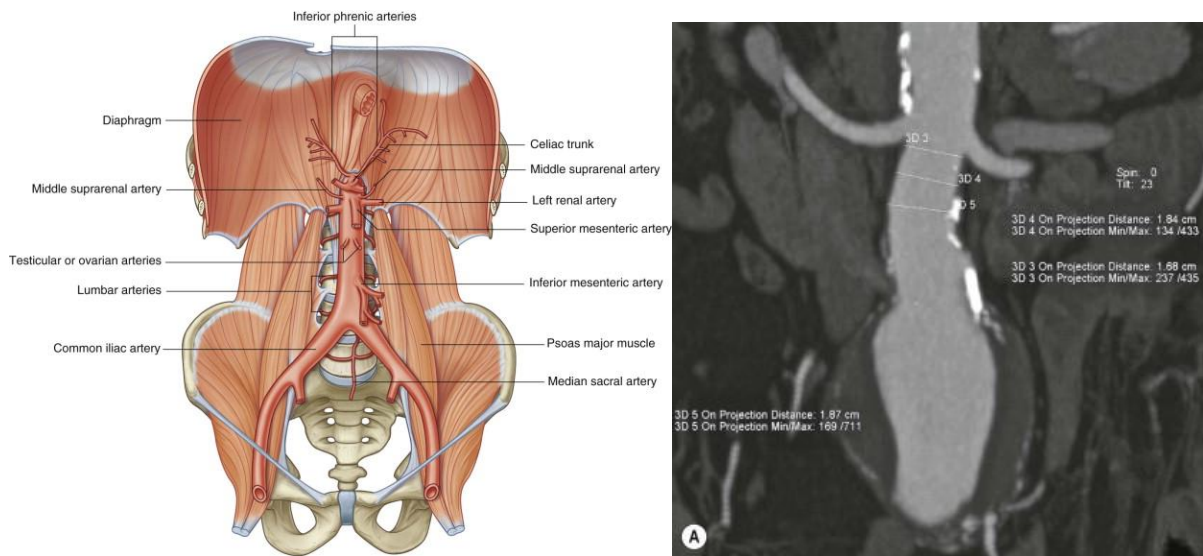


Figure 1 and 2: on the left (1) representation of the abdominal aorta with all its branches.¹¹ On the right (2) a CT-A image with vascular contrast of an abdominal infra-renal aneurysm with a long sized neck including measurements. The white areas on the aortic wall are calcifications.¹²

A successful treatment of an AAA is achieved by removing the pressure on the aneurysm before it ruptures. In 78% of the operations the treatment of choice is minimally invasive surgery; the endovascular aneurysm repair (EVAR), which aims to exclude the aneurysmal sac from blood circulation by placing an endovascular stent graft in the abdominal aorta.^{13,14} The technical background will elaborate on this approach. Another surgical procedure to treat AAA is the open repair (OR), which replaces the aneurysmal sack with a prosthesis during a laparotomy. OR showed to have higher per- and post-operative complication rates.^{15,16} OR shows similar patency rates as EVAR after a follow-up period of 6 years, yet higher free re-intervention rates than EVAR (81.9% versus 70.4%, respectively, $p=0.03$).¹⁵ Stather et al. compared various randomized trials and found that EVAR had short term benefits compared to OR, though long-term EVAR showed to suffer from higher re-intervention rates and risks of rupture.¹⁷ Possible explanations for the higher re-intervention rates might be the complexity of the EVAR procedure, complex anatomy of the patients, and experience which is an important factor for success. The long-term patency of EVAR continues to improve with more new endovascular devices entering the market each year.¹⁸ Though Bahia et al. found that over a period from 1969-2011 the 5-year follow-up clinical outcome of elective infra-renal AAA repair has shown only minor improvement (log odds ratio: 0.027, confidence interval: 0.012-0.042), despite technical and procedural advancements.¹⁹

The endovascular stent graft varies between vendors, alternating between complex combinations of metals, polymers and drug eluting materials to create stent grafts for varying patient cases.^{20,21} The technical background

in this thesis will elaborate further on this topic. Most commonly used materials for aortic stent grafts are nitinol stents with a graft of Dacron (PolyEthyleneTerephthalate (PET)) or expanded-PolyTetraFluoroEthylene (ePTFE), which result in good management of the AAA over a 6 year period of time and often longer.^{15,16,21,22} EVAR results in a higher rate of no-mortality (ranging from 98.3% to 99.5%) than OR (ranging from 95.2% to 97%), however, there are several complications such as high secondary intervention rates due to endoleaks and secondary aneurysm sac rupture, which need solutions/improvements.^{15,16,18,22–26} In addition, a standard EVAR procedure is not suitable for approximately one third of the patients. This might result in: the use of more complex stent grafts such as fenestrated or chimney, OR instead of an EVAR, or a decision not to be operated at all.²⁷

Complications encountered after EVAR are often due to complex anatomy or a technical failure which results in endoleaks and/ or migration of the deployed stent graft. These complications ensue the risk of rupture of the aneurysm.¹⁵ In addition, the angulation of the neck, existence of thrombosis/ stenosis, as well as involvement of renal and iliac arteries are important factors for the outcome of an EVAR. Therefore, during planning these anatomical differences act as indicators for potential complications or even as contra-indications for an EVAR procedure. Figure 3 and 4 show visual representations of some of these factors, which are a part of the description of hostile neck anatomy (HNA) as well.²⁸ Additionally, there is a classification system for endoleaks shown in table 8, Appendix 9.1.^{29–33}

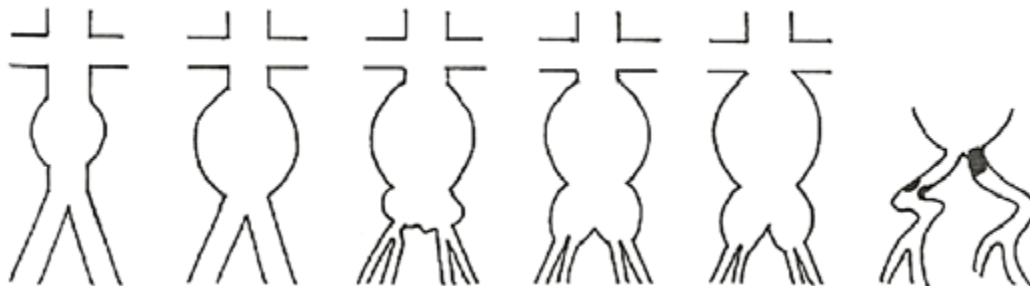


Figure 3: Morphological variations of aortic aneurysms with regards to renal and iliac arteries. From left to right: infra-renal aneurysm (early stage), infra-renal aneurysm (late stage), infra-renal aneurysm (including partly communal iliac aneurysms), infra-renal aneurysm (including full communal iliac aneurysms), juxta-renal aneurysm (including full communal iliac aneurysms) and aneurysm with stenotic and occlusive vascular disease of the iliac communal arteries.²⁸ Note the decrease in length of the neck (see Figure 4 as well).



Figure 4: Visual interpretation of aortic angulation and shapes of necks above aneurysms. From left to right: straight, tapered, conical, angulated, bulged.²⁸

The above-mentioned factors should be considered during the planning of EVAR procedures, even more so when using patient specific stent grafts. The stent grafts are being improved continuously allowing surgeons to perform EVAR on patients with increasingly complex anatomy as shown in Figure 3 and 4.^{22,34} An example of such difficult anatomy is a short neck i.e. short landing zone, (in this case the aneurysm is close to the renal arteries, see Figure 3), where obtaining appropriate sealing is difficult or even impossible. A good seal is a stent graft deployed to the neck without any gaps between the stent graft and the aortic wall. Inappropriate sealing may lead to endoleaks and/or stent graft migration, ensuing the risk of rupture¹⁵. When a stent graft is deployed over the renal arteries or the coeliac trunk artery complications such as renal failure, major intestinal ischemia, or even

death may occur. Therefore, custom-made stent grafts such as fenestrated stent grafts can prove useful to obtain proper sealing above the renal arteries without blocking the major branching arteries.³⁴ In addition, it is reported that Aortic Neck Dilatation (AND) for supra-renal stent grafts is 2% versus 25% for infra-renal stent graft placements. AND increases the risk for migration and/or endoleak type I.³⁵ Supra-renal stents may therefore prove beneficial to all AAA patients.

TECHNICAL BACKGROUND

To understand a standard EVAR procedure a short description is given of the steps taken during surgery. Furthermore, the various EVAR stent graft products are discussed.

EVAR procedure

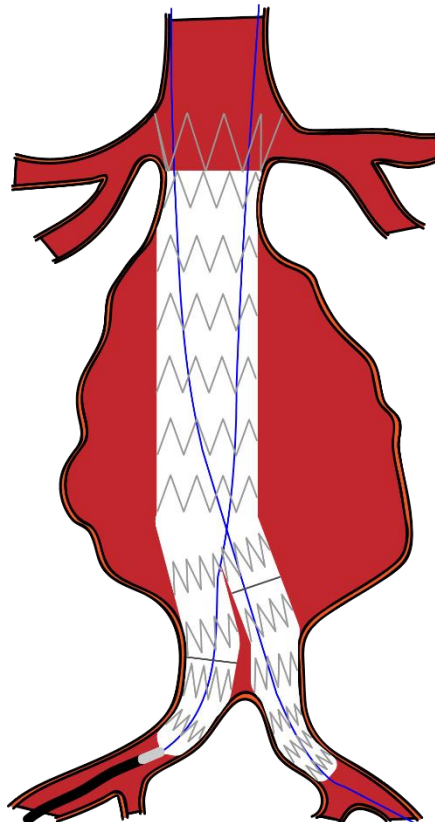


Figure 5: Abdominal aorta with aneurysm and an almost fully deployed stent graft. The grey z-shaped lines are referred to as the stent or 'skeleton', the white area covering the stents from the inside is referred to as the graft.

After all preoperative imaging has been performed and the dimensions have been measured, a suitable EVAR device is chosen from the portfolios of the manufacturers. The surgery is electively planned. Generally, after two to three weeks the patient will undergo surgery. When anaesthesia has been administered the EVAR procedure starts with accessing the femoral arteries (in some hospitals this is performed under ultrasound guidance) where guide wires are inserted and thereafter the catheters. Making use of a hybrid OR allows for immediate insertion and positioning of the main device. This main device consists of the proximal neck part, a body, and one long and one short leg. Next, an angiographic image is made using 7 or 15 ml of contrast with a flow of 60 ml/min or 20 ml/min, respectively. Thereafter the main device is repositioned, if required, and deployed. Then the extensions of the legs are inserted and deployed in the communal iliac arteries, while preventing over-stenting of the internal iliac arteries. To help prevent over-stenting often a blowback image is made, where a mix of contrast and NaCl fluid is injected into the catheter of the iliac leg with a syringe using high force. This image shows the communal, internal, and external iliac arteries. To ensure good positioning and seal with the aortic wall the proximal and distal landing zones are pressurized with a highly compliant balloon. A control angiographic image

is made to ensure no endoleak type 1 is present (see appendix 1 for elaboration on endoleak types). Finally, the puncture holes in the femoral arteries are closed with a closure device or by pressing on the hole for at least 10 minutes. Figure 5 depicts a self-expandable stent graft in the abdominal aorta during the final stage of deployment.

EVAR systems

The endovascular approach for treating aneurysmal disease is preferred to open repair as stated in the clinical background, this minimally invasive approach is used by a variety of stent grafts on the market. From the available devices three distinctions can be made: self-expandable stent grafts, balloon-expandable stent grafts and 'special' stent grafts. The latter category contains devices such as the 'Nellix' stent graft; a system that consists of two stents surrounded with endobags which are filled with a hardening polymer in vivo (see Figure 6). The Nellix fixates the stents in the aneurysm and proximal and distal sealing zones, forming the endobags compliant with the patient's anatomy. Which aneurysms are suitable for these self- and balloon-expandable stent grafts is determined by the manufacturers/vendors. For instance, the Endurant is indicated for aneurysmal neck angle of up to 60°. The Aorfix is indicated for neck angles of up to 90° (see Figure 6).

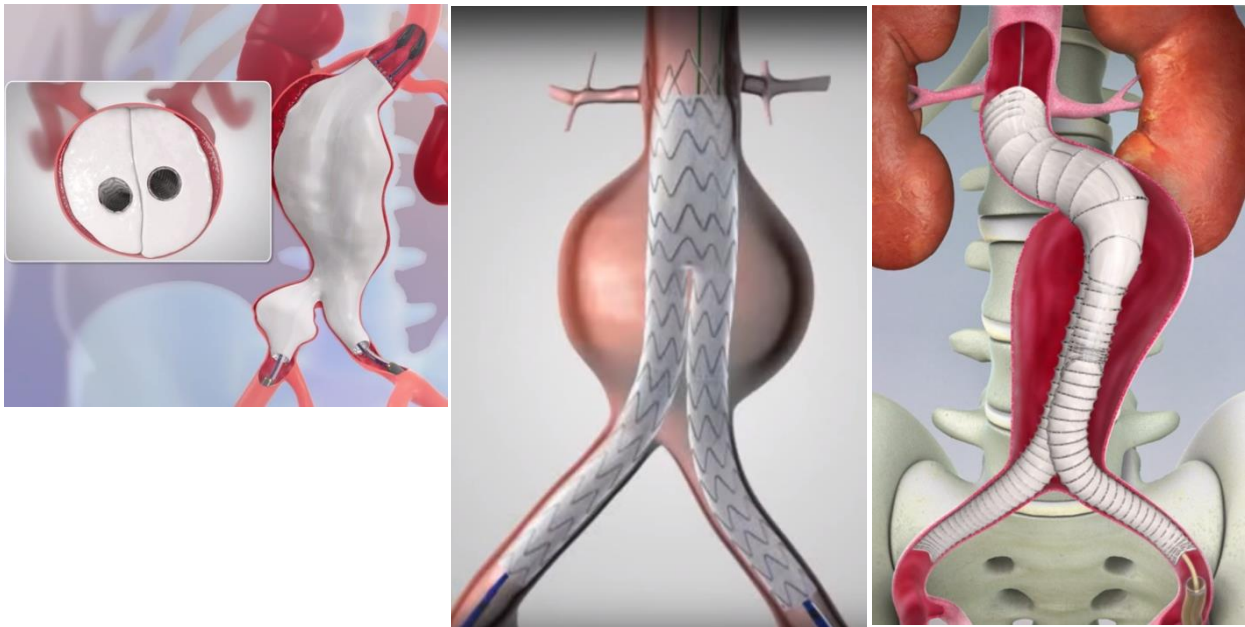


Figure 6: From left to right: Nellix by Endologix³⁶, Endurant II by Medtronic³⁷, Aorfix by Lombard Medical³⁸.

To be able to treat complex aneurysms involving branches of the abdominal aorta, some manufacturers developed three, or even five, stent grafts combinations to be able to perform techniques such as the chimney stent technique, snorkel approach, and sandwich technique. Such stent grafts allow for immediate surgery due to their standardized sizes. However, when the stent grafts are deployed in the aorta, gutters are formed due to the stent grafts' circular profile and thereby not closing off the entire neck (see Figure 7). This might result in occlusion of the renal stent graft branches due to thrombosis forming of blood in those gutters.

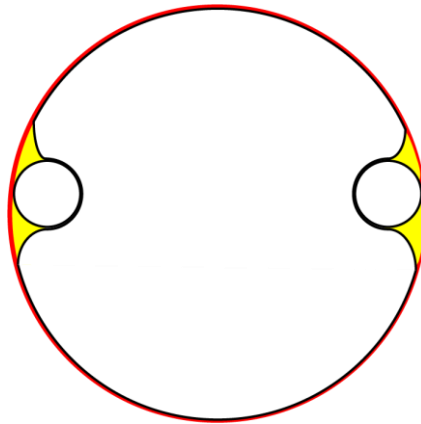


Figure 7: In red the aortic wall, in black the stent grafts and in yellow the gutters that are formed after deployment of the stent grafts.

Despite all these advances stent grafts are often non-personalized 'simple' straight tubular constructs. Though developments are made in the design of the graft as well. This involves creating multiple layers of braided grafts which are interconnected allowing flow into the aneurysm sac whilst the returning flow is reducing the speed of the inward flow at the same time. Therefore, causing stasis of flow in the aneurysm sac allowing for thrombus to form and thereby reducing the aneurysm lumen to the point it reaches the stent graft and no flow is present outside the stent graft. In addition to these EVAR systems, products have been developed that allow for correction of the sealing zone. For instance, endo-anchors which are coiled wires that fixate the stent graft to the vessel wall at the required sealing zone.²²

Producing personalized stent grafts with fenestrations or branches to prevent blocking of the branching arteries is costly (roughly 3 times the standard price) and has an average production time of 6-8 weeks.³⁹ Successful treatment is achieved by eliminating the aneurysm and thereby preventing rupture, during production, however, the risk of rupture ensues. Even more so, due to the production time of 6-8 weeks an acute treatment with personalized stent grafts is not possible to date.^{39,40}

2. EXPLORATION

IMPROVEMENT OPPORTUNITIES FOR STENT GRAFTS

As described in the previous chapter multiple stent graft systems are available. However, currently the major problems of those EVAR systems are long-term patency and their higher re-intervention rate when compared to open repair, often due to stent graft migration and endoleaks. To illustrate opportunities for improvement a patient case is discussed.

Case of an abdominal aneurysm with a conical neck

A patient with lower back pain appeared at the emergency room. At that point in time the aneurysm was physically examined and found not symptomatic, however, the patient returned a week later with persistent back pain and this time with a pressure sensitive aneurysm. A CT-A scan was performed and the patient went into surgery 4 days later. The morphology of the patient was not ideal, a 5.3cm infra-renal aneurysm over a length of 10cm with a conical neck (see Figure 8). The latter is cause for worry due to increased risk for an endoleak type I. However, an Endurant II stent graft was placed successfully (see Figure 9) and the aneurysm has shrunk when measured during the last follow-up.

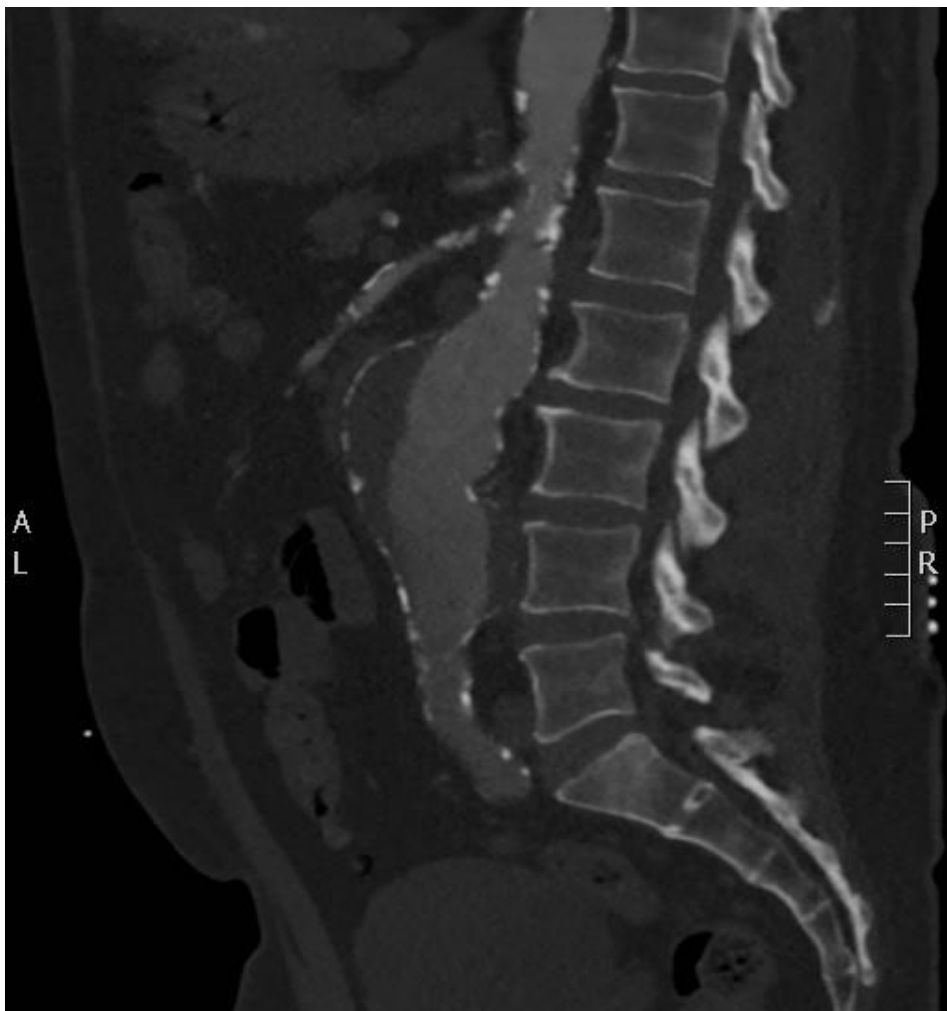


Figure 8: A CT-A scan in which a 5.3cm in diameter infra-renal aneurysm with a conical neck can be seen. Note the calcifications proximal to the aneurysm.

According to the instruction for use (IFU) of Medtronic for the Endurant II stent graft system, the aortic neck should be in the range of 19-32 mm in diameter. Furthermore, the neck should not have any significant

calcifications or thrombi. Depending on the length of the neck that is usable as a landing zone the maximum angle is determined; for less than 10 mm landing zone the angle should be lower than 60°, for less than 15 mm landing zone it should be lower than 75°.41 This is the angle between proximal aorta and the aneurysm sac. Another requirement is the diameter of the aortic neck should be 10-20% lower than the diameter of the chosen stent graft (i.e. oversizing of 10-20%).41 Often patients meet these requirements and deployment of the Endurant device succeeds. However, in this case a conical neck is present which nearly has a 4 mm diameter increase over a 10 mm length. Citing from the IFU: 'The safety and effectiveness of the Endurant II/Endurant IIs stent graft system has not been evaluated in patients who have a reversed conical neck, which is defined as a >4 mm distal increase over a 10 mm length (infrarenal EVAR only)', this therefore might result in unexpected outcome.41 Though experience from the vascular surgery team and Medtronic resulted in agreement that treatment with the Endurant II system would succeed. The successful result can be seen in Figure 9.

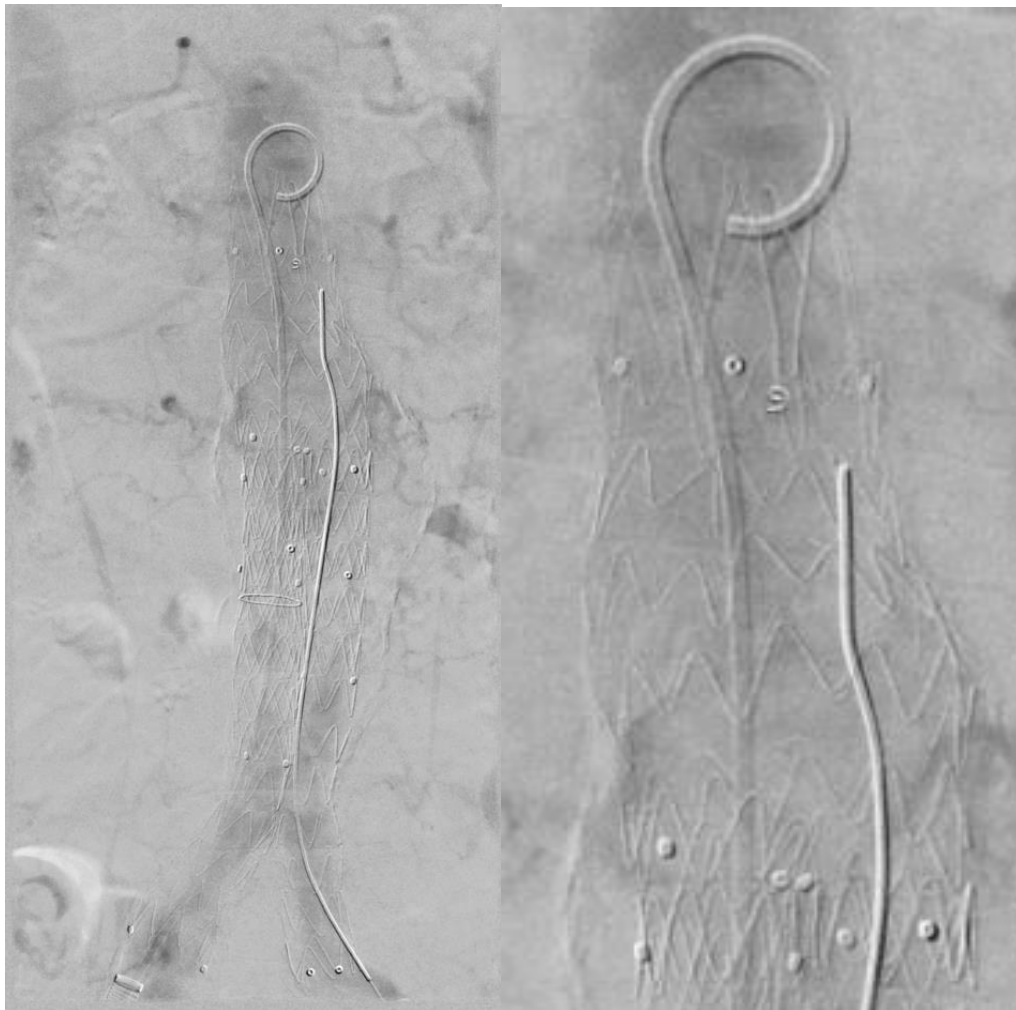


Figure 9: On the left an overview of the placed stent-graft (with a guide wire and pig tail in-situ), on the right a zoom on the conical neck. Note the adaptability of the self-expanding stent graft (z-shape lines) to follow the aortic neck. Furthermore, opaque dots (markers) are visible, as well as the letter e which is in line with the bifurcation and indicates correct rotational positioning of the stent graft (i.e. the bifurcation is aligned with the iliac arteries).

The use of the Endurant II stent graft for this patient case was indicated by the IFU. Though the lack of a customized fit might result in use of stent grafts outside the IFU, exclusion of patients for EVAR or open repair with its added perioperative complication risk. Kristmundsson et al. have investigated the CT-A scans of 241 patients and compared them with the IFU's of Zenith, Excluder and Endurant stent grafts. They concluded that the Endurant had the highest suitability percentage; 48.1%.42 Van Keulen et al. performed an evaluation of 100 patients treated with an Endurant stent graft. They compared the IFU of the Zenith, Excluder, Talent and

Endurant stent grafts with the CT-A scans of those 100 patients. It was concluded that 52, 60, 73 and 81% of the patients, respectively, would fall under the IFU of those stents.⁴³ Due to the common stent graft its limited applicability for complex cases, use of stent grafts outside the IFU to cope with such complex cases is considered.

Oversizing, in case of this conical neck, is considered to compensate for the change in diameter. The oversizing for this patient case is based upon the largest diameter. However, may therefore result in unnecessary high stresses in the vascular wall on the smaller diameters. Sternbergh et al. have shown that excessive oversizing, more than 30 percent, increases the risk for migration 14-fold compared to oversizing of less than 30 percent. The risk for aneurysm sac expansion at 24 months was increased 16-fold.⁴⁴

Optimizing the stent graft fit for each patient might overcome oversizing problems and thereby prevent complications like migration, endoleaks or sac expansion. This personalized fit with the patient's anatomy should increase the operability of patients with morphologically complex aneurysms i.e. it should result in an IFU which includes indications for those complex cases. Furthermore, in order to treat patients in an acute setting (with or without a complex aneurysm) a more efficient and quicker process to produce customised stent grafts for AAA is necessary. Such a new production process may enable surgeons to treat even those patients with personalized stent grafts. Thereby, re-iterating that surgeons might improve clinical outcome for complex cases as well as the less complex ones by using personalized devices.

RESEARCH QUESTION

The overall research question of this master thesis is: How can we improve/ re-invent the personalized stent graft and its production process in treating patients with an abdominal aortic aneurysm, for both normal and morphologically complex aneurysms?

3. ANALYSIS

Patients with infra-renal aneurysms are treated with stent grafts that preferably land at an infra-renal landing zone (i.e. neck). This ensures no fenestration or branches are needed into the renal arteries. If no suitable infra-renal neck is found, a supra-renal stent graft is considered. When this is possible a custom-made stent graft with fenestrations for the various branches of the aorta is needed. This adds complexity during placement of the main body. A risk that is sometimes taken when patients have no suitable landing zone below the renal arteries and open repair is not indicated due to contra-indications. This chapter will discuss materials used in stent grafts, its geometries, furthermore, compliance and usability will be addressed, resulting in an overview

MATERIAL

Stent grafts are manufactured using a variety of materials. The wire mesh stent, also called 'skeleton', is most often produced using nitinol followed by stainless steel and cobalt chromium. To be able to exclude the aneurysm from the blood circulation a graft is fixated to the stent, forming the stent graft. This graft is made from a polymer, often being Dacron or ePTFE.

Nitinol

Nitinol is used in many stent grafts providing the rigid form it requires as well as its capability to self-expand to a pre-set diameter when deployed. The self-expansion is also known as the shape memory effect (SME). Nitinol is therefore a smart material; smart is described as a material that has self-adaptability, is self-sensing, has shape memory or multiple of these functionalities combined in one material.⁴⁵⁻⁴⁹ The shape memory of nitinol exists in two forms; thermal memory and mechanical memory. The first converts heat into a change of the crystalline structure of the nitinol; from so called martensite to austenite. The latter allows deformation of the nitinol without plastic deformation (permanent deformation) also known as super elasticity, this only happens when the temperature is high enough ensuring a full austenitic phase of the nitinol.^{45,47,50,51} Furthermore nitinol is biocompatible, hemodynamically stable and amongst others practically non-corrosive.^{52,53} Nitinol's super elasticity (SE) can mimic the elasticity of healthy vessel wall. Mimicking the native artery results in less complications and ensues longer lasting implants.^{21,54} However, atherosclerotic plaques and thrombosis adversely influence the compliance of the native artery. Due to this reduction in compliance the effect of mimicking native artery compliance might be ineffective.

Most stent grafts are made of nitinol to allow for deployment flexibility; the capability to adjust the stent graft by small amounts to optimize the positioning in the designated landing zone during deployment. This possibility, to adjust the stent graft placement during deployment, is highly beneficial and reduces post-operative complications such as renal artery blockage.

Nitinol can be produced via laser based Additive Manufacturing (AM) processes, albeit currently in proportions of micrometres. Properties of a Shape Memory Alloy (SMA) produced via AM are close to that of conventionally processed SMA, i.e. AM produced SMA has a shape memory effect comparable to conventional produced SMA.^{51,55} The machine settings for AM need to be chosen carefully, for the properties of SMA change drastically with the smallest change. In addition to these settings the percentage of nickel and titanium as well as other metals in the powder mixture requires consideration as well. Differences in the composition or impurities can alter the material characteristics drastically.^{55,56}

Successes are reported on the use of nitinol in endovascular devices; properties such as biocompatibility, hemodynamical stability and corrosion resistance. Fatigue and long term patency, especially for thinner stents, amongst others need to be further investigated.⁵⁷

Other skeleton materials

Nitinol is not the only material used in stent grafts, stainless steel (SS) and cobalt-chromium (CoCr) versions are on the market as well. These latter two are balloon expandable stent grafts, and have no shape memory. The advantage of balloon expandable stent grafts is their increased crush resistance and hoop strength resulting in a strong fixation in the vessel wall. An additional benefit is the stable stress on the landing zone of the stent graft. Whereas nitinol stent grafts cause a continually increasing stress on the vessel wall, due to oversizing, balloon expandable stent grafts induce a stable stress level in the vessel wall. Though the stress level is stable, the increased rigidity of the balloon expandable stent graft results in reduced compliance, i.e. the stent graft does not pulsate as the surrounding artery does. According to the Windkessel model this might result in reduced flow in a healthy aorta, which in turn might have adverse effects on the patency of the stent graft. For parts of the stent graft that come into contact with atherosclerotic plaques or thrombi the difference between self- and balloon expandable might be smaller due to the inherent lower compliance of those pathologies. Additionally, balloon-expandable stents cannot be directly controlled over how they expand, compared to self-expandable stents which expand in the pre-set shape.

The Windkessel model describes the entire vascular system as a compliant reservoir with a pump. The heart rests in between contractions and fills with blood. When the heart is not contracting there is no flow and thus a stasis of blood which can cause several problems such as thrombosis. Therefore, the arteries have a 'pumping function' as well. After the heart has contracted, the dilation of the vessel walls (due to their compliance and sudden increase in blood volume during contraction) is returned to their initial balance state before contraction of the heart. This results in the blood being pushed forward while the heart is in diastole, smoothing the flow curve and allowing for continuous flow (albeit a pulsatile flow).⁵⁸

A summary of the aforementioned characteristics of nitinol, and the reasons for being the material of choice for this design:

- Primary reason is the shape memory characteristic of nitinol which allows for each stent graft to be patient specific and deployed in the same shape it was fabricated, for balloon expandable materials this is uncontrollable as mentioned above;
- Furthermore, it has super elasticity allowing higher compliance, closer to that of the native artery, than the balloon expandable materials;^{21,54}
- It is biocompatible, hemodynamically stable, and non-corrosive;^{52,53}
- It has proven to have higher fatigue resistance than balloon expandable stents.⁵⁷
- And it allows for adjustments during deployment helping prevent renal artery blockage.

Graft

The most common grafts are made of PET or ePTFE; materials which are biocompatible and have strong wear and tear resistance. These characteristics are important for a graft to be able to withstand the continuously pulsating blood. This requires grafts to be relatively thick when compared to other materials like polyurethane (PU) or ultrahighmolecularweightpolyethylene (UHMWPE). Research by Guan et al. has shown that the current limiting factor is the graft (in this case PET) when it comes to mimicking the native artery. When using PU it is shown that the compliance of the stent graft increases (by a factor of 17) to the point where the stent skeleton itself becomes the limiting factor. This increase in compliance approaches that of the native aorta.⁵⁹ In addition, PET and woven polyesters might play a role in inducing a more severe post implantation syndrome (PIS) when compared to ePTFE. Therefore, it might prove beneficial to consider other materials like ePTFE and PU for the graft.^{60,61}

Additionally, considering the various geometries Lin et al. have shown that z-shape stents cause more damage to the graft during a 168h pulsatile flow test than circular stents.⁶² Therefore, when choosing the graft material one should consider the amount of damage the stent geometry will cause to the graft for this might result in choosing a material that is more fatigue resistant.

The production of a graft can comprise various techniques amongst others: electrospinning, submersing the stent in molten graft material, stretching graft material over the stent and using fibres to weave a graft which is sewn onto the stent.²¹ Which graft material suits the product requirements best is still unknown and should be investigated. Further elaboration can be found at the end of this chapter.

GEOMETRY

The variety in geometrical shapes manufacturers produce for their stent grafts all have their own effect on the vessel wall, blood flow, long-term patency and so forth. These shapes can be classified in 5 classes according to overall geometry: sequential rings (rings with bridging), individual rings (rings without bridging), woven, helical, and coil. As can be seen in Figure 10. Subdivision can be made according to geometry per ring: z-shape and circular, and the connection between rings: regular, periodic, and closed cell connection. As can be seen in Figure 11.⁶³

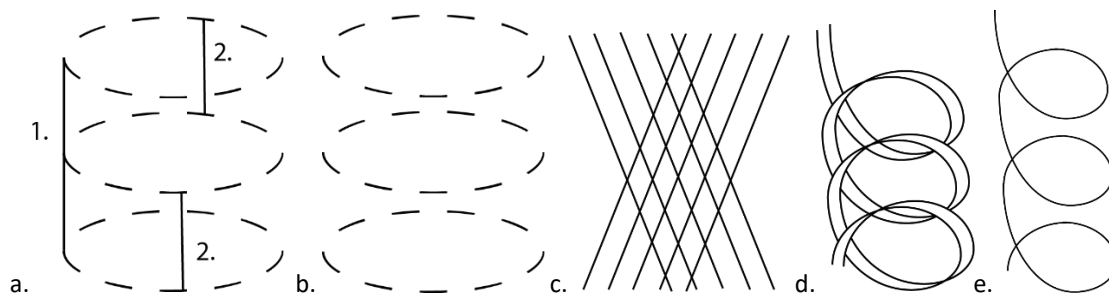
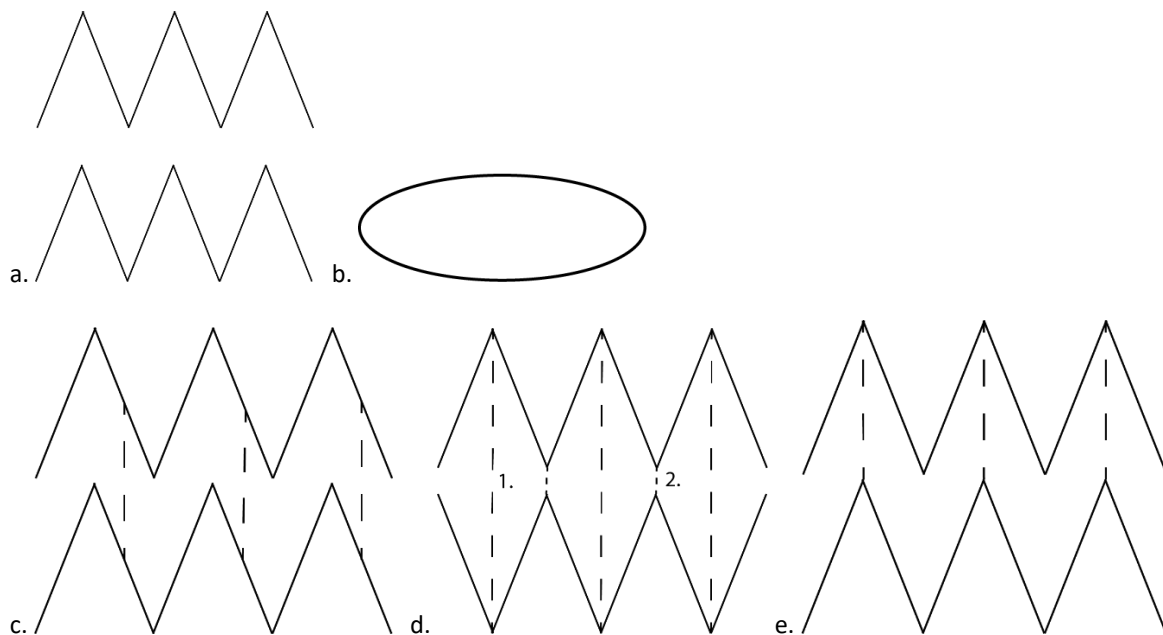


Figure 10: 5 classes of stent geometries; a) sequential rings (with bridging 1,2), b) individual rings (without bridging), c) woven, d) helical, and e) coil.



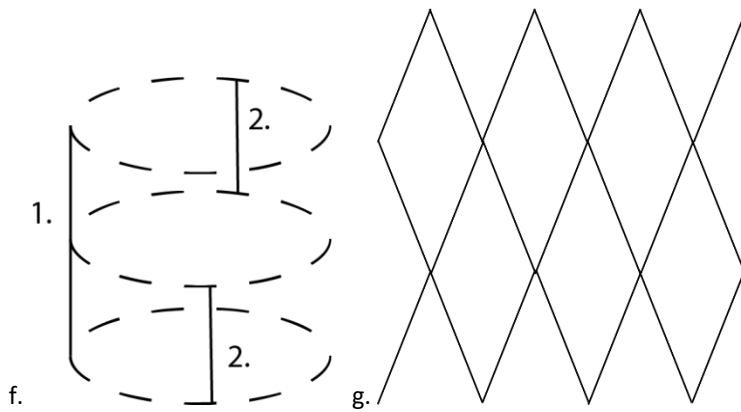


Figure 11: subdivision of ring geometry: a) z-shape, b) circular and subdivision according to bridging: c) mid-strut to mid-strut, d) peak to valley; 1. long, 2. short, e) regular, f) periodic (1. is a longitudinal bridge and 2. are periodic bridges both 1 and 2 with c, d or e placement), and g) closed cell.

The geometry and material also influence two parameters used in self-expandable stents: Chronic Outward Force (COF) and Radial Resistive Force (RRF). The COF describes the ability of the stent to fixate itself in the vessel wall due to the unloading force created in the nitinol during the crushing process. The RRF indicates the force required to crush the stent (i.e. the force the stent can withstand without collapsing or the loading force according to the stress-strain loading curve of nitinol).^{64,65} As can be seen in Figure 12.

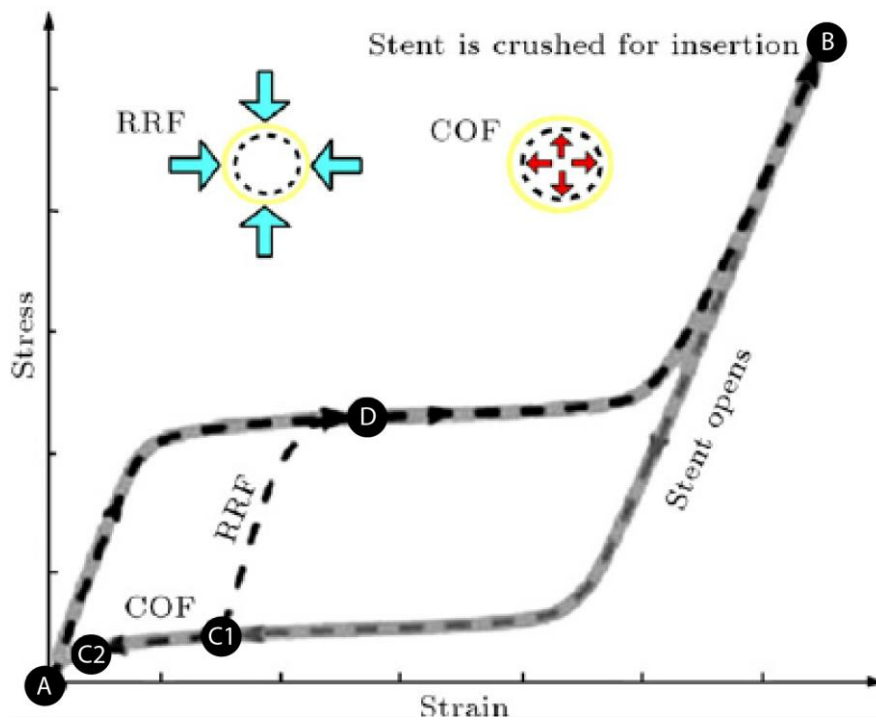


Figure 12: A typical hysteresis loop (i.e. stress-strain curve), by Nematzadeh et al., for super elastic nitinol. The loop consists of a loading curve, path A-B, describing the increase of stress and strain when the stent graft is crushed to the required insertion diameter. Then an unloading curve follows, path B-C, which describes the deployment of the stent graft in the vessel until it reaches a stress equilibrium with the vessel wall at point C1. This equilibrium has two curves as well, the COF (path C1-C2), describing the remaining stress, or outward force, in the stent graft (i.e. the unloading curve). The second curve is the RRF, path C1-D, which describes the loading curve of the stent graft or the force required to crush the stent at that equilibrium point C1.⁶⁵

The COF and RRF have an impact on the stability of the inlet-outlet ratio. The ratio of the inlet diameter at the neck with the outlet diameter at the iliac legs (d_{in}/d_{out}) increases with an increasing AND (i.e. increasing neck

diameter). This ratio is exponential to the overall force exerted on the stent graft according to Georgakarakos et al.⁶⁶ Therefore, the force on the stent graft will increase with an increasing AND, which might result in stent graft migration and even endoleaks.⁶⁷⁻⁶⁹ However, Monahan et al. did not report any endoleak type I or migration due to AND after a mean follow-up of 59 months in 49 patients. Therefore, neck diameter as a determinant for migration outcome as reported by Jim et al. and Stanley et al. might require further investigation.^{70,71} Optimizing the neck and iliac diameters ratio might prove beneficial to prevent migration and endoleaks, and should therefore be included in the design considerations.

Strut thickness

Kastrati et al. and Pache et al. performed studies on strut thickness comparing coronary stents with varying strut thickness.^{72,73} In two studies, they included 651 and 611 patients and found reduced relative risks for angiographic restenosis (0.58, $p=0.003$ and 0.57, $p<0.001$ respectively) and reduced relative risk for clinical restenosis and therefore intervention (0.62, $p=0.03$ and 0.56, $p=0.002$ respectively) for strut thickness of 50 μm compared to 140 μm .^{72,73} Furthermore, the thickness of the struts becoming smaller is an important factor in positive clinical outcome.⁷⁴ The geometrical orientation of the struts did not affect the outcome. Important to mention is that these results come from a study concerning coronal stents. Due to difference in size and goal this might not be applicable to an EVAR design. Important to note as well is that the COF and RRF increase with the strut thickness, therefore a balance should be found in required COF, RRF and clinical outcome. For instance, to obtain a similar COF and RRF with thinner struts a larger oversizing percentage should be chosen. Considering the aforementioned, the effect of strut thickness of EVAR stent grafts should be investigated, its effect on the vessel wall and functional properties might be significant and therefore an element to take into account while designing the optimal stent graft.

COMPLIANCE OF STENT GRAFT AND AORTIC WALL

Guan et al. gave an overview of research performed on stent graft design and its impact on the biomechanical properties of the native aorta. Two properties of stent grafts, amongst others, need to be considered when the new stent graft is designed. Firstly, when the diameter of the stent graft is lower than the diameter of the aortic neck, in systole, this might result in stent graft migration. This can occur due to AND, where the diameter of the aortic neck becomes greater than the stent graft which at systole reaches its maximum diameter and becomes nearly non-compliant.⁷⁵ Therefore, it is necessary to be precise when determining the diameter of the neck of the stent graft. These measurements are performed often in CT-angiographic images, it is unclear at what point of the cardiac cycle the images were taken. The diameter change of the aortic neck can be as big as 13.3%.⁷⁶ This change might impact long-term patency of the stent graft and might result in early re-intervention.⁷⁷

The second property is the inherent compliance mismatch between stent graft and native artery which causes flow disturbances that might cause stenosis and proliferation of cells at both ends of the stent graft. Creating a stent graft in which the compliance approaches that of the native artery might resolve those flow disturbances. Guan et al. described the influence of blood pressure condition of the patient as a factor in determining the necessary compliance of the stent graft. Normo- and hypertensive patients benefit more from higher compliant stent grafts, hypotensive patients benefit less from higher compliant grafts.⁵⁹ Due to the lower pressure less compliance is required to follow native artery distensions. The low compliance difference between stent graft and native artery in patients with low blood pressure results in less flow disturbances.

Morris et al. compared stent graft compliance with the compliance of a silicone phantom, whose characteristics approximate the native aortic wall. The 'Zenith Flex' and 'Fortron' stent graft showed no significant compliance difference with the silicone phantom. Raising the question why, this might be due to their geometry, material combination, strut thickness and/or graft, further investigation is required.⁷⁸

USABILITY

The use of different market available stent grafts (spiral, circular, and z-shape with and without bridging) in tortuous anatomical cases is investigated by Demanget et al. in 2013. They have shown that spiral and circular stents obtain higher flexibility results while having lower internal stresses and low luminal reduction rates. These results are created during 90° and 180° bending tests.⁷⁹

Through personal experience visibility of the stent graft in vivo is highly preferable. The procedure requires good visualization of the stent graft, though with the current radiopaque beads and opacity of the stent visualization sometimes lacks the required unambiguity. This results in valuable time being lost discussing its current position and presentation on screen. Incorporating more radiopaque material in the final powder composition of the nitinol ensures better visibility perioperative, furthermore an intuitive radiopaque bead placement should be developed.

PRODUCTION PROCESS

The vascular system of each patient is vastly different, to cope with such variation a production process with high adaptability is required. 3D printing allows for such adaptability it is, therefore, the production method of choice to produce personalized stent grafts. Other production methods currently used are laser cutting and braiding, amongst others. The first is limited by the requirement of a tube from the desired material. Creating a tube matching the patient anatomy in tortuosity and diameter is difficult, set aside that it requires a laser system with 5 or 6 axes. The latter is mostly used for digestive track stents and has device characteristics not ideal for use in EVAR. Choosing the optimal design for 3D printing requires research into the composition of the nitinol powder as well as the geometry for some geometries require more support which would result in unwanted extra labour to remove these supports when printing is finished.

Using nitinol requires post-processing this helps in acquiring homogenous material characteristics throughout the entire stent. This can be achieved through a variety of ways, commonly by using heat, which is possible to perform in some 3D printers that can act as an oven.

OVERVIEW

Nitinol will be the material of choice for this design. Nitinol is preferable over CoCr due to the reasons mentioned earlier, though CoCr is already printable. Whether these characteristics will be present in 3D printed nitinol remains to be seen. Considering the materials used in stent grafts, its geometries, compliance and usability, preferences can be noted as to which of the aforementioned would suit the final goal best. An overview of geometries and graft types is given in Table 1 and 2. First important characteristics are explained, thereafter the overview is given in the table.

Table 1 important characteristics:

- *COF*: the chronic outward force should be balanced, it should ensure a proper seal, however, it should not cause unnecessary high wall stresses.
- *RRF*: the stent graft should be able to withstand changes from the body that cause an outside pressure. Commonly agreed; the higher RRF the better.
- *3D printable*: 3D printing requires supports to print geometries for instance with an overhang. Difficult geometries are therefore harder to print than more simple geometries would be.
- *Graf-able*: a graft can be applied to the stent in multiple ways, however, stent geometry plays a role in how accessible they are in various graft application methods.
- *Anatomically shape-able*: certain stent geometries are less ideal for shaping to the anatomy of a patient, due to their inherent larger profile.
- *Fatigue resistant*: the various geometries all behave different and therefore result in varying fatigue behaviours.

- *AND*: under influence of the COF and the geometry, *AND* might be prominent than in others.
- *Dislodgement force*: the force the stent graft can withstand before it migrates.

Table 1: Indications of the forces to be expected and the behaviour of the stent regarding its overall functionality.^{78,80,81}

Stent geometry	COF	RRF	3D printable	Graft-able	Anatomically shape-able	Fatigue resistant	AND	Dislodgement force
	+++ = balanced	+++ = higher	+++ = best	+++ = best	+++ = best	+++ = best	+++ = lowest	+++ = highest
Z-shape	++	+++	++	++	++	+	+	++
Circular	+	+++	++	++	+++	+++	++	+++
Closed cell	+++	+	+++	+++	+	+	+	++
Woven	+++	+	N.A.	+++	+	++	+++	+
Helical	++	++	+	+	++	++	++	+
Coil	++	++	++	+	+++	+	+++	+

The z-shape and circular stent geometries offer balanced characteristics, of which 3D printability and anatomically shape-able are the most important for this research project its goals, therefore z-shape and circular will be included in the concept designs. Though the closed cell, woven, and helical stent design are superior in some characteristics, in others they are inferior. Therefore, a balanced stent design might offer overall better results.

Table 2 important characteristics:

- *Compliance*: the compliance of the graft indicates the possibility to approach compliance of a healthy aortic wall. Higher compliance is therefore preferable.
- *Endothelization*: the graft plays an important role in accepting the stent graft and reducing PIS. The amount of endothelium that grows over the graft differs per graft type and porosity. A graft that offers quick and stable endothelization is preferable.
- *Abrasion resistant*: due to the pulsatile environment, an abrasive resistant graft is required.
- *Graft-able*: the graft should be mouldable to the patient anatomy and quickly applied to the stent.
- *Low PIS*: inflammation can cause major complications, therefore, PIS induction should be as low as possible.
- *PWV*: the graft should have, ideally, no influence on the flow profile of the blood.

Table 2: Indications of the characteristics of the graft.^{54,59,82}

Graft type	Compliance	Endothelization	Abrasion resistant	Graft-able	Low PIS	PWV
	+++ = higher	+++ = better	+++ = better resistant	+++ = better	+++ = low induction	+++ = Low influence
ePTFE	+	+++	+	+	+++	++
Dacron (PET)	+	+++	++	+	+	+++
PU	+++	?	?	+++	+++	+
UHMWPE	+++	?	?	+++	?	?
Dyneema	+	+++	+++	+	?	?

Considering the graft material, there are still unknowns therefore, a standardized study into the functionalities of these graft materials is essential before a decision for one can be supported. However, compliance and graft-

ability are important characteristics for this research project, therefore, PU or UHWMPE seem the most likely candidates as graft material.

DESIGN REQUIREMENTS

To be able to properly identify requirements for the stent graft design user have been identified as well as their requirements, which can be found in table 3. A total of 6 requirements from users have been identified through a quick question round with the vascular surgeons:

- *Lower costs*: the amount of money a surgery costs, specifically the cost of the used stent graft systems which should be as low as possible for these stakeholders.
- *Quantity*: the amount of operations that can be performed with the stent graft systems used, operational wise the system should be able to be produced easily to allow for large quantity production.
- *Revenue from product*: the margins on the product should be as high as possible.
- *Higher treatability*: the complexity of the cases able to be treated with the stent graft system should be greater than what is currently available.
- *Safe product*: the product should be safe to use in all cases.
- *Lower complication rate*: the amount of complications that occur with the used stent grafts.

Table 3: Users and user requirements; the vascular surgeon, hospital and producer have the most requirements in this project.

User	Lower costs	Lower complication rate	Quantity	Revenue from product	Higher treatability	Safe Product
Vascular surgeon		X	X		X	X
Interventional radiologist			X			X
Operating assistants			X			X
Patient		X			X	X
Healthcare insurance	X	X				X
Society	X	X				X
Producer			X	X	X	X
Material industry			X	X		
Hospital	X	X	X		X	X
CE Marking		X				X
FDA		X				X

List of requirements

Some requirements have been identified above, all the requirements can be found in the list below and are formed based upon literature, personal communication with my supervisors and OR time. The requirements are subdivided into four categories: functional (what should it do), operational (how does the production chain look like), technical (how should it perform) and transitional requirements (how is it implemented into the workflow).

Functional

- Should be able to be used for either all abdominal aneurysms or at least one of the following: infra-, juxta- and supra-renal abdominal aneurysms.
 - Stent graft should include branches for renal and visceral arteries.
 - Should also be used for infra-renal aneurysms with a small neck
- Should be inserted via the femoral artery.
 - Compatible with guide wires.
 - Profile lower than 20 French (smaller is better).⁷⁴
- Should have a user interface similar or more intuitive to current EVAR products.
 - Positioning via radiopaque beads should indicate locations of top and bottom as well as fenestrations/branches.
 - Stent should be as radiopaque visible in its entirety as possible.
 - Should be able to be manipulated during placement.
 - Deployment should be controlled via rotating handles on the interface-end.
 - Should self-expand during deployment. (requires nitinol)
 - Should self-adhere to vessel wall through COF and RRF inherently in the stent.
- Custom made for better match with patient's anatomy.
- Should be long enough to provide an artificial landing zone for subsequent stent grafts to be placed.
- Should be compatible with other brands of stent grafts as an artificial landing zone.

Operational

- Should use Angiographic images to produce data for use in the design of the stent graft.
- Should produce a 3D model of the stent graft in a file compatible with the AM method (current is a STL file).
 - Should use a semi-automatic or automatic method to produce that model.
- Should be produced with an AM method (3D printing).
 - Printer should be compatible with reactive metal printing (use of Argon gas).
- Should have as low as possible material costs.
 - Should be capable to produce multiple products in the same manufacturing instance.
- Should withstand post-processing annealing to ensure homogeneous material characteristics.
 - Nitinol requires annealing to ensure homogeneous super-elasticity and shape memory.
- Should be able to be covered with a polymer film.
 - Already certified and much used polymers: e-PTFE and Dacron.
 - Less used but interesting: PU and UWHMPE.²¹
- Should prevent graft erosion and abrasion as much as possible.^{21,82,83}
- Should be able to withstand a surface treatment for sterilization, both nitinol and the polymer.²¹

Technical

- Should have similar characteristics to conventional produced stent grafts.
 - Composition of the powder for 3D printing should be fine-tuned.
 - Should comply with CE Marking and FDA approved standards.
- Should have full patency longer than 2 years (comparison mid-term current devices).²³
- Should cope with high alternating pressure inside the blood vessel.
 - Should have high endurance and little to no chance of breaking/fatigue.
- Should not induce too much AND → COF should be balanced with the vessel wall.
- Should be flexible to retain profile without kinking → A high enough RRF should be ensured.
- Should allow for a polymer film to be created over the stent, therefore the space in between struts should be small.
- Should not migrate or leak.
 - Should be oversized by 10-20% to ensure good radial force, this should be in balance with potential vascular wall damage.

- Should have a top stent with barbed wires to hook into the vessel wall.
- Should have a graft design that prevents endoleaks type III and IV.
- Should be biocompatible.²¹
 - Bio-inert towards blood.
 - Promote low vessel wall ingrowth.
 - Demote sclerotic plaque forming.
 - Low corrosion levels.
 - Should have a form of porosity or patterned holes for improved endothelialisation and increased flexibility.
 - Should not be toxic, allergic, or carcinogenic.
 - Should have a low PIS effect.
 - Should not cause thrombosis, haemolysis, foreign body reaction or inflammatory response.

Transitional

- Should reduce production time to less than one week from delivery of CTA scans.
- Should be placed as first stent graft to provide the operator with an artificial neck/landing zone.

4. CONCEPT PHASE

A variety of stent grafts are available on the market. Evidence for the superiority of a specific design is not yet available. As mentioned in the second chapter for some of the design choices such as: thin- versus thick-struts and high compliant versus low compliant stent grafts choices must be made which will be implemented into the final design. One should take into account that the EVAR procedure is minimally invasive and therefore is bound to a user interface which cannot always accommodate all the movements a surgeon wants. The design should be adapted to this and be as simple as possible to prevent the surgery becoming unnecessary difficult.

At first the design should focus on the supra-renal to infra-renal part. Considering that 'off the shelf' stent grafts can be placed inside the custom-made stent graft part (see Figure 13); as a first design, an artificial infra-renal neck is suggested for the off the shelf stent graft to land on. This design is technically less complex since it does not include fenestrations for renal arteries, a next iteration of the design should include juxta- and supra-renal stent grafts.

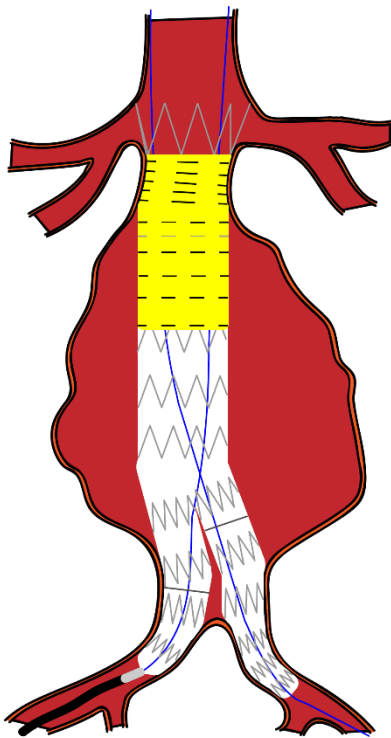


Figure 13 legend

Yellow: Custom-made stent graft.

Black dashed line: Anatomically shaped rings in custom-made stent graft.

Grey dashed line: Proximal ring from the off the shelf stent graft.

Figure 13: A sketch of the off the shelf stent graft inside the custom-made supra- / infra-renal stent graft.

Considering the list of requirements two design concepts are made in Solidworks. A fishmouth stent and a z-shape stent. Both designs have a straight tubular version as well as one that is matched to the anatomy of a conical aortic neck (see Figure 18 the set-up of Ansys).

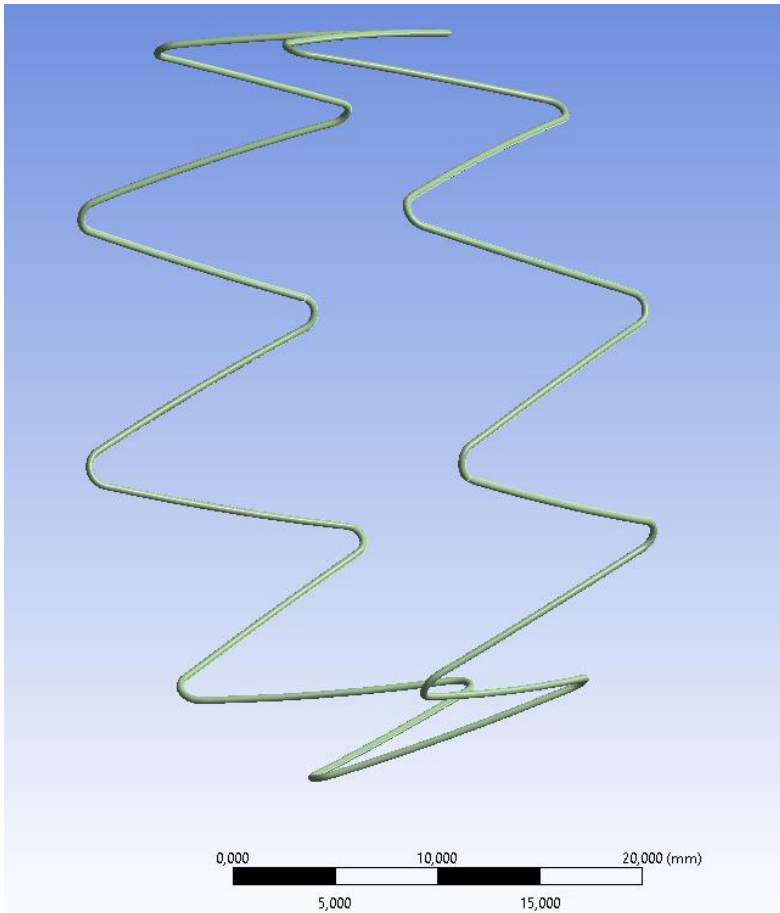


Figure 14: Personalized Z-shape stent of 36 to 32mm diameter and a strut thickness of 0.1763mm.

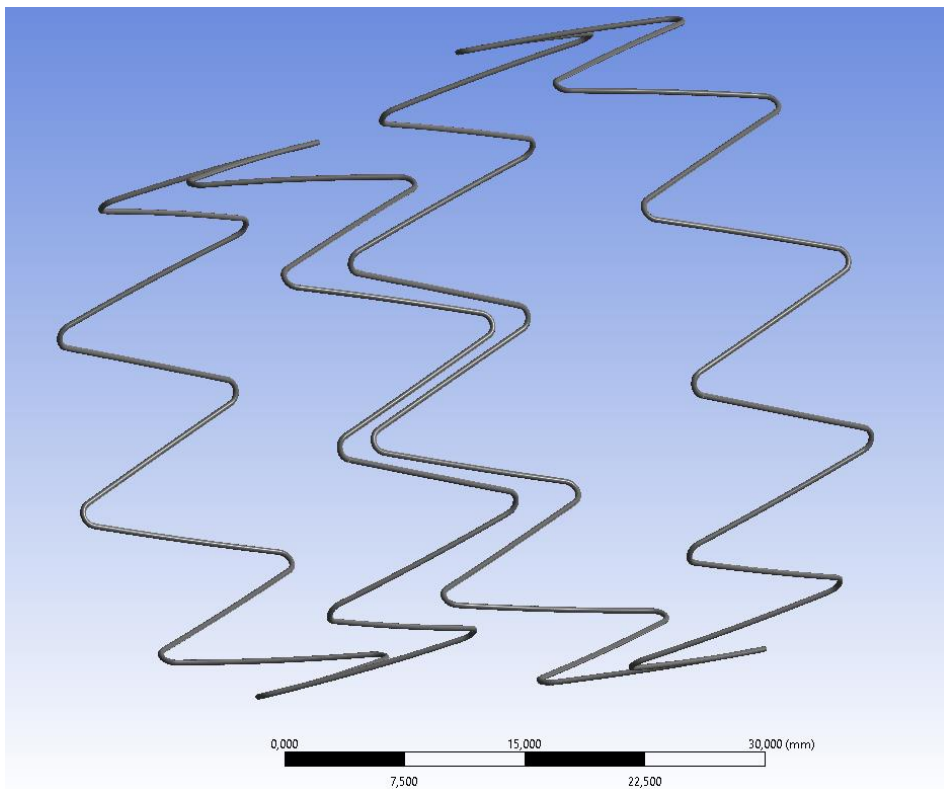


Figure 15: Z-shape stents of 32 and 40 mm diameter and a strut thickness of 0.1763 mm.

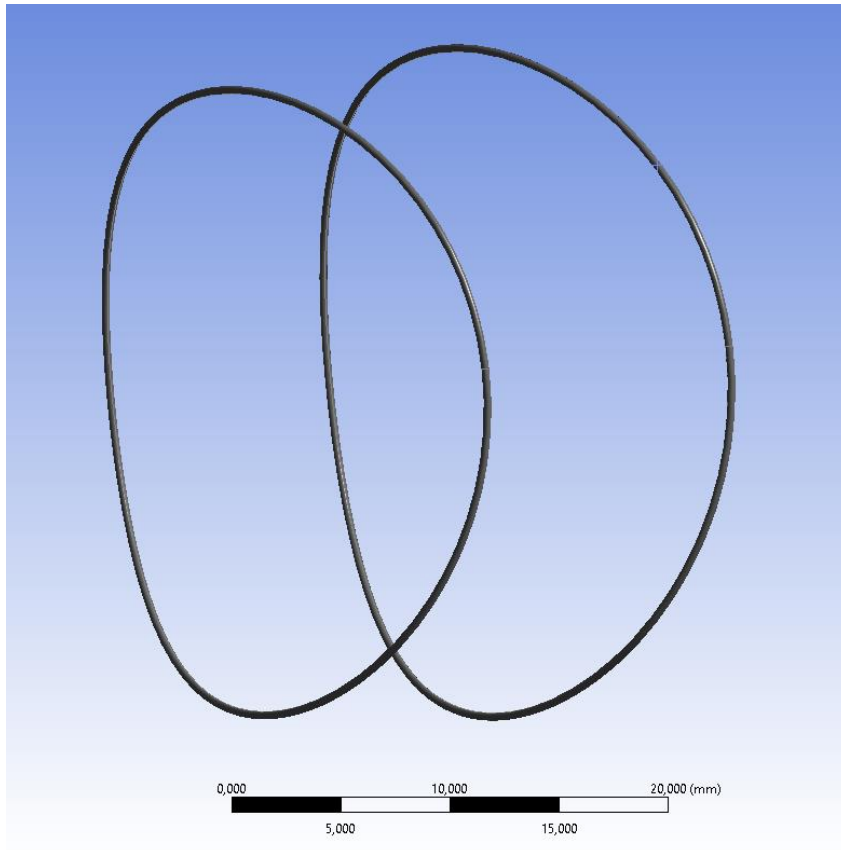


Figure 16: Left image: Fishmouth stent of 28mm (left) and 30 mm (right) diameter and a strut thickness of 0.1763 mm.

5. EMBODIMENT PHASE

To test the functionalities of the designs and their impact on the vascular wall simulation are performed using the finite element method. Due to the early stage of the project some indications on whether these designs will have a positive effect on the vascular wall is preferred before money is invested in manufacturing the stents. This approach allows for simulation of various aortic necks and stent designs and quick evaluation of subsequent iterations of the stent designs. Furthermore, detailed data can be acquired regarding the stent, the aortic neck, and their effect on each other. Good simulation practice requires hand calculations and experimental data. The calculations are performed below, the experimental data is acquired from the literature.

PRE-SIMULATION CALCULATIONS - GOVERNING EQUATIONS FOR A FINITE ELEMENT

ANALYSIS OF A STENT

$$\begin{bmatrix} \sigma_x \\ \sigma_y \\ \sigma_z \\ \tau_{yz} \\ \tau_{xz} \\ \tau_{xy} \end{bmatrix} = \frac{E}{(1+\nu)(1-2\nu)} \begin{bmatrix} 1-\nu & & & & & \\ & 1-\nu & & & & \\ & & 1-\nu & & & \\ & & & 1-2\nu & & \\ & & & & 1-2\nu & \\ & & & & & 1-2\nu \end{bmatrix} \begin{bmatrix} \varepsilon_x \\ \varepsilon_y \\ \varepsilon_z \\ \gamma_{yz} \\ \gamma_{xz} \\ \gamma_{xy} \end{bmatrix} \quad (1)$$

The matrix above describes the stresses of one infinitesimal small cube of material in three dimensions, as a function of the strains. Furthermore, E is Young's modulus, ν is Poisson's ratio, σ is stress, τ is shear stress, ε is strain and γ is shear strain. The strain-displacement relations describe the strains on a small cube of material. Which is a ratio of the change in dimensions of the cube due to forces and its initial dimensions.

$$\varepsilon_x = \frac{\partial u}{\partial x}, \varepsilon_y = \frac{\partial v}{\partial y}, \varepsilon_z = \frac{\partial w}{\partial z}, \quad (2)$$

$$\gamma_{yz} = \frac{\partial v}{\partial z} + \frac{\partial w}{\partial y}, \gamma_{xz} = \frac{\partial w}{\partial x} + \frac{\partial u}{\partial z}, \gamma_{xy} = \frac{\partial u}{\partial y} + \frac{\partial v}{\partial x} \quad (3)$$

These equations (1, 2 and 3), based upon Hooke's law, are only valid for the linear elastic behaviour of the material, if the yield threshold has been reached the behaviour of the material will change into nonlinear and these equations will not represent the changes in the cube anymore.

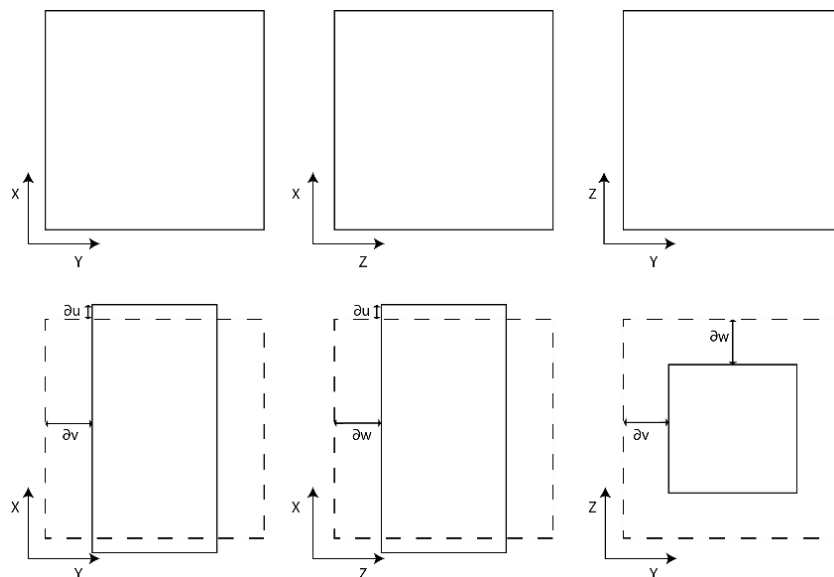


Figure 17: a cube is changed into a bar due to forces which causes the original diameters (x , y , and z) to change with u , v , and w . This is an exaggerated form for functional display.

EXAMPLE CALCULATIONS - ADAPTED VERSION OF HOOKE'S LAW

According to Boron and Boulpaep's Medical Physiology book, the change in length of the blood vessel and its wall thinning during distension is not a major factor. Therefore, Laplace's law can be used to describe the wall tension (T) in a blood vessel considering only the transmural pressure and the radius of the vessel.⁵⁸ Comparable to pulling together the ends of a longitudinally separated vessel wall.

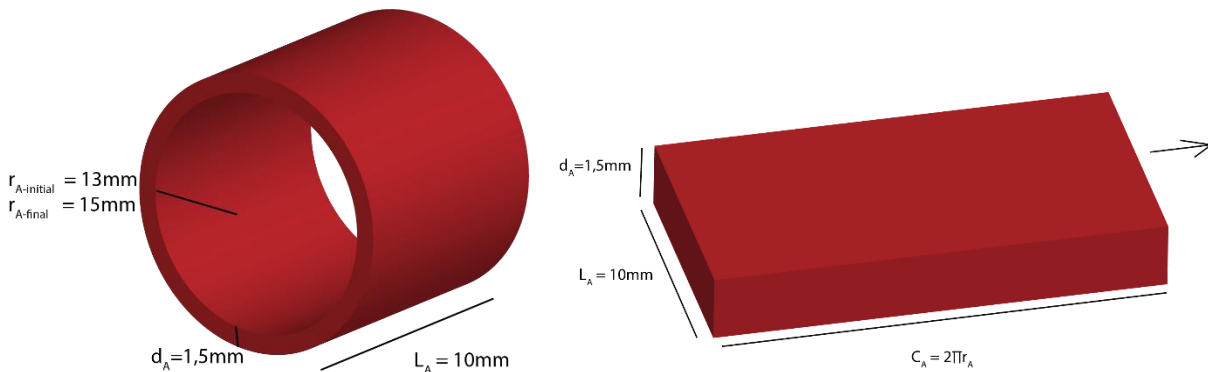


Figure 18 and 19: on the left dimensions of the aorta neck are shown; the radius r , the thickness d , and the length L . On the right the aorta 'sheet' is shown with its thickness d , width L and circumference/length C and the pulling direction indicated by the arrow.

A blood vessel, when longitudinally cut, can also be described as a sheet of material. The wall tension can then be described through the adapted version of Hooke's Law which describes the blood vessel like it were an elastic band that is stretched.⁵⁸

Boron and Boulpaep's adapted version of Hooke's Law⁵⁸:

$$\frac{F}{A} = E \times \frac{L_1 - L_0}{L_0} \quad (4)$$

The Young's modulus of the aortic wall is 4.46×10^{10} Pa and its Poisson's ratio is 0.49.⁸⁴

Using the adapted version of Hooke's Law (4), the force required to strain the sheet of aorta by 12.57mm (a 4mm diameter increase) can be calculated:

$$\frac{F}{A} = 4.46 \times 10^6 \times \frac{9.42 \times 10^{-2} - 8.17 \times 10^{-2}}{8.17 \times 10^{-2}}$$

$$\frac{F}{A} = 6.82 \times 10^5 \text{ N/m}^2$$

$$F = 6.82 \times 10^5 \times (1.5 \times 10 \times 10^{-6})$$

$$F = 10.2 \text{ N}$$

Therefore, the stent requires a minimal force of 10.2N to strain an aortic wall of 10mm width from 13 to 15mm in radius.

A similar calculation can be made for a nitinol ring whose dimensions are: length/ circumference: 15mm to 13mm / 94.3mm to 81.7mm, width: 0.2mm and thickness 0.2mm.

The Young's modulus of a sample of nitinol is 4.0×10^{10} Pa and its Poisson's ratio is 0.46.⁸⁵

$$\frac{F}{A} = 4.0 \times 10^{10} \times \frac{9.42 \times 10^{-2} - 8.17 \times 10^{-2}}{8.17 \times 10^{-2}}$$

$$\frac{F}{A} = 6.12 \times 10^9 \text{ N/m}^2$$

$$F = 6.12 \times 10^9 \times (0.2 \times 0.2 \times 10^{-6})$$

$$F = 245 \text{ N}$$

Therefore, the force provided by the stent to expand itself is larger than the force required to expand the aortic wall thus the stent will not collapse under the aortic wall. However, the stent will not reach its final dimensions of 15mm radius due to the counteracting force of the aortic wall.

This calculation does not take into account the compression using Poisson's ratio. This ratio has a value ranging from -1 to 0.5. Metals often have their ratio around 0.3, in this case the aortic wall has a ratio of 0.49 that means that the volume of the cube would be almost constant and the force required to change its volume would almost be infinitely large. For metals, a small change in dimensions of the cube is possible. Calculating the stress in the x direction for the aortic wall and the nitinol ring gives an indication of what the results from the simulation should look like.

CALCULATION OF AORTIC WALL FORCES NEEDED TO EXERT A 4-MM ENLARGEMENT OF THE DIAMETER.

Using the assumptions Boron and Boulpaep made regarding vessel length and wall thickness, only a pulling force is exerted in both x-directions of the cube resulting in a normal and shear stress on the cube in both x directions.⁵⁸

If this is filled into the governing equations together with $X = 2\pi \times 1.3 = 8.17 \times 10^{-2} \text{ m}$ and $\partial u = 2\pi \times 1.5 - 8.17 = 1.25 \times 10^{-2} \text{ m}$ the stress in the x direction with its corresponding shear stresses can be calculated.

$$\sigma_x = \frac{4.46 \times 10^6}{1.49 \times 0.02} \times 0.51 \times \frac{1.25 \times 10^{-2}}{8.17 \times 10^{-2}} = 11.7 \times 10^6 \text{ Pa}$$

$$\tau_{xz} = \frac{4.46 \times 10^6}{1.49 \times 0.02} \times 0.02 \left(\frac{0}{0.94} + \frac{1.25 \times 10^{-2}}{1.5 \times 10^{-3}} \right) = 24.9 \times 10^6 \text{ Pa}$$

$$\tau_{xy} = \frac{4.46 \times 10^6}{1.49 \times 0.02} \times 0.02 \times \left(\frac{1.25 \times 10^{-2}}{0.01} + \frac{0}{8.17 \times 10^{-2}} \right) = 3.74 \times 10^6 \text{ Pa}$$

$$F_x = 11.7 \times 10^6 \times (1.5 \times 10 \times 10^{-6}) = 176 \text{ N}$$

CALCULATION OF FORCES NEEDED TO CRUSH A CIRCULAR NITINOL STENT.

To be able to be inserted, the stent must be crimped to a diameter of 6 mm in a realistic scenario, though for this calculation we assume a reduction of 4 mm (i.e. a diameter of 26 mm) is enough for insertion. This will give the minimal stress created in the stent to crush it to 26 mm from 30 mm.

If this is filled into the governing equations together with $x = 8.17 \times 10^{-2} \text{ m}$ and $\partial u = 1.25 \times 10^{-2} \text{ m}$ the stress in the x-direction with its corresponding shear stresses can be calculated:

$$\sigma_x = \frac{4.0 \times 10^{10}}{1.3 \times 0.4} \times 0.7 \times \frac{1.25 \times 10^{-2}}{8.17 \times 10^{-2}} = 8.24 \times 10^9 \text{ Pa}$$

$$\tau_{xz} = \frac{4.0 \times 10^{10}}{1.3 \times 0.4} \times 0.4 \times \left(\frac{0}{0.94} + \frac{1.25 \times 10^{-2}}{2 \times 10^{-4}} \right) = 1.92 \times 10^{12} \text{ Pa}$$

$$\tau_{xy} = \frac{4.0 \times 10^{10}}{1.3 \times 0.4} \times 0.4 \times \left(\frac{1.25 \times 10^{-2}}{0.01} + \frac{0}{8.17 \times 10^{-2}} \right) = 38.5 \times 10^9 \text{ Pa}$$

$$F_x = 8.24 \times 10^9 \times 0.04 \times 10^{-6} = 330 \text{ N}$$

As can be seen in the calculations the stent requires far greater forces to reach the desired deformation than it would for the aortic wall. This makes sense if you look at the Young's modulus of both materials and its definition. The Young's modulus is the force per cross-sectional area required to stretch the material to twice its initial length. However, the forces required to deform the stent are high and do not represent reality.

For z-shape stents the forces are calculated differently. The geometry of the nitinol stent should be taken into consideration. Therefore, if a stent is crimped with a z-shape geometry the cross section of the stent will have a compressive and a tensile part. Equilibrium dictates that the forces on these parts are equal but opposite to each other.

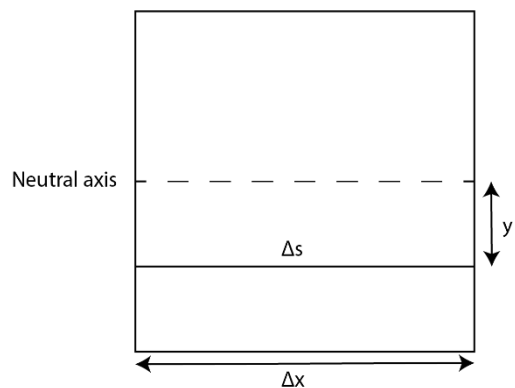


Figure 20: Stress free cross section of the stent; Δx = width of the cube, Δs = width of the cube at location y , y = location along the radius of the stent.

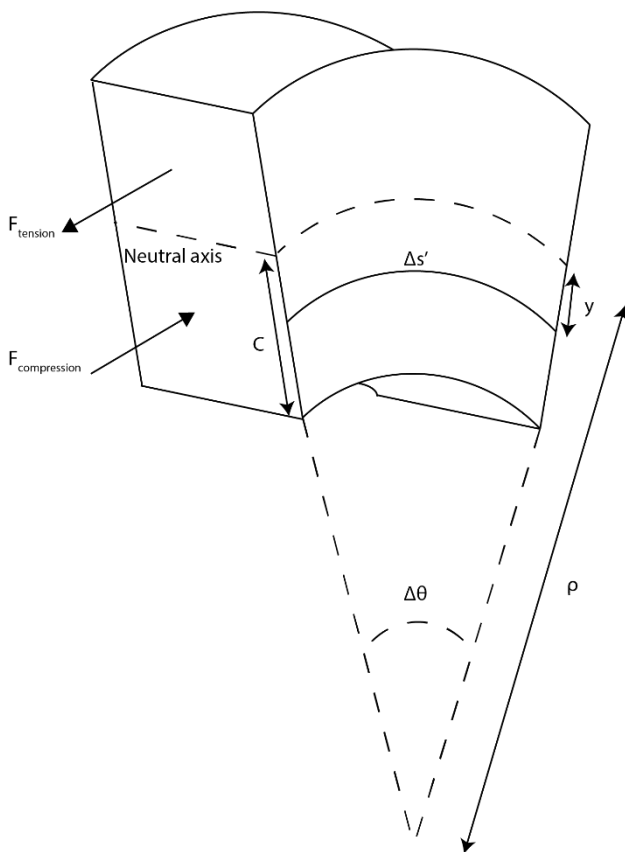


Figure 21: A side view of the cross section indicating different parameters; $\Delta \vartheta$ = change in angle, ρ = radius of the curve, C = radius of the stent, $\Delta s'$ = width at location y , y = location along the radius of the stent. Note the tension force and compression force in their respective areas.

For small deformations, we can assume:

$$\Delta x = \rho \times \Delta \theta \rightarrow \Delta s' = (\rho - y) \times \Delta \theta \quad (5)$$

The strain is also known as:

$$\varepsilon = \frac{\Delta s' - \Delta s}{\Delta s} = \frac{(\rho - y)\Delta \theta - \rho \Delta \theta}{\rho \Delta \theta} = \frac{-y}{\rho} \quad (6)$$

If the stent is crimped from 15 mm to 13 mm in radius, the angles between the struts (7 times 2 in total; $360/7 = 51.43^\circ$) are reduced by a factor 13/15. This results in an increase of angle ϑ by a factor of 15/13. Therefore, the $\Delta \vartheta$ is:

$$\Delta \theta = \frac{15}{13} \times 51.43 - 51.43 = 7.91^\circ$$

Δx is approximately 5.8 mm and y is the maximum radius, therefore $y = C = 0.1$ mm. Therefore, the ρ can be calculated as well as the resulting strain ε (using equations 5 and 6):

$$\rho = \frac{\Delta x}{\Delta \theta} = \frac{5.8}{7.91} = 0.73 \text{ mm} \rightarrow \varepsilon = \left| \frac{-y}{\rho} \right| = \left| \frac{-0.1}{0.73} \right| = 1.36 \times 10^{-1}$$

This strain can then be used for calculating the stress with the governing equations:

$$\sigma_x = \frac{4.0 \times 10^{10}}{1.3 \times 0.4} \times 0.7 \times 0.136 = 7.34 \times 10^9 \text{ Pa}$$

The force exerted on either the compressive or the tensile area is calculated by multiplying their respective areas with the stress.

$$F_x = 7.34 \times 10^9 \times 0.2 \times 0.1 \times 10^{-6} = 146.9 \text{ N}$$

When compared to the aortic wall force requirement (176N) it can be concluded that the stent will expand itself into the vessel wall until an equilibrium has been reached. The stent lacks the strength to push the aortic wall to the 4mm diameter increase, therefore a COF remains. Overall 176N and 122N quite high and most likely do not represent realistic scenarios. More often stent crushing forces of around 5-15 N are found.⁸⁶⁻⁸⁸

One extra calculation must be performed; the required 122N is calculated assuming 1 spring extending by 4 mm. However, there are 14 similar springs/struts in the stent geometry oriented in a circle. Therefore, we can assume equal distribution of force:

$$F_{x,per \text{ strut}} = \frac{146.9}{14} = 10.5 \text{ N}$$

10.5 N is in the range of 6-15 N and is therefore a feasible result. A similar approach applies to the aortic wall on which these 14 struts have their effect:

$$F_{aorta,per \text{ strut}} = \frac{176}{14} = 12.6 \text{ N}$$

This results in a chronic outward force i.e. the equilibrium with the vessel wall (see Figure 12). Which can be calculated by determining an equilibrium factor.

$$\text{Equilibrium factor} = \frac{10.5}{12.6} = 0.83$$

$$F_{stent,released} = 10.5 \times 0.83 = 8.75N$$

$$F_{COF} = 10.5 - 8.75 = 1.75N$$

Morris et al. have tested various marketed stent grafts with circumferential loading tests resulting in a maximum loading force (at 20% diameter reduction) of 5N, rapidly dropping to a 0.5N when the force is removed, after which it 'slowly' returns to its initial diameter and zero outward pressure is measured.⁷⁸ Therefore, the calculated 1.75N might be too high, most likely due to the linear elastic assumption which overestimates the amount of stress required to strain the stent.

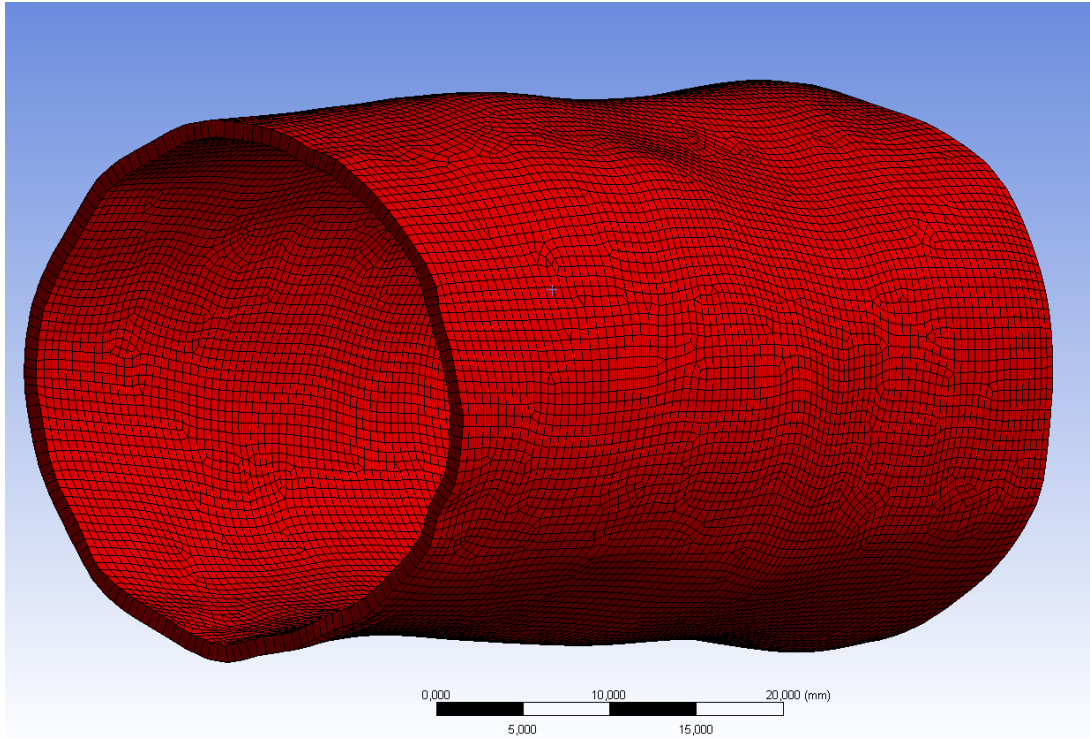
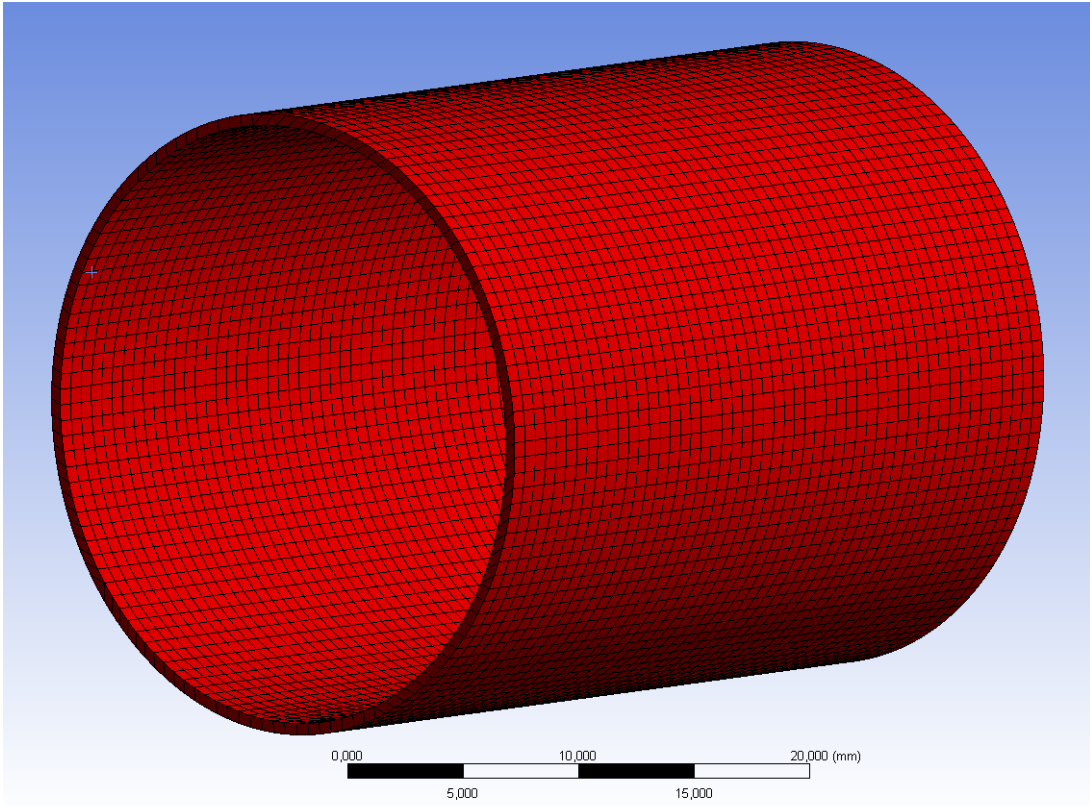
The N/m² (i.e. Pa) can also be calculated in order to compare with other stent grafts. The total length of the stent is 237.14mm its width is 0.2mm.

$$P_{net,outward} = \frac{1.75}{237.14 \times 0.2} \times 10^6 = 3.69 \times 10^4 Pa = 36.9 kPa = 276 mmHg$$

Which is outside the normal range of blood pressure in the aorta (10-16 kPa; 80-120 mmHg), likely due to the linear elastic assumption. Though it might overstress the vascular wall, however, it might also indicate a proper seal.

SET-UP OF ANSYS

Ansyes is a finite elements analysis program allowing for a variety of simulations. For this purpose, a static structural analysis was chosen, this allow for stresses and strains to be measured in the simulated bodies. This type requires bodies (stents and aortic necks), materials (formulations and properties), boundary conditions to work within, and forces/displacements to simulate. In the set-up of the static structural analysis three vessel walls are used to mimic the aortic neck, of which the latter two in Figure 22 are derived from patient scans.



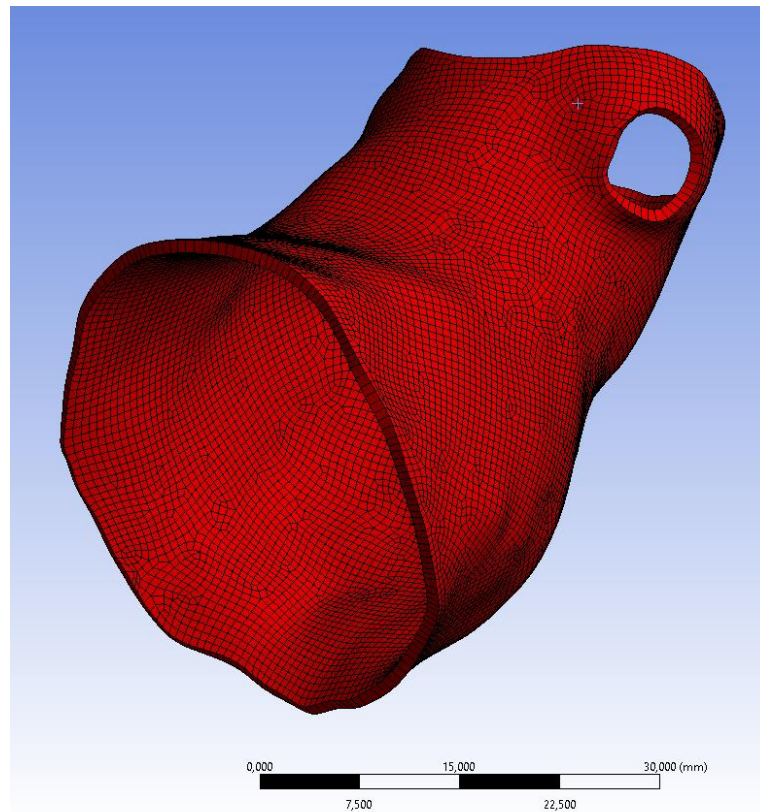


Figure 22: Aortic necks; on the top an artificial straight tube for direct comparison (diameter 26 mm), in the middle a straight anatomical shape (around 30 mm diameter). On the bottom, a conical shape with a varying diameter of 26-32 mm. All with a wall thickness of 1 mm. The latter two are derived from patient scans.

Based upon literature material descriptions were chosen for the aortic wall and nitinol stent, these descriptions assume simplified behaviour. In those studies, the material models were verified with experiments. For the aortic wall, a 3rd order polynomial description was chosen. Which results in non-linear hyper-elastic isotropic behaviour.⁸⁹ Whereas the aortic wall in fact is anisotropic it is assumed isotropic to simplify the simulation, thereby only influenced by circumferential compliance. Which is in line with the statement of Boron and Boulpaep concerning sole influence by circumferential compliance.⁵⁸ This polynomial approach does approximate the aortic wall in its circumferential compliant behaviour according to Zhao et al., however, they added the intima and adventitia layers as well, which have been left out in this simulation.⁸⁹

Nitinol has difficult behaviour to simulate, Ansys does have a shape memory algorithm, however, this is computationally more demanding. Therefore, an elastoplastic behaviour description was chosen to approximate the super elastic characteristic of nitinol. Demanget et al. validated this with experiments, they used material properties from the experiments of Kleinstreuer et al.^{85,90}

Table 4: Material properties of nitinol and aortic wall.^{85,89}

Nitinol, material properties					
Austenite elasticity (MPa)		40,000	Martensite elasticity (MPa)		18,554
Austenite Poisson's ratio		0.46	Martensite Poisson's ratio		0.46
Start of transformation loading (MPa)		390	End of transformation loading (MPa)		425
Aortic wall, material properties					
Artery, layer: media;	C ₁₀ (MPa)	0.03828	C ₂₀ (MPa)	0.01885	C ₃₀ (Mpa)
					0.02067

Ansys also offers a super elasticity material description, however, this description is not yet compatible with beam elements. Beam elements are used, to mesh the stents, due their short computation times when compared to 'standard' solid elements. Similar reasoning applies to shell elements versus 'standard' solid elements, which are used to mesh the aortic neck.

In the set-up of the simulations a static structural analysis is chosen wherein the geometry is loaded into SpaceClaim (a design modeler from Ansys) that allows for initial set-up of the required bodies (see for an example Figure 25). Thereafter Ansys Mechanical is used to describe the steps the simulation must take which are summarized in the following two Figures 23 and 24.

The above-mentioned material models are verified performing two verification simulations. For the verification simulations, similar steps are taken as for the main simulations. However, without the expansion step since it is only necessary to measure the crushing force required, furthermore, only two crushing plates are used orthogonal to and on either side of the two diamond shaped cells (see Figure 28 in Chapter 6).

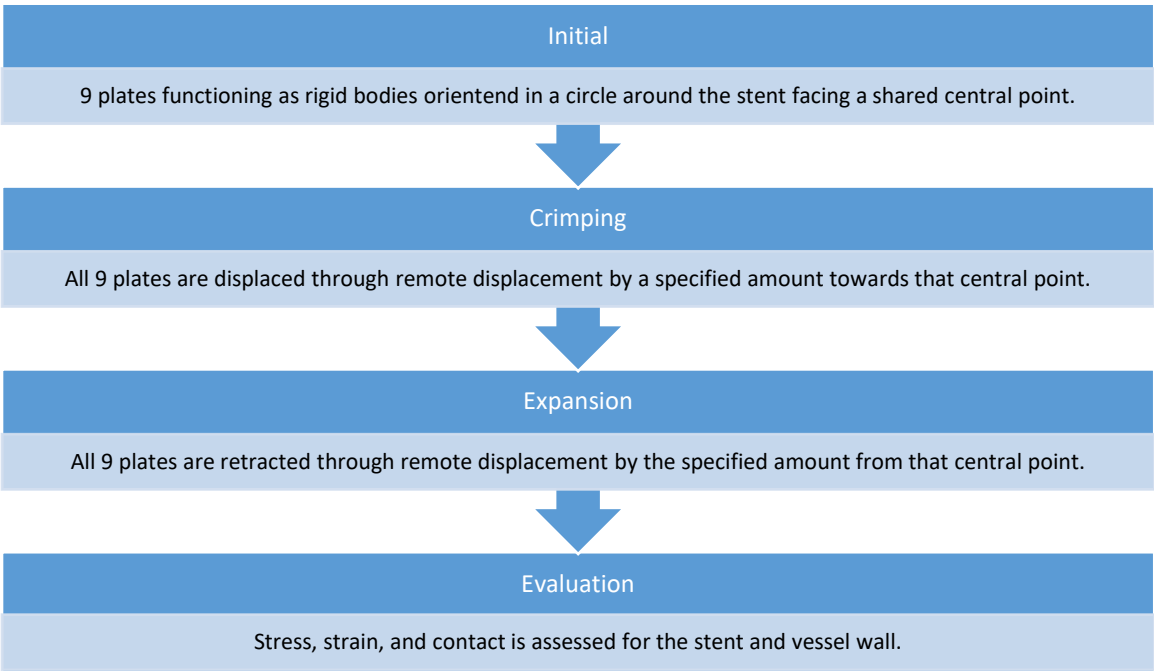


Figure 23: Stent crimping without aortic neck.

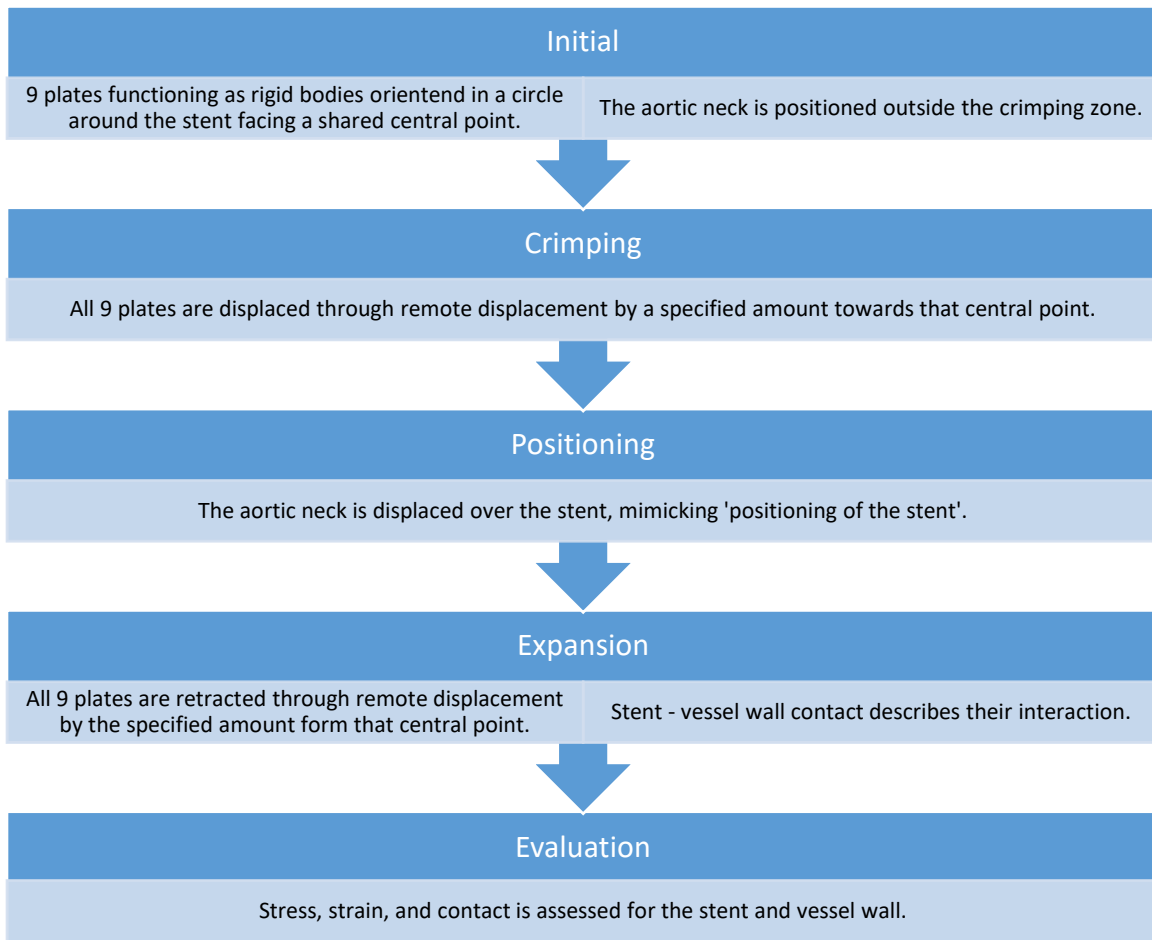


Figure 24: Stent crimping with aortic neck.

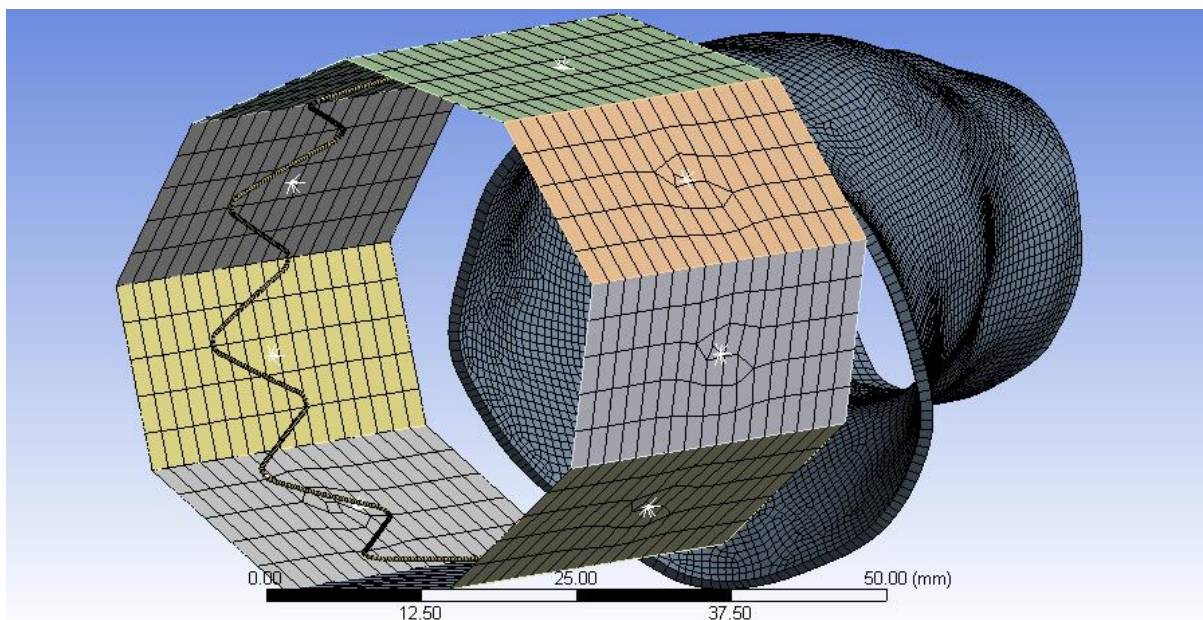


Figure 25: The initial set up for a simulation, in this case a straight z-shape stent with a conical aortic neck.

In Figure 25 the initial set up for a simulation can be seen. This set up allows, as a first step, to crimp the stent to the required diameter. Followed by displacement of the aortic wall to mimic the positioning of the stent;

performing this with the aortic wall was computationally more advantageous due to the relative simple geometry of the aortic neck, the results are similar.

Two contact regions are defined: the stent with the rigid body (plates) and the stent with the aortic wall. Both contact are frictional contacts. This aids in stabilizing the simulation. Furthermore, the stent-rigid plate contact description uses a Newton-Rhapson approach thereby updating the stiffness matrix at each equilibrium iteration. Per iteration it converges to an equilibrium (i.e. solution) for the current problem, after a few iterations it finds that solution and moves on to the next problem with an updated stiffness matrix based upon the previous solution. The stent-aortic neck contact description uses a direct solver approach, which eliminates equations instead of finding solution in an iterative fashion. Direct elimination requires the factorization of an initial very sparse linear system of equations into a lower triangular matrix followed by forward and backward substitution using this triangular system.

The stent/ rigid plate contact is divided into 9 contact regions for the plates each require their own contact description. The contact settings are similar for all the stent / rigid plate contact descriptions, see table 5.

Table 5: Table from the Ansys Mechanical window showing the set-up values for the stent / rigid plate contact.

Definition	
Type	Frictional
<input type="checkbox"/> Friction Coefficient	0.2
Scope Mode	Manual
Trim Contact	Off
Suppressed	No
Advanced	
Formulation	Program Controlled
Elastic Slip Tolerance	Program Controlled
Normal Stiffness	Manual
Normal Stiffness Factor	0.8
Update Stiffness	Each Iteration, Aggressive
Stabilization Damping Factor	2.
Pinball Region	Radius
Pinball Radius	0.35 mm
Time Step Controls	None
Geometric Modification	
Interface Treatment	Add Offset, No Ramping
<input type="checkbox"/> Offset	0.2 mm
Target Geometry Correction	None

The stent / aortic wall description consists of one contact description with all the inner faces of the aortic wall as contact and the stent as target, see table 6. A normal Lagrange formulation is chosen to force the stent and aortic wall to have contact compatibility without any contact penetration. Other formulations allow for contact penetration which causes the simulation to not-converge due to a too large penetration depth.

Table 6: Table from the Ansys Mechanical window showing the set-up values for the stent / aortic wall contact. Note the friction coefficient changes per simulation depending on the required stability, the range is from 0.05 to 0.4.

Target Shell Face	Bottom
Shell Thickness Effect	No
Definition	
Type	Frictional
<input type="checkbox"/> Friction Coefficient	0.2
Scope Mode	Manual
Trim Contact	Off
Suppressed	No
Advanced	
Formulation	Normal Lagrange
Elastic Slip Tolerance	Program Controlled
Stabilization Damping Factor	2.
Pinball Region	Radius
Pinball Radius	0.25 mm
Time Step Controls	None
Geometric Modification	
Interface Treatment	Adjust to Touch
Target Geometry Correction	None

The stent, rigid plates and aortic wall are all meshed sizing them accordingly to obtain proper aspect ratios of the elements. Quality is determined based upon the aspect ratios, quality of at least 0.5 is required. Therefore, quads are employed as much as possible. Quads often offer a good aspect ratio when the element size is chosen correctly for the body being meshed. However, a trade-off was made between the maximum allowed elements and nodes (including both mesh and contact created nodes and elements) and the quality of the mesh.

Table 7: the number of elements and their quality per model.

Body	Size of elements	Number of elements / Nodes	
Plates / rigid bodies (9 in total)	2.5mm	1035 (115 per plate)	3546 (394 per plate)
Aortic wall (shell elements)			
Conical	0.7mm	8209	8331
Straight	0.7mm	9893	10004
Tube	0.55mm	11096	11248
Stent (beam elements)			
Z-shape	0.3mm	782	1566
Fishmouth	0.3mm	304	608

In order to stabilize the simulation, ensuring the bodies do not move all over the place, boundary conditions and constraints are added. For the rigid plates, a remote displacement was chosen to move the plates in- and outwards. The stent and aortic wall were constrained with nodal displacements and orientations (often with one node). This restrained the stent to be allowed only to change in the radial x-direction. For the aortic wall the same restriction applied, however, a nodal displacement in the z-direction was added to simulate the movement of the aortic wall over the stent (this displacement varied per simulation) and constraint further movement after displacement.

Since this simulation is difficult a manual determination of sub steps was chosen. Initial sub steps were set at 20 with a minimal amount of 5 sub steps and a maximum amount of 5000 sub steps. Results are gathered for both the stent and the aortic wall as well as their contact. These results consist of images and data per time step wherein the maximum principal strain and equivalent von-Mises stress are shown and compared. Normal and

personalized z-shape and fishmouth stents in straight, anatomical straight and anatomical conical aortic necks are compared to acquire insight into the effect of personalized stents.

6. EVALUATION AND RECOMMENDATIONS

In this chapter, the results from the simulations are shown. The figures showing maximum principle elastic strain or equivalent (von-Mises) stress in stents or aortic necks have a colour coding legend wherein red is the maximum encountered value in the measured object and blue is the lowest encountered value.

VERIFICATION TESTS

Two verification tests were performed, first a single ring of diamond shaped cells undergoing a 100mmHg (13.3 kPa) pressure from inside out (Figure 26 and 27). Secondly two diamond shaped cells were subjected to two crushing plates on either side of the cells as can be seen in Figure 28. The maximum principal elastic strain and equivalent stress (von-Mises) were measured (Figure 29 and 30).

Verification test 1

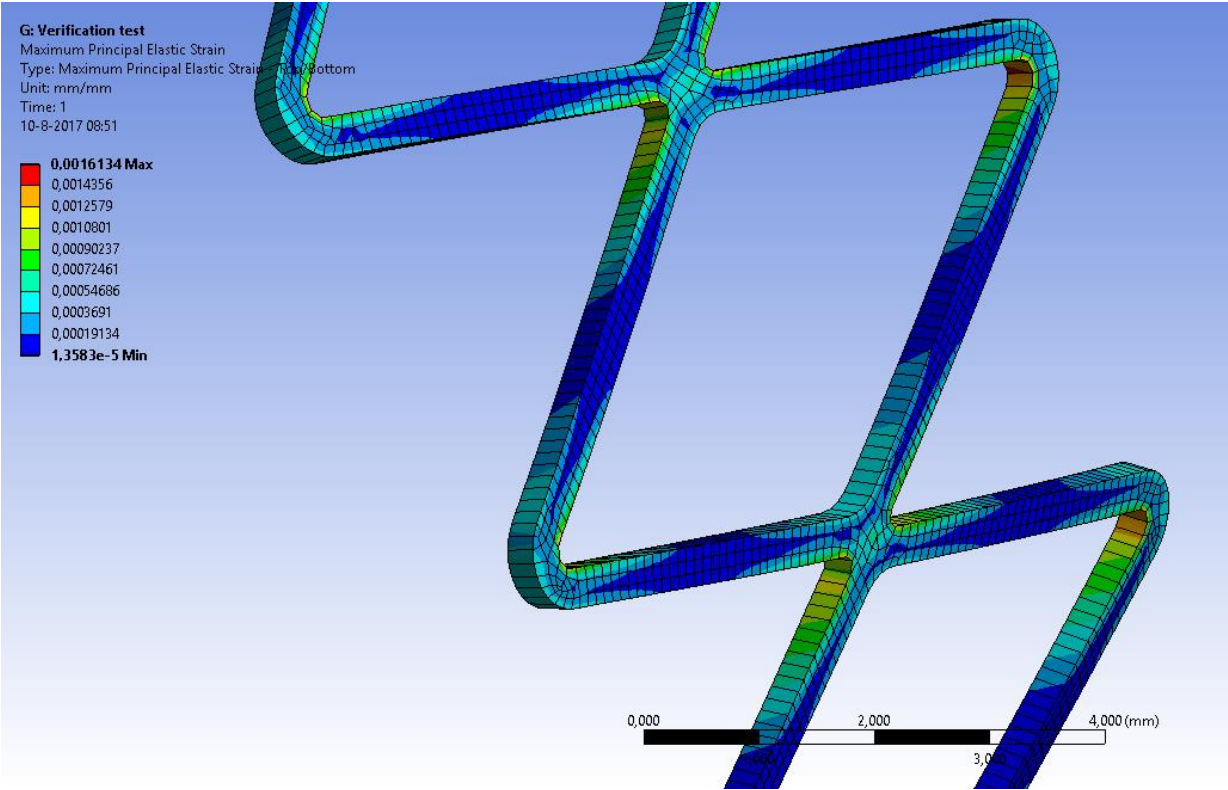


Figure 26: The maximum principal elastic strain of a diamond cell geometry with a 100mmHg pressure pushing from inside out, reaching a maximum of 1.6×10^{-3} mm/mm. Note the red areas inside the cell at the points and at the connection points on the outside of the stent, indicating the highest encountered strain. The middle areas of the struts are showing little to no strain (blue).

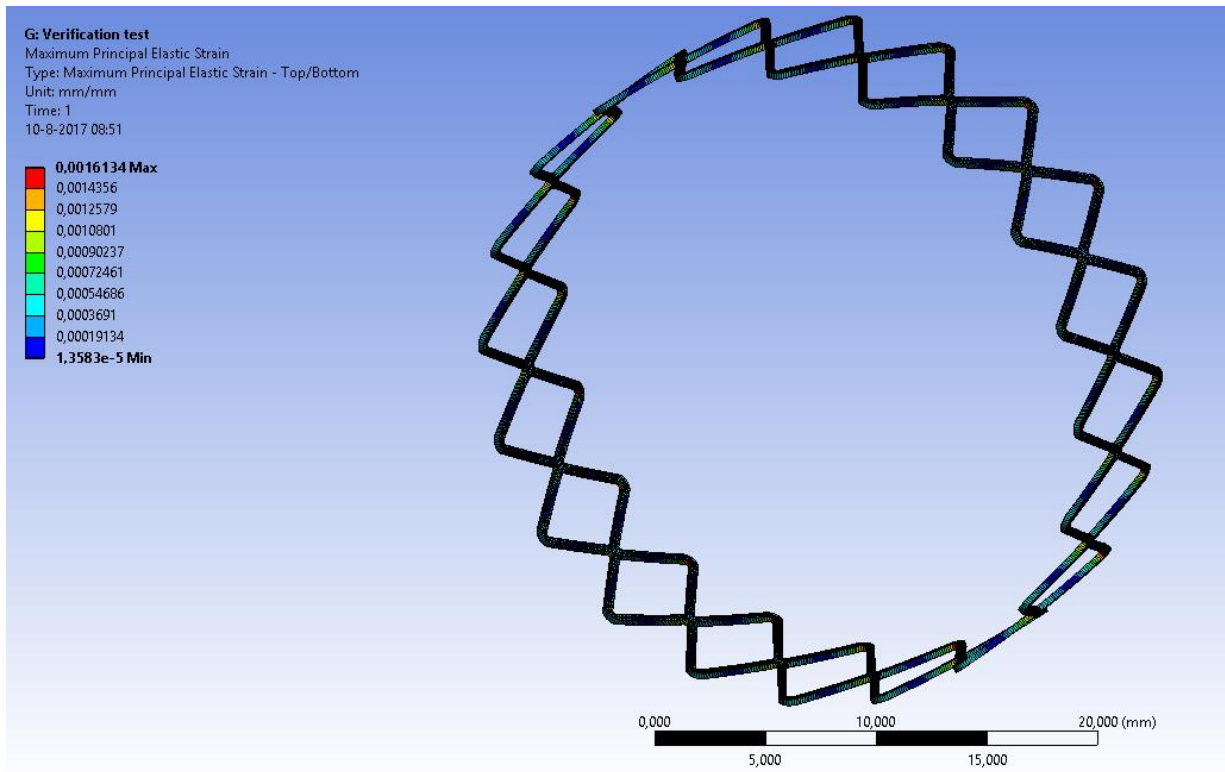


Figure 27: The maximum principal elastic strain of the same diamond cell geometry and simulation (Figure 26) in full view.

Verification test 2

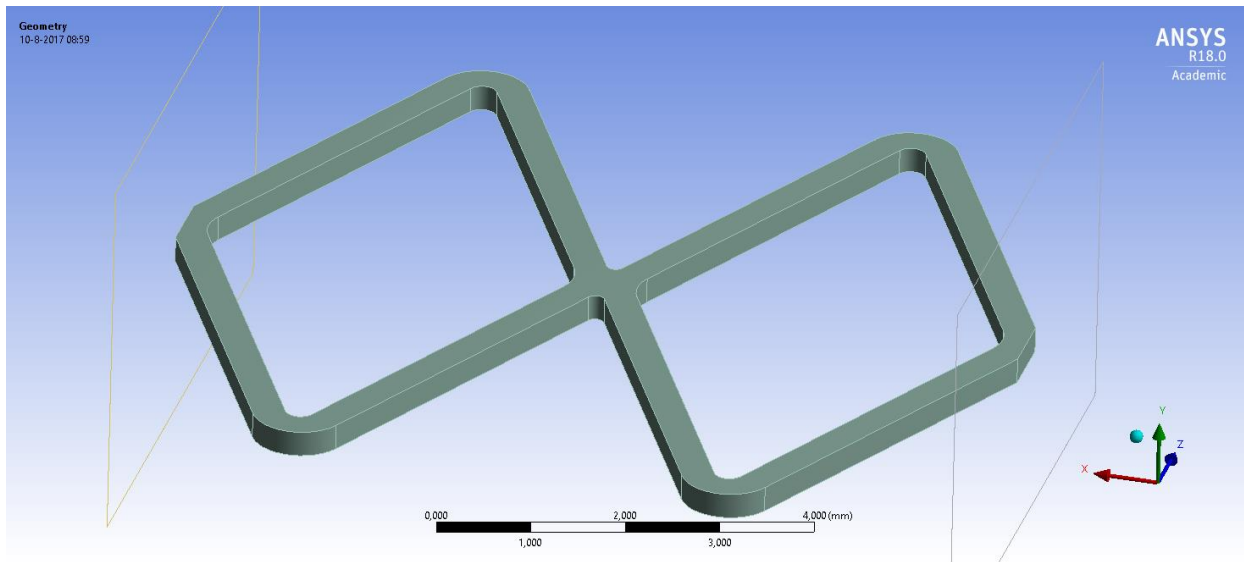


Figure 28: The initial set-up for the double diamond cell crushing test. Showing in grey the double diamond cell and on either side the transparent plates for crushing the stent. (black and white scale bar below indicating: 0-4 mm)

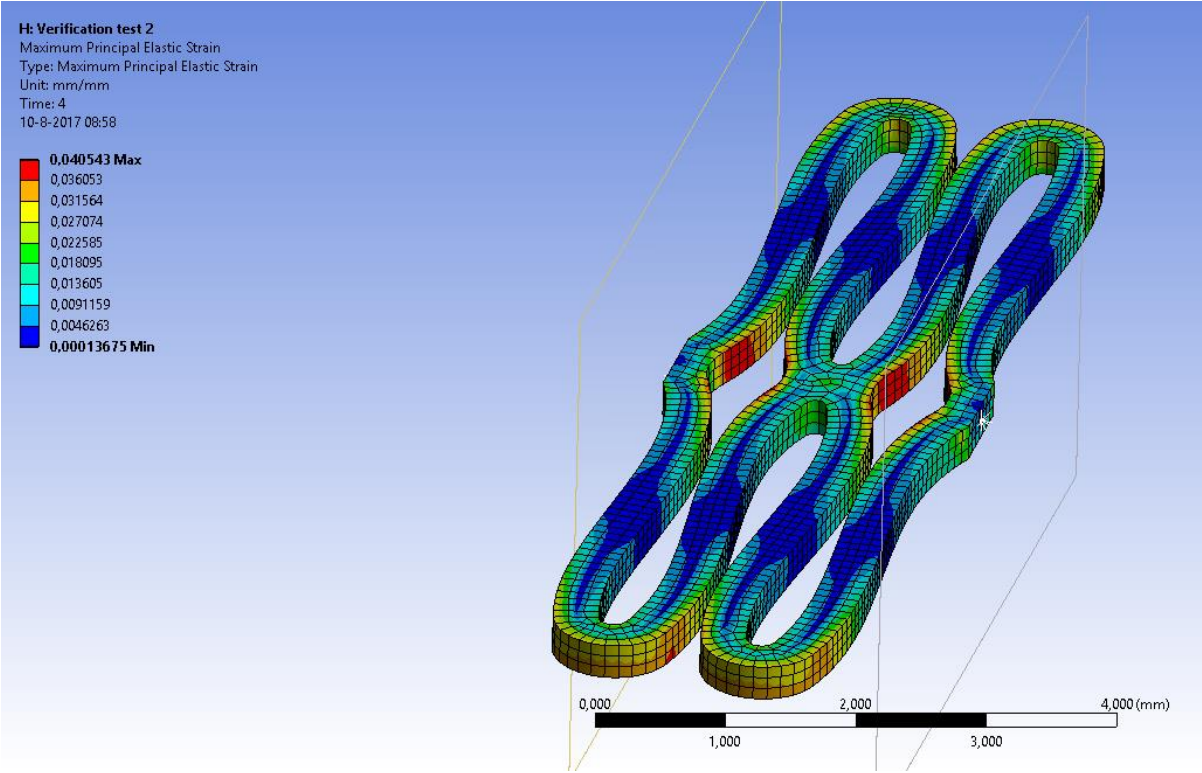


Figure 29: The maximum principal elastic strain for a completed crushing test of the double diamond cell., reaching a maximum of 4.05×10^{-2} mm/mm. The highest strain is encountered on the inside of the stent at the connection points with the other cells. The points of the double diamond cell have medium-high strain (yellow-orange). The middle areas of the struts are showing little to no strain (blue)

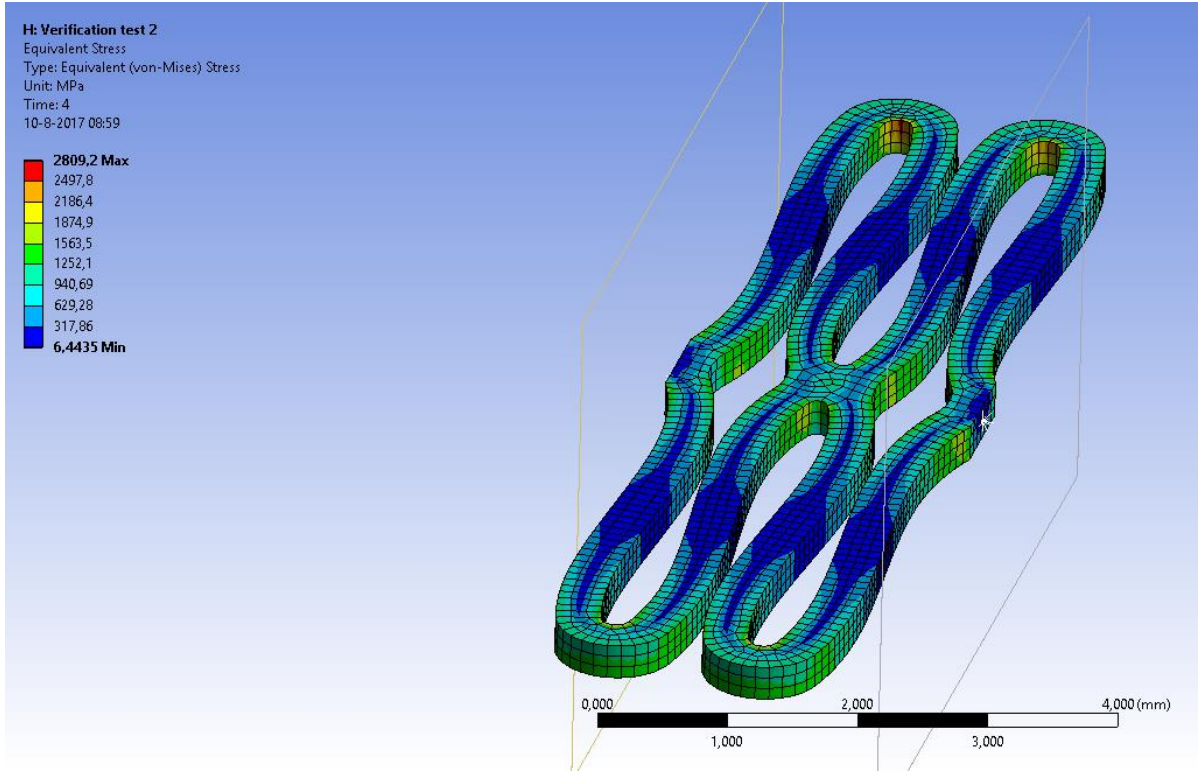


Figure 30: The equivalent stress (von-Mises) for a completed crushing test of the double diamond cell, reaching a maximum of 2.81 GPa. The highest stress is encountered at the points on the inside. The middle areas of the struts are showing little to no strain (blue)

ANATOMICAL CONICAL – STRAIGHT VERSUS PERSONALIZED STENT

The straight and personalized z-shape stent (Figure 14 and 15) were crushed with the 9 rigid plates (as seen in Figure 25) and inserted into the conical vessel, subsequently it was released after which it reached an equilibrium with the vessel wall. The results from that equilibrium are found in Figure 31 - 37. The maximum principal strain and equivalent (von-Mises) stress were evaluated.

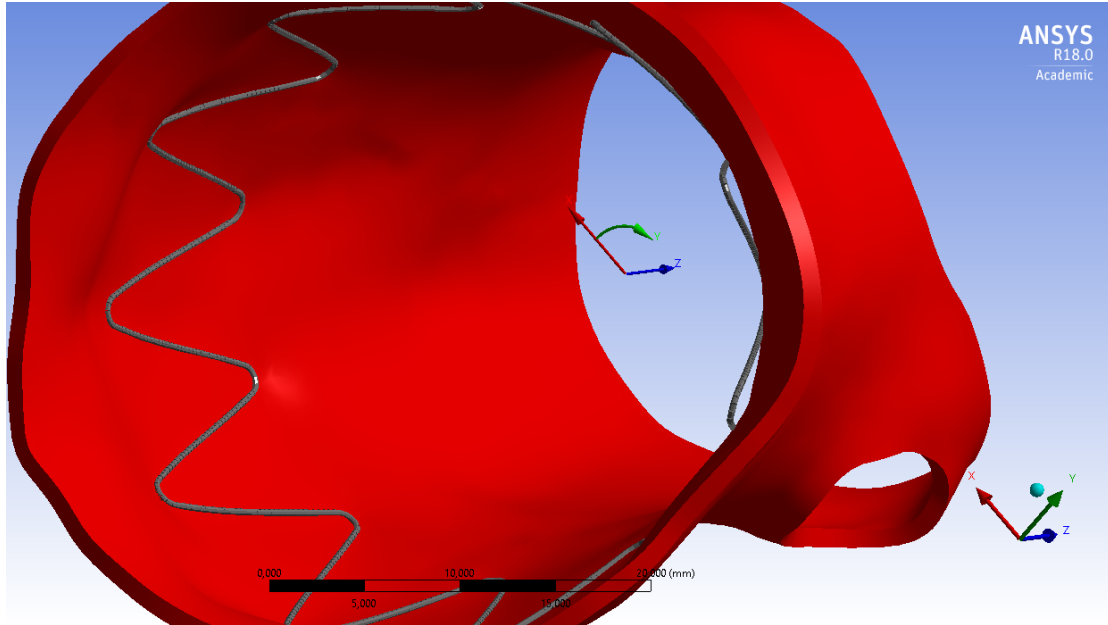


Figure 31: An image without measurements of the end equilibrium stage of the conical neck with a straight z-shape stent, note the stent conforms to the anatomy of the aorta.

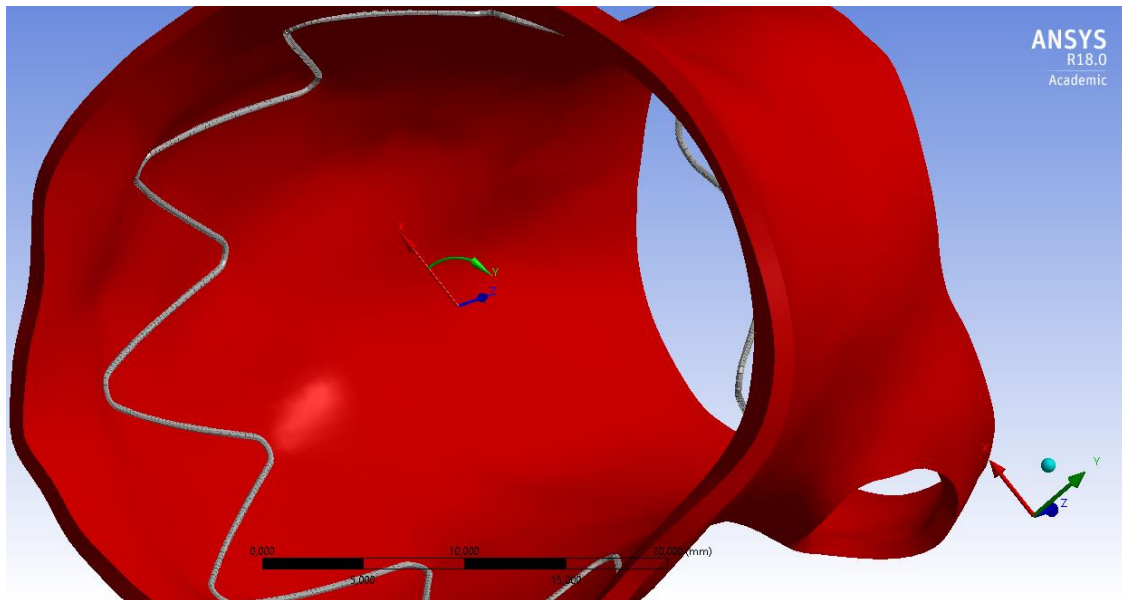


Figure 32: An image without measurements of the end equilibrium stage of the conical neck with a personalized z-shape stent, note the stent conforms to the anatomy of the aorta.

Important to note in Figure 31 and 32 is the conformability of both stents to the aortic neck, as well as some points of the z-shape sticking out into the lumen, though visually they do not seem to differ after deployment.

In the following two figures, the conformability of the straight and personalized stent to the conical neck is shown.

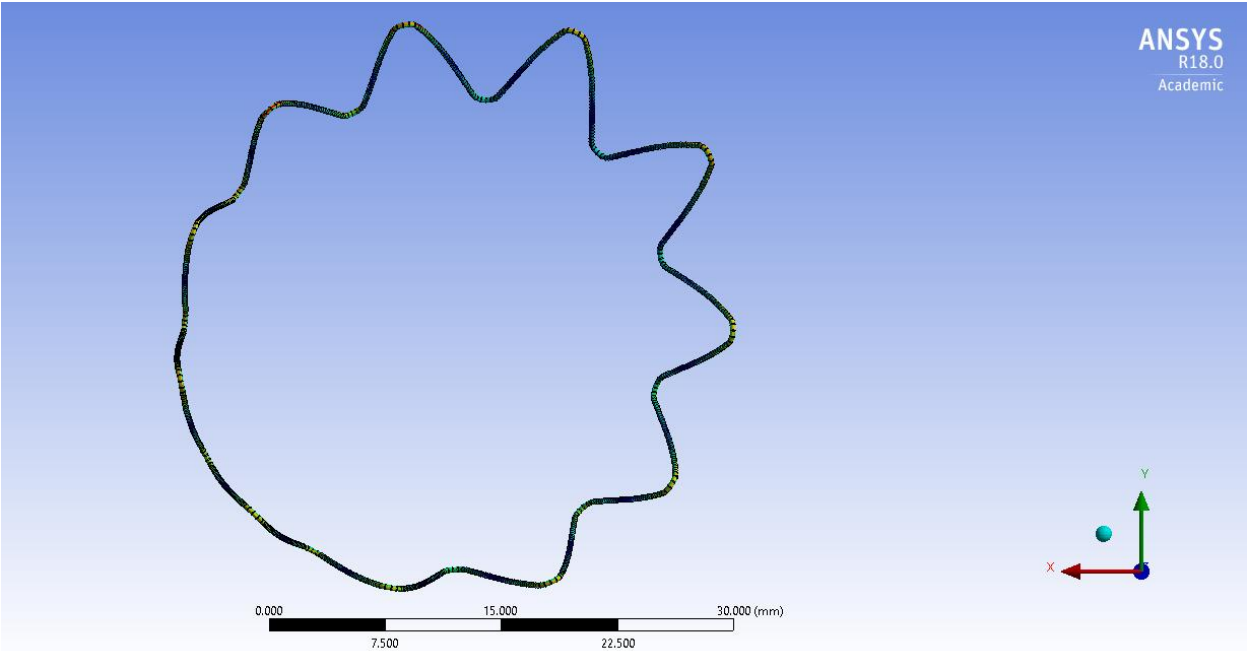


Figure 33: the straight stent deployed in a conical neck results in deformation of the stent after conforming to the aortic neck. On the top and right it follows the conical shape, on the left it follows the straighter part of the neck.

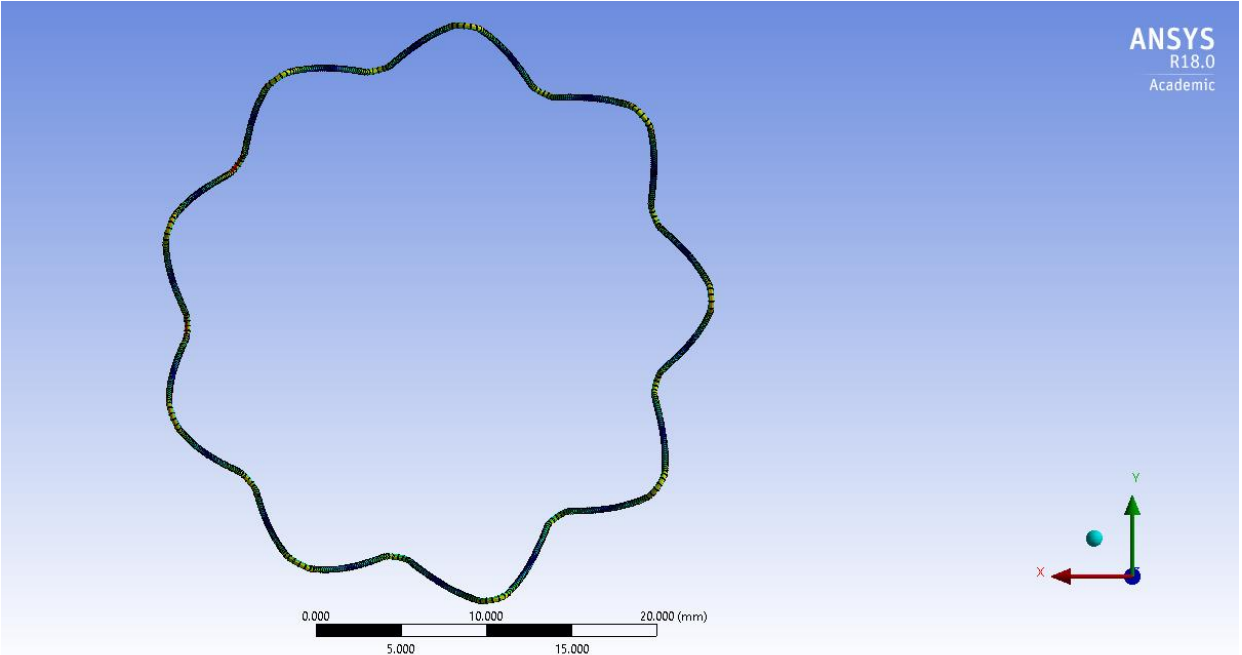


Figure 34: the personalized stent deployed in a conical neck results in little visible deformation after conforming to the aortic neck.

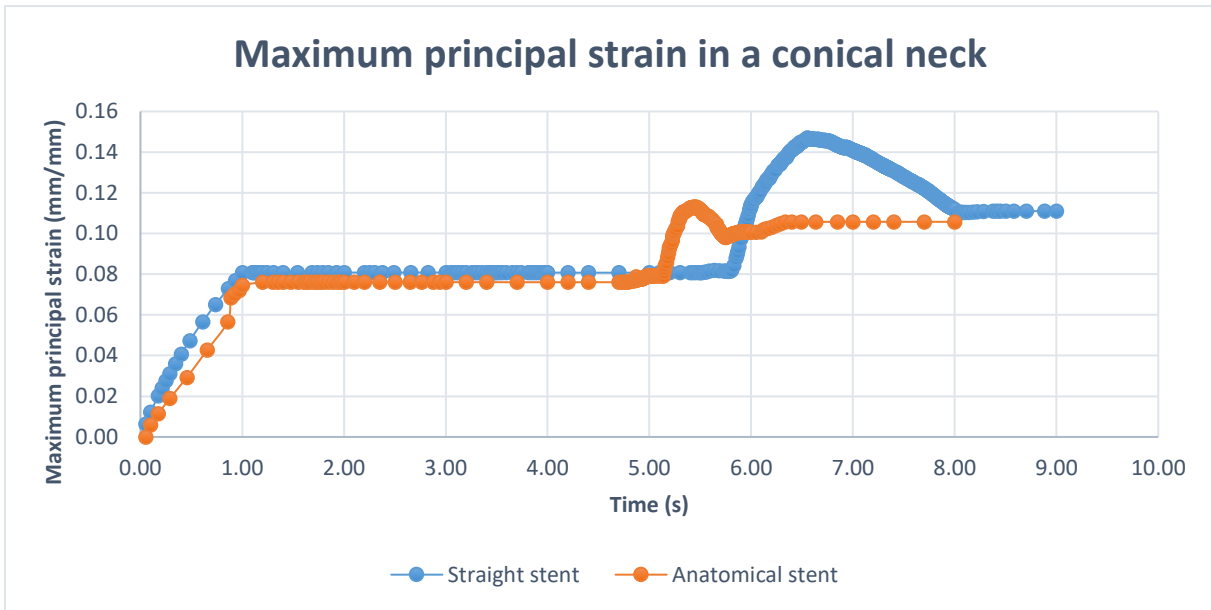


Figure 35: A graph comparing the maximum principal strains in the conical neck caused by the straight and anatomical z-shape stent.

In Figure 33 the strain of the aortic neck is measured. The first second increase is the angio-tension force enacted on one end of the aortic neck. The flat part of the graph is the crushing of the stent as well as the movement of the aortic neck over the stent, which has no effect on the strain. Thereafter the stent is deployed, which increases the strain in the neck, until it finds an equilibrium at the end. Note the peak in the amount of strain for both straight and personalized stent, as well as the almost equal equilibrium end points.

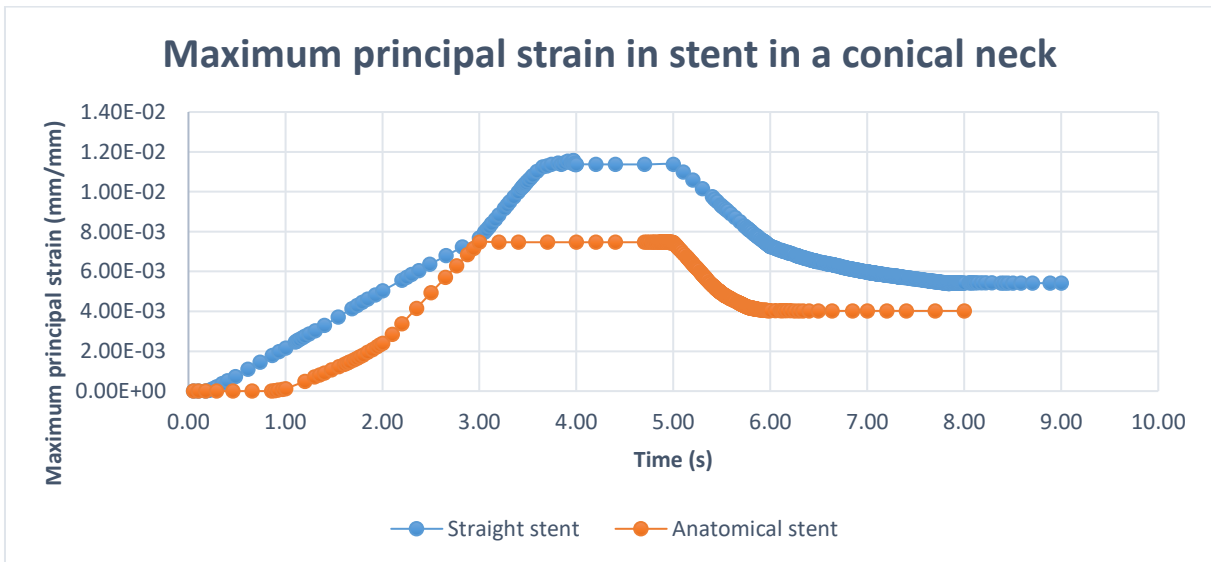


Figure 36: A graph comparing the maximum principal strains of the straight z-shape stent with that of the anatomical z-shape stent, in a conical neck.

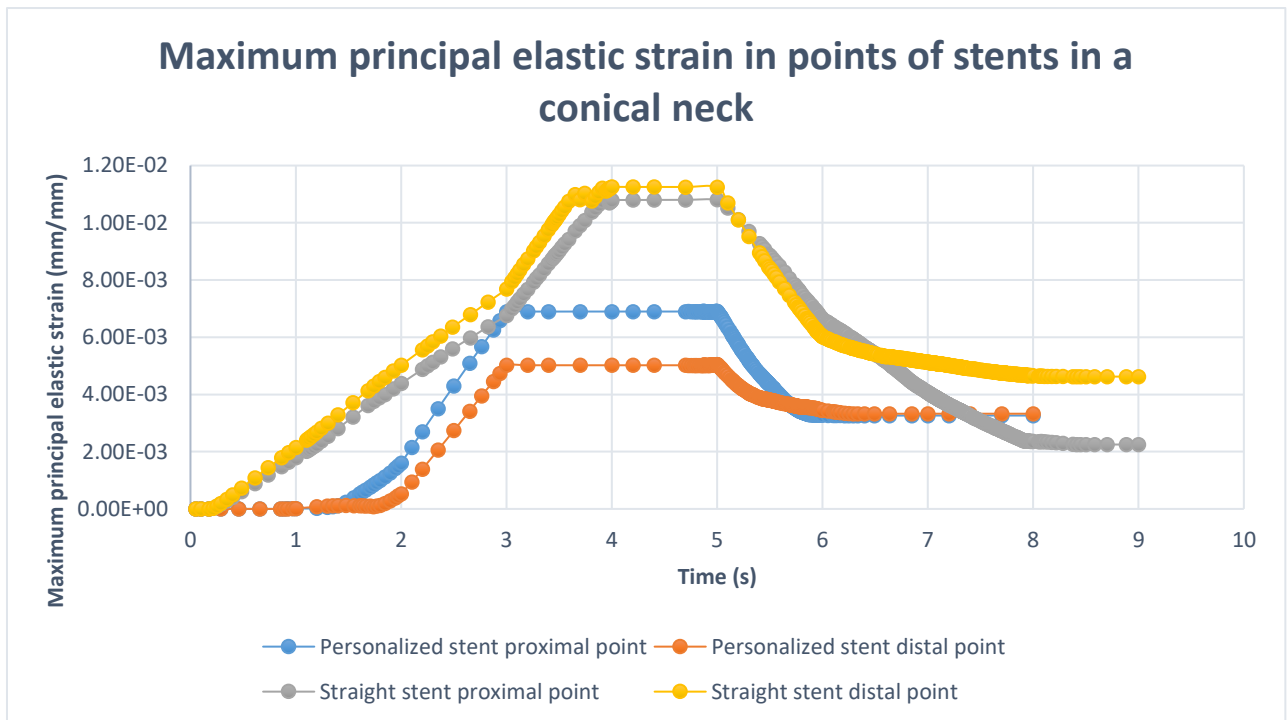


Figure 37: The maximum principal elastic strain measured in one of the proximal points of the straight and personalized stent deployed in a conical neck.

In both graphs (Figure 34 and 35) the crushing and deployment process of the stent can be seen; the initial increase of strain in the first three to four seconds, the flattened part of the graph where the aortic neck is moved over the stent in the fourth and fifth second, and finally the deployment of the stent in the vessel finding an equilibrium. Important to note in Figure 35 is the difference between the proximal and distal point of the straight stent, whereas the personalized stent has no difference between those two points at the moment of equilibrium. Noteworthy as well is during movement of the aortic neck the difference in strain, of the proximal and distal points of the personalized stent.

Of all these graphs, their stress equivalents can be found in Appendix 9.2, as well as the whole-body view of the stents and aortic necks. All showing similar results as shown here.

STRAIGHT TUBE – STRAIGHT Z-SHAPE STENT

The straight Z-shape ring (Figure 15) was crushed with the 9 rigid plates (as seen in Figure 25) and inserted into the vessel, subsequently it was released after which it reached an equilibrium with the vessel wall. The results from that equilibrium are found in Figure 38 and 39. The maximum principal strain and equivalent (von-Mises) stress were evaluated.

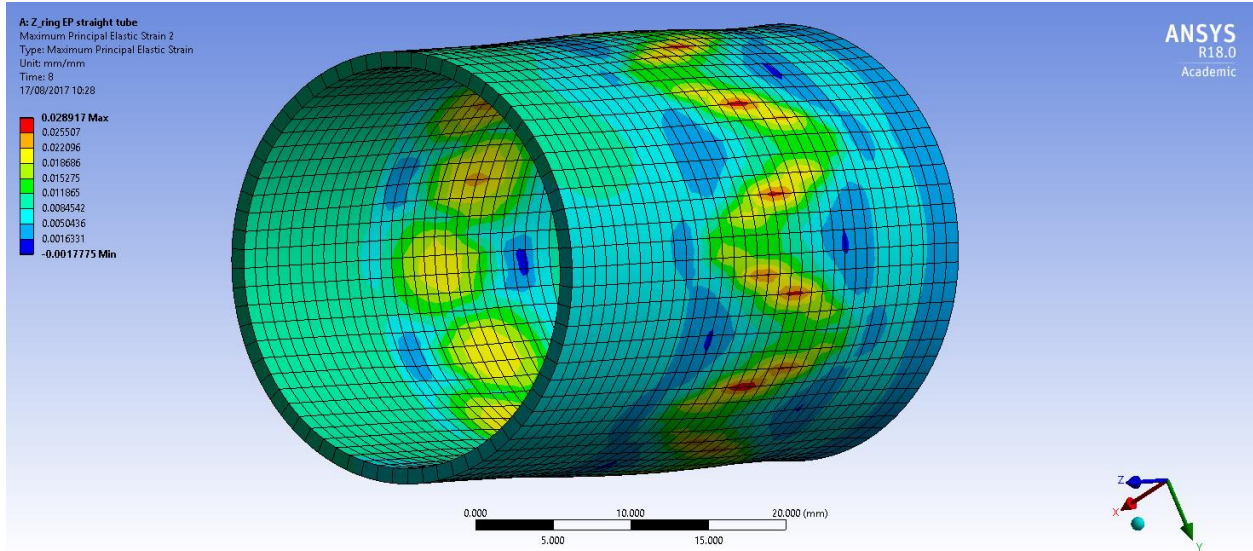


Figure 38: Maximum principal elastic strain of a z-shape stent in a straight tube, reaching a maximum of 2.89×10^{-2} mm/mm. The highest strains are encountered along the z-shape of the stent, where the centre with direct contact has the most (red) and the area around it has one level lower (orange) and so on, forming a 'hill'.

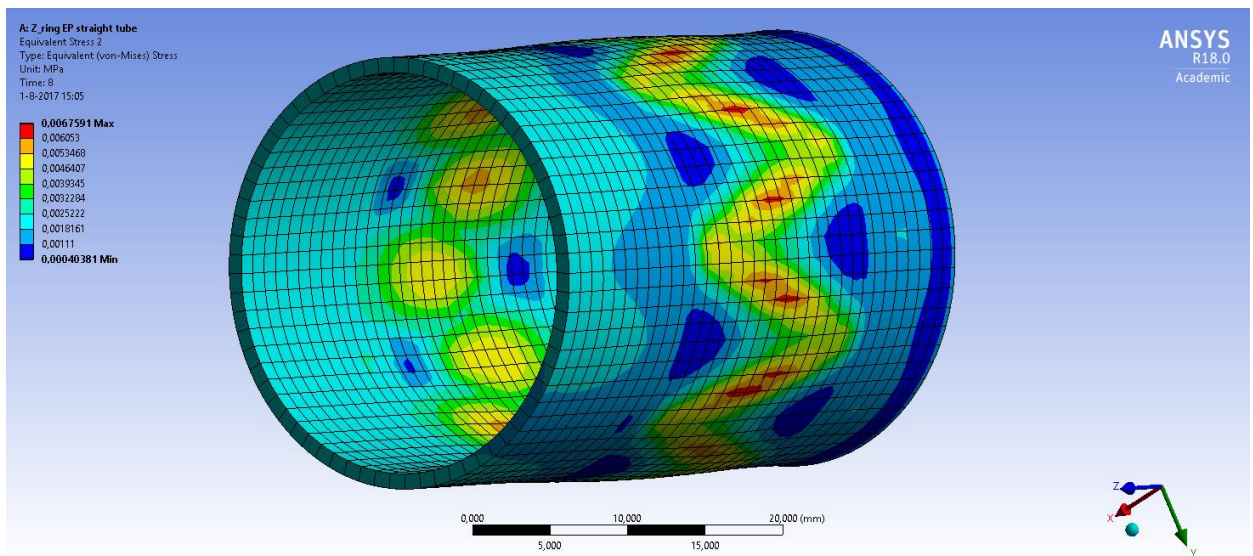


Figure 39: Equivalent (von-Mises) stress of a z-shape stent in a straight tube with aortic wall characteristics in units of MPa, reaching a maximum of 6.76×10^{-3} MPa. The highest stresses are encountered along the z-shape of the stent, where the centre with direct contact has the most (red) and the area around it has one level lower (orange) and so on, forming a 'hill'. Note that the points of the stent (yellow / green) have lower stress values than the centres (red areas) of the struts do.

Note in both figures the area over which the stent divides its outward force, also indicated by the amount of green, yellow, and orange.

STRAIGHT TUBE – FISHMOUTH STENT

The straight fishmouth ring (Figure 16) was crushed with the 9 rigid plates (as seen in Figure 25) and inserted into the vessel, subsequently it was released after which it tried to reach an equilibrium with the vessel wall. The results from that attempt at equilibrium are found in Figure 40 and 41. The maximum principal strain and equivalent (von-Mises) stress were evaluated at last converged time step of 6.44 s. This equates to about 50% deployment of the stent.

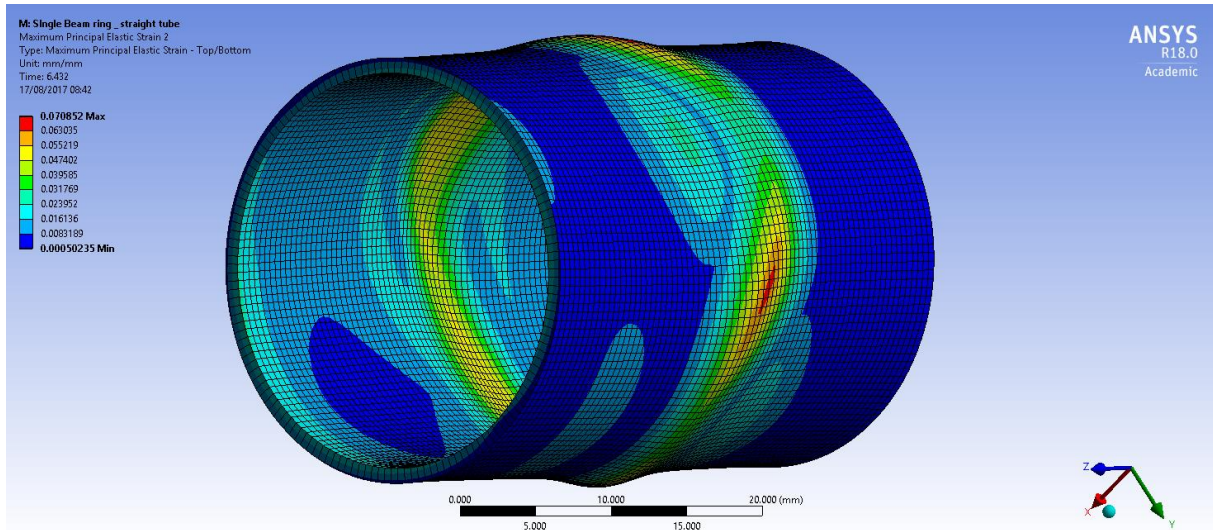


Figure 40: Maximum principal elastic strain of a fishmouth stent in a straight tube, reaching a maximum of 7.09×10^{-2} mm/mm. The highest strains are encountered on the corners of the fishmouth stent (red areas). Note the slope / hill around the stent pressing into the vessel wall.

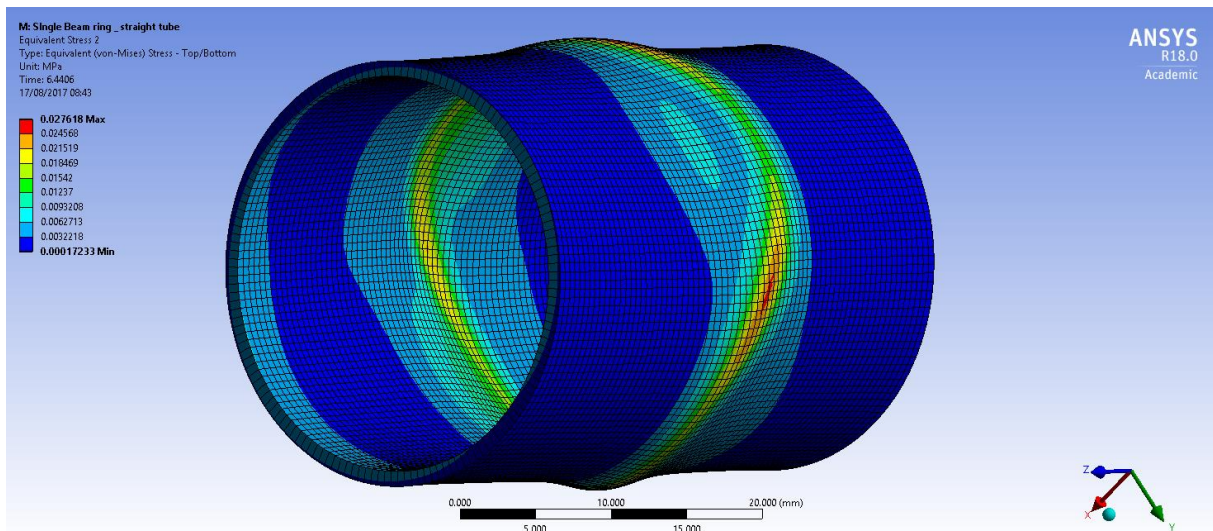


Figure 41: Equivalent (von-Mises) stress of a fishmouth stent in a straight tube, reaching a maximum of 2.76×10^{-2} MPa. The highest stresses are encountered on the corners of the fishmouth stent (red areas). Note the slope / hill around the stent pressing into the vessel wall.

Note in both figures the area over which the stent divides its outward force also, indicated by the higher peak strain. Also indicated by the amount of green, yellow, and orange.

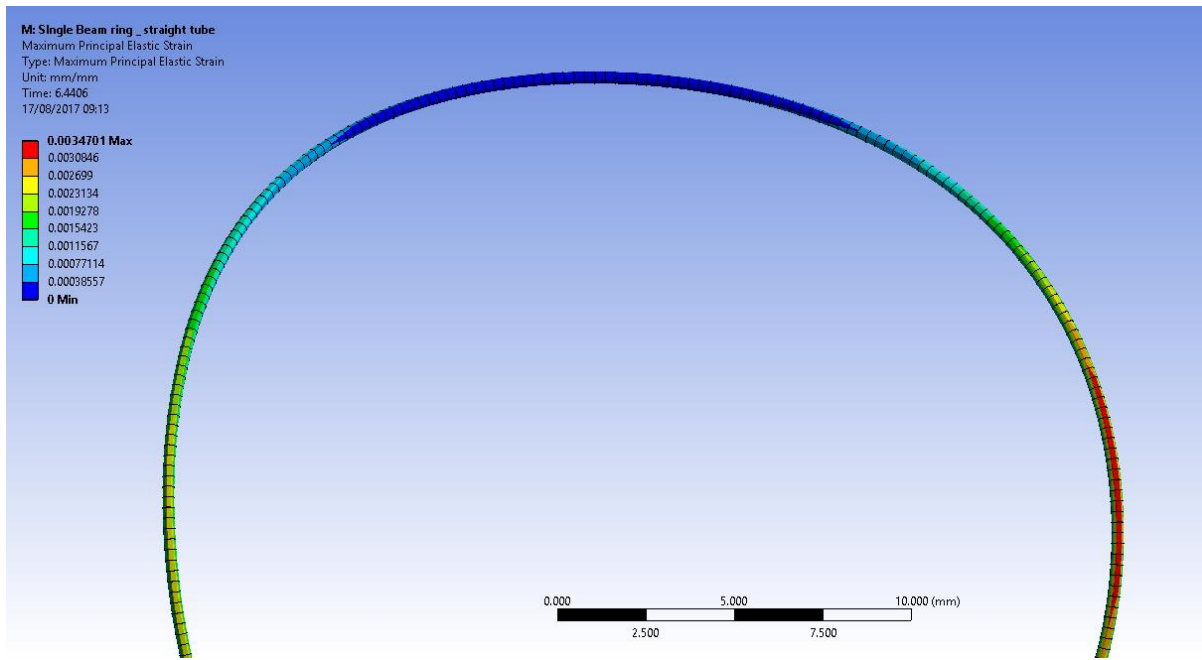


Figure 42: The maximum principal elastic strain in the fishmouth stent, not fully, deployed in a straight tube, reaching a maximum at 3.47×10^{-3} mm/mm. Note the highest strain is encountered on the side of the fishmouth stent (red/orange areas), whereas the top has apparently no strain (blue area) this strain is on the other side and of the same magnitude as visible on the side here.

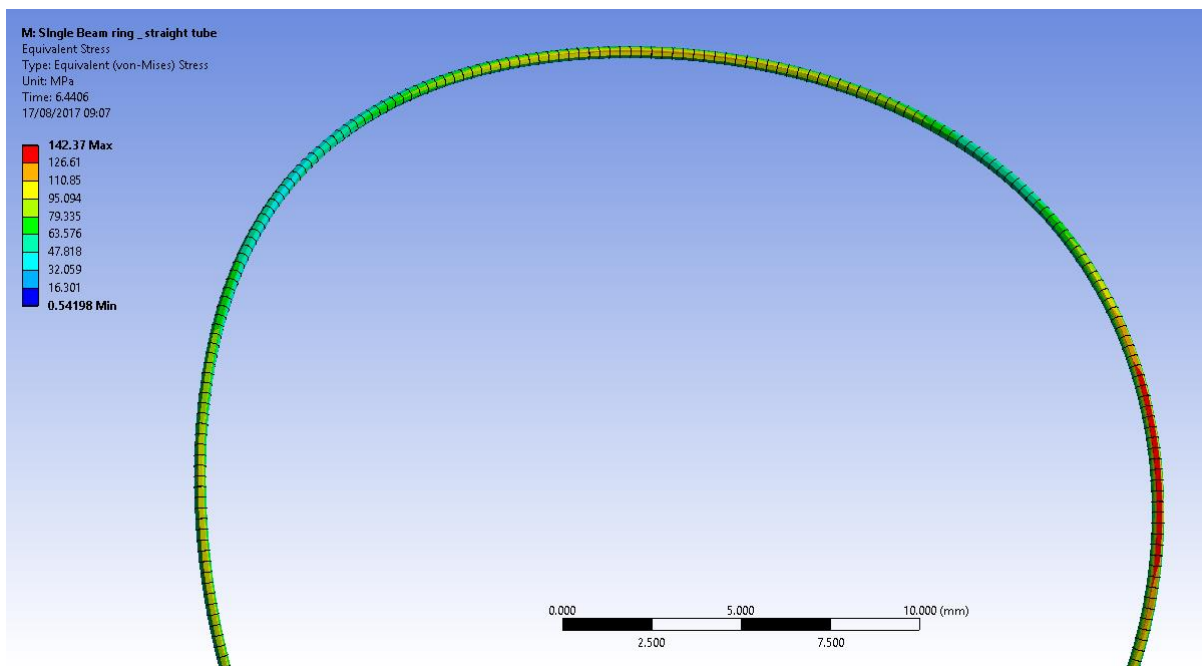


Figure 43: The equivalent (von-Mises) stress in the fishmouth stent, not fully, deployed in a straight tube, reaching a maximum at 142 MPa. Note the highest stress is encountered at the top and side of the stent (red / orange areas).

ANATOMICAL STRAIGHT NECK – STRAIGHT Z-SHAPE STENT

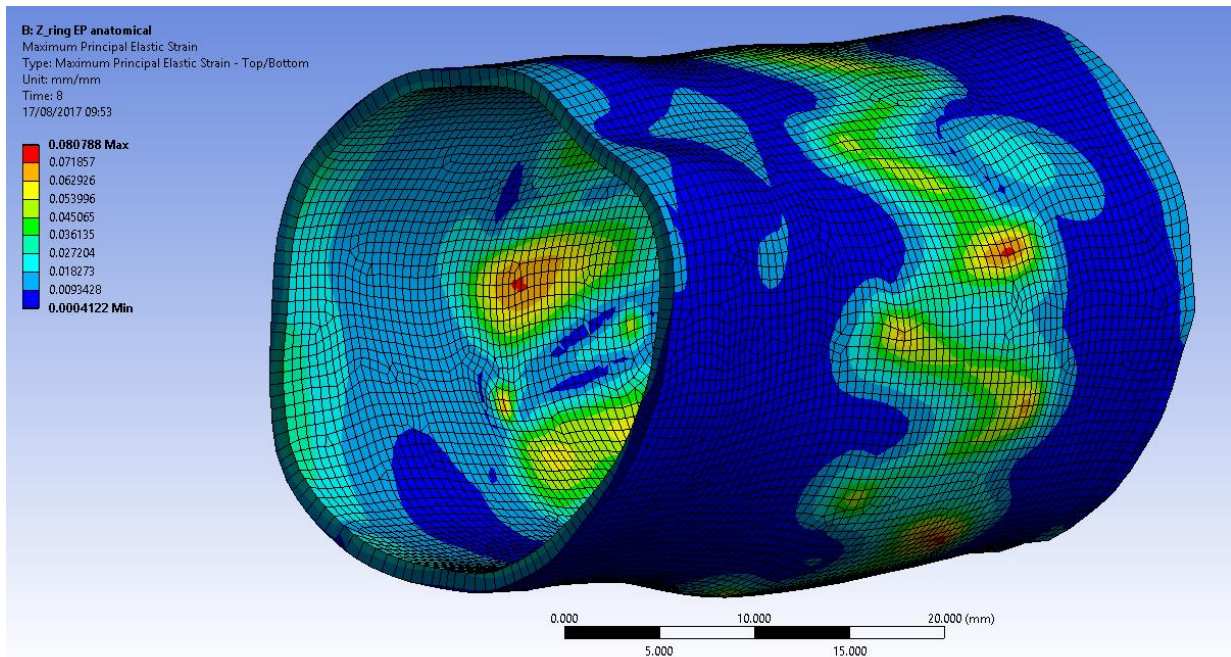


Figure 44: The maximum principal elastic strain in the anatomical straight neck due to a deployed straight z-shape stent, reaching a maximum at 8.08×10^{-2} mm/mm. Note the highest strain is found at the peaks of the z-shape stent, furthermore note the distribution of strain at mid-strut level of the z-shape stent.

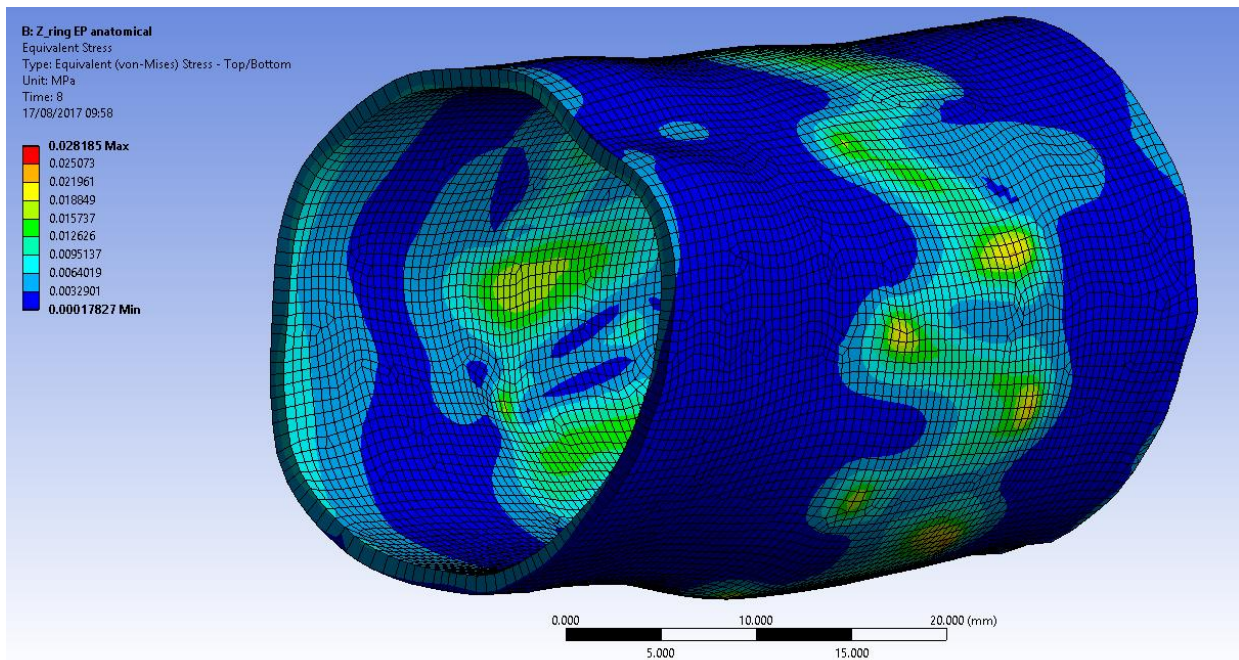


Figure 45: The equivalent (von-Mises) stress in the anatomical straight neck due to a deployed straight z-shape stent, reaching a maximum at 2.82×10^{-2} MPa. Note the highest stresses are encountered at the peaks of the z-shape stent. Furthermore, note the stress distribution at mid-strut level.

DISCUSSION

This research has investigated the effect of personalized stents versus straight stents. Additionally, it considered two different stent geometries most usable in 3D printing (the desired production process), the fishmouth and z-shape stent, in answering of the research question how to re-invent the personalized stent graft and its production process. It was found that personalized stents have a more equal distribution of strain (and stress) in the stent. And might thereby induce less stress and strain in the vascular wall, however current results show little change in the strain of the vascular wall. Despite the encountered differences between both stent geometries, superiority of one geometry over the other remains to be seen.

Verification

Both verification tests (Figures 26-30) showed comparable results to the study of Kleinstreuer et al., however, differences are present, most likely due to a variety in the geometry since the dimensions given did not match the nominal diameter they indicated to be using.⁸⁵ The two diamond cells were used to reproduce the crushing of the stent, a full ring was not possible due to a restriction in elements and nodes that can be used in the educational licence, however, the data is of the same magnitude and therefore most likely to match reality.

The z-shape stents in a conical neck (Figures 31 and 36) when compared to the final perioperative images of the EVAR procedure (Figure 9) show similar adaptable behaviour of the z-shape stent in following the morphology of the aortic neck, which is an indication that these simulations do approximate reality.

Straight versus personalized

The conformability of the straight and personalized z-shape stent in a conical neck is considered reasonable due to the stents having points of the z-shape sticking out into the lumen, where it should have full conformability to the aortic wall to create a larger seal (Figures 31-34). In the next design iteration, the stent should follow the aortic wall even more to prevent points of the stent sticking out into the lumen. If we look closer at Figures 33 and 34 the difference between deformation of the stents in conforming to the aortic wall is clear. The personalized stent is suited better to the conical neck than the straight stent, however, a similar conformation to the straighter part of the aortic neck on the left of the stent was expected, in a future iteration of the design this conformation needs to be included to create a better seal with the vessel wall. Thereafter a re-evaluation of the personalized stent is required.

The effect of the personalized stent can be seen in the graphs, a lower principal strain and equivalent stress in both the stent and the aortic neck (Figures 35 and 36). Though the difference is small for the aortic neck at the equilibrium stage, the maximum encountered stress is significantly lower for the aortic neck under influence of the personalized stent. This is a direct result of the personalized shape of the stent, ensuring the right amount of oversizing for each diameter in the aortic neck might therefore aid in reducing vascular wall stress. The peaks encountered in the graphs of Figure 35 are due to the elastic behaviour of the aortic wall. The stent expands quicker than the equilibrium with the vessel wall can set in, therefore an 'overshoot' happens thereafter the stent and vessel wall find their equilibrium due potential energy that is stored during the overshoot in the vessel wall pushing the stent back.

This personalized approach in oversizing affects the amount of strain (and stress) in the points of the stents (see Figure 37). At the distal points of the straight stent ring higher strains were found than at the proximal points, which might seem counterintuitive at first. Due to the straight geometry of the stent and the conical shape of the neck the distal part of the stent has more room to expand, thereby reducing the strain in the proximal points (see Figures 49-59 (in appendix 10.2) for stresses and body views). Furthermore, the difference in strain of the proximal and distal point of the personalized z-shape stent during aortic neck movement is due to the nominal diameter difference. The larger diameter (proximal point) has the higher strain (and stress) levels for the same reason as the straight stent at the equilibrium.

As stated in the beginning of this discussion the z-shape stent does approximate realistic behaviour, however, the simulation stops after the deployment, it does not simulate AND which happens thereafter. Straight stents might extend further (see Figure 46) under influence of the pulsatile environment and sick aortic wall, thereby causing additional unwanted AND. Simulations and in-vitro experiments should investigate the influence of the pulsatile environment on personalized stents and whether this might reduce AND or alter the way the neck dilates.

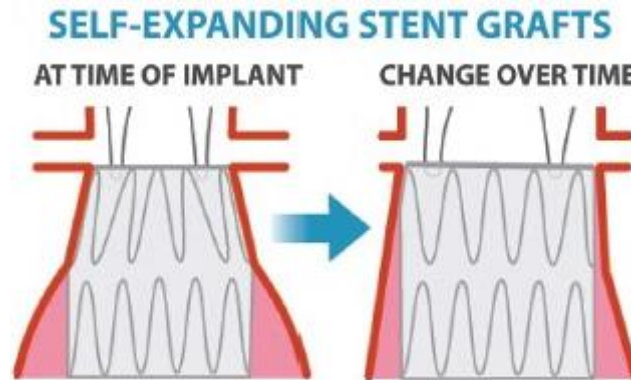


Figure 46: The loss of sealing due to AND over time, adapted from Manish Mehta.⁹¹

Z-shape versus Fishmouth

The fishmouth stents induce a larger peak stress than the z-shape stents do (Figure 38 versus 40 and 39 versus 41), however, the area over which this peak stress occurs is smaller than with the z-shape stent. The residual compliance of the aorta is smaller at the peak areas due to the elasticity modulus of the vascular wall, therefore energy looking for a way to be stored in the vessel wall will first transfer into the valley areas before transferring into the peak areas. Based upon these results, Z-shape stent graft systems might benefit less from higher compliant grafts than the fishmouth stent grafts would. Therefore, when considering the graft type for the future design of the fishmouth stent graft a highly compliant material should be chosen such as PU. A note for future consideration is the effect of ageing on the aortic wall, it has been reported that the strength of the wall decreases with the age, i.e. the compliance decreases.⁹² This might result in less benefit of this compliance difference due to the stiffening of the aorta.

Fishmouth stent

During simulation of the fishmouth stents achieving convergence was difficult. Often the simulation failed due to distorted elements and subsequent failure to repair and converge. The z-shape stent has a larger area over which the force is distributed than the fishmouth stent does. This higher force might result in the simulation of the vascular wall not coping. Increasing the amount of sub steps and taking more time for the remote displacement of the stent back to its original position did not help in convergence. Subsequently the diameter of the fishmouth stent has been reduced to approximately 10% oversizing, however, the desired convergence was not achieved. Elemental distortion and errors in element formulations kept arising. Reduction of the element size did not result in full convergence either. Therefore, only partial convergence is shown in Figures 40-43. The stress and strain distribution is as would be expected from the fishmouth stent. The exact reason as to why full convergence is not achieved is still unknown, further investigation is required. With more elements and nodes allowed in an advanced license might aid in convergence reducing the probability of elements distortion. The way the stent is constrained might be of effect as well, by using symmetry one can remove in stent constraints and use symmetry constraints this might aid convergence.

Z-shape stent

When comparing Figure 38 and 39 with Figure 44 and 45 it is clear that the maximum strain and stress has shifted from mid-strut to the peaks of the z-shape stent. Considering the design of the stent, the mid-strut areas are higher than the peaks (peak to peak it has barrel-like shape). Therefore, in the straight tube mid-strut areas will induce a larger effect on the vascular wall. For the anatomical straight neck, the stent encounters a rough surface causing a varied effect on the vascular wall.

Design

Furthermore, as noted before in Figure 31 and 32, the points of the stent can be seen extending inwards to the lumen instead of parallel to the vascular wall. Since the graft is fixated to the stent this results in the graft being lifted into the lumen. This might cause several problems such as flow disturbances and graft abrasion due to peak stresses in the graft around those points as well as a reduced area of seal which might result in stent graft migration and/or endoleaks. For personalized stent grafts these effects might be reduced due to better matching diameters, however too big diameter changes might induce the above-mentioned effects instead of preventing them.

The influences of varied geometry on flow and compliance of the native aorta should be investigated. Through simulation and/or in-vitro experiments an optimal balance should be created to reduce the influence of the stent graft on the native aortic wall. Morris et al. concluded significant influences due to geometry, graft type and design choices in 5 different stent grafts.⁷⁸ Currently no single EVAR device on the market is superior to the rest, each has its own anatomical specialization. This raises the question if it is feasible to produce a universal stent design to accommodate all anatomical variations. In any case, knowledge on the effects of varying geometry and devices dimensions is limited. This thesis succeeded to broaden that knowledge, by showing the reduction of stress and strain through personalized stents on the vascular wall, however, questions remain which should be investigated in future research.

Method

The Finite Element Method (FEM) main principle is that a large difficult model is described as multiple smaller simpler models. These models consist of algebraic equations describing small elements which, when solved, are substituted into the larger model to solve for the entire model. It can be depicted as multiple smaller combined tangent lines describing a non-linear curve. These simulations approximate reality and offer an estimation of how real models would behave. This should be considered when performing future research with real models and comparing those results with the current ones. Literature offers some insight on what formulations of material and tissue describe reality well. However, the chosen formulations might not be the most optimal. The nitinol formulation is based upon an elastoplastic description. Whereas a specific super elasticity formulation would be preferred, however this formulation is not yet available for beam elements in Ansys. The artery wall is described by a 3rd order polynomial and experimental data, most studies used their own formulation and data of the artery wall often based upon in-vitro testing. Therefore, comparison with other studies is difficult. The authors' limited knowledge about Ansys prevented implementation of such advanced formulations, however, it is strongly suggested for future research to consider implementing those advanced formulations for a more accurate approximation of reality. In addition to the formulations, limitations in computer power and an educational license restricted the number of nodes and elements that could be used. In future research, it is suggested to implement symmetry in the geometrical models to reduce the number of elements and nodes required and/or acquire an extended license to allow for a larger number nodes and elements to be present in the simulation.

The elastoplastic formulation created for these simulations produces results that are in the same order of magnitude however do not fully comply to the literature results from Kleinstreuer et al. Such linear formulations might overestimate the amount of stress in the vascular wall and stent, due to the lack of proper formulation of the difficult strain hardening behaviour of nitinol.⁸⁵ That behaviour allows for more strain without a proportional

increase in stress (see Figure 12). Therefore, this elastoplastic formulation should be compared to experimental data to verify whether it is a suitable formulation.

The interaction between beam and shell elements proves to be a challenge. The stent and vascular wall interact with prescribed contact, this contact can utilize various formulations (pure penalty, augmented Lagrange, and normal Lagrange, amongst others). Pure penalty and augmented Lagrange allow for contact penetration, which means elements can have a bit of overlap when coming into contact. Though this can aid in convergence in some simulations, for these simulations it prevented convergence by stopping at the first point of contact. This might be due to the overlap the results from the equilibrium equation for the stent did not match those from the vascular wall causing a non-convergence. The normal Lagrange formulation forces both bodies to come into contact without allowing for any penetration, this resulted in convergence for the z-shape stents. For the fishmouth stents contact did have an expected expanding effect on the vessel wall, however, it did not converge fully.

Vascular wall simulation

The vascular wall simulated in this thesis is a simplified model as noted in the set-up of Ansys part. A real blood vessel behaves anisotropic and has multiple layers with varying characteristics. The 3rd order polynomial and experimental data on which the used model is based was created by Zhao et al. They made a model that employed the three layers of the artery as well as soft and calcified plaques.⁸⁹ It is suggested to extend the current vascular wall model to incorporate these additions, this will aid in approximating real-life behaviour of the vessel wall and thereby give more insight into the effect of anatomical shaped stents on various aortic necks.

Production process

3D printing is not yet a proven suitable production process for nitinol stents. Therefore, it might be that printing nitinol stents is not possible yet this should, therefore, be the first step in future research. During this research, multiple technical medicine students have worked on this project. Some with a goal towards 3D printing of nitinol. Tests, based upon ASTM standards, have been developed to evaluate the printed nitinol parts: a tensile strength test, differential scanning calorimeter analysis and crushing test. These tests allow for standardized measurements of nitinol parts allowing us to gain insight into the characteristics of the printed nitinol and the effects of varying powder compositions. Defining the right powder composition and printer settings should be the next research step.

CONCLUSION

In this thesis, the personalized and straight stent designs were evaluated through finite element analysis. The results showed that stress and strain in the aortic neck can be reduced through personalizing stent grafts. The evidence strengthens the confidence in the necessity for personalized stent grafts. In addition, fishmouth stents have been compared to z-shape stents, however, currently the evidence presented is not strong enough to support a claim of superiority for either one design. Furthermore, 3D printing is the desired production method for its capability of producing complex shapes allowing for exact personalized stent design. Therefore, it can be concluded that the first important steps have been set for improving the personalized stent graft design, however, additional research into effects and behaviour of the personalized stent graft and its production process is required.

7. OUTLOOK

The current stent graft design hypothesis only focusses itself on the infra-renal part of the procedure by creating an artificial landing zone infra-renal. During the decision making whether to implant a stent graft results are weighed against potential complications, for instance renal ischemia occurring with some juxta- and supra-renal stent grafts. Personalization of the stent grafts to accommodate branched devices as well might prove beneficial in reducing complications with juxta- and supra-renal aneurysms. On a side note: often the inferior mesenteric artery is being sacrificed due to expected good collateral flow, however, this may cause problems in some patients causing ischemia to the transverse colon, descending colon, sigmoid colon, and rectum. It may prove beneficial for patients to receive a stent graft that matches their entire anatomy including those branches that are now often sacrificed. Furthermore, considering branched and fenestrated stent grafts, supra-renal stent placement is beneficial compared to infra-renal stent placement due to AND that is less present for supra-renal stents (2% versus 25%).³⁵ Therefore, performing research into producing patient specific supra-renal stent grafts using 3D printers might prove beneficial for clinical outcome.

Not present in the simulations is the graft that envelops the stent. The impact of the graft on the compliance of the stent has been found significant by multiple studies and should therefore be part of future simulations of the various stent graft designs. This graft study should investigate the required graft characteristics which would suit the personalized stent grafts best. Furthermore, the effect of bridging should also be investigated, the effect of the presence of a bridge on the flexibility of the stent graft might be significant, thereby influencing the compliance of and flow through the stent graft.

The stents in this thesis are designed to oversize approximately 20% in diameter this should ensure good sealing at the neck and prevent any migration during normal pulsatile behaviour of the aorta. According to Sternbergh et al. this is comparable to a stent graft that is 3-5mm in diameter larger than the targeted aortic neck.⁴⁴ However, during CT-A scanning of the abdominal aorta the pulsations of the vascular system are not taken into account. Instead, in the Meander Medical Centre, a 2mm inaccuracy threshold is used. Only measurements outside the threshold are considered significant. This results in reduced accuracy of the measurements since it is not clear whether the measurements are performed in systole or diastole and how this relates to the effects of angiotension (i.e. the Windkessel effect). Van Herwaarden et al. found that the outward change in diameter can be as big as 13.3% from the initial diameter.⁷⁶ Therefore, choosing a stent graft which achieves 20% oversizing, might be too large which can result in overstressing of the vascular wall and induce AND. By combining the CT-A scan with for instance an ECG, one can know the status of the vascular cycle at the time of acquisition. It might be beneficial to combine scans and ECG post-acquisition to determine the dimensions of the aorta. This might result in a more accurate estimation of the size of the aorta. Which in turn might result in more accurate oversizing thereby reducing vascular wall stress.

Depending on the outcome of the future research into printing of nitinol, a plan b might be required. Using patient specific fabricated nitinol rings might be the solution for the problem. This would envelop using the data from the CT-A scans to extract the required data for the dimensions of the to be fabricated rings. Thereafter the rings are produced with common production methods and welded together with nitinol bridges. The grafting technique designed for the initial plan can be used on this plan b as well. This results in a fully functional stent graft made patient specific. However, it might take extra manual labour to create such a stent and therefore be less desirable than the initial plan. Another option might be using CoCr or Stainless Steel 316-L to produce the stents, already, both are used in producing stent grafts for EVAR, moreover, they are already usable in 3D printers.

8. ACKNOWLEDGEMENT

First, I would like to thank my supervisors for their continuing support and valuable input during this graduation internship. Vincent your never-ending enthusiasm made every hurdle a little smaller. Kees, the feedback sometimes came in riddles, but was always on spot. Bregje your unbiased questions and sincere interest helped me making huge steps in my personal progress. Thank you all.

Furthermore, I would like to thank Gerben te Rietog Scholten and Henny Kuipers for their practical insight in 3D printing, Richard Loendersloot for his help in tackling FEA and Ansys. Peter Besselink for his boundless knowledge of nitinol and Henk Anema for his enthusiasm and knowledge on 3D printing of metals. Moreover, I want to thank Arjan, Anouk, Daan, Claire, Michiel, Kevin, Rens and Tara for their hard work and input for this research project, during their master 2 internships. Lastly, I want to thank, of course, my family, Laura, and friends for sharing my frustrations and euphoria's.

9. REFERENCES

1. Jongkind, V. *et al.* Juxtarenal aortic aneurysm repair. *J. Vasc. Surg.* **52**, 760–7 (2010).
2. Reimerink, J. J. *et al.* Endovascular repair versus open repair of ruptured abdominal aortic aneurysms: a multicenter randomized controlled trial. *Ann. Surg.* **258**, 248–56 (2013).
3. Szilagyi, D. E., Smith, R. F., DeRusso, F. J., Elliott, J. P. & Sherrin, F. W. Contribution of abdominal aortic aneurysmectomy to prolongation of life. *Ann. Surg.* **164**, 678–99 (1966).
4. Powell, J. T. *et al.* Final 12-year follow-up of surgery versus surveillance in the UK Small Aneurysm Trial. *Br. J. Surg.* **94**, 702–8 (2007).
5. Lederle, F. A. *et al.* Immediate repair compared with surveillance of small abdominal aortic aneurysms. *N. Engl. J. Med.* **346**, 1437–44 (2002).
6. Lederle, F. A. *et al.* Rupture rate of large abdominal aortic aneurysms in patients refusing or unfit for elective repair. *JAMA* **287**, 2968–72 (2002).
7. Moll, F. L. *et al.* Management of abdominal aortic aneurysms clinical practice guidelines of the European society for vascular surgery. *Eur. J. Vasc. Endovasc. Surg.* **41 Suppl 1**, S1–S58 (2011).
8. Cao, P. *et al.* Comparison of surveillance versus aortic endografting for small aneurysm repair (CAESAR): results from a randomised trial. *Eur. J. Vasc. Endovasc. Surg.* **41**, 13–25 (2011).
9. Chaikof, E. L. *et al.* SVS practice guidelines for the care of patients with an abdominal aortic aneurysm: executive summary. *J. Vasc. Surg.* **50**, 880–96 (2009).
10. Erbel, R. *et al.* 2014 ESC guidelines on the diagnosis and treatment of aortic diseases. *European Heart Journal* **35**, 2873–2926 (2014).
11. Drake, R. L., Vogl, A. W. & Mitchell, A. W. M. *Gray's Anatomy for Students*. (Elsevier, 2015).
12. Schaefer-Prokop, C. & Dixon, A. K. *Grainger & Allison's diagnostic radiology. The chest and cardiovascular system*. (Elsevier, 2016).
13. Craig, K. Clinical practice. Abdominal aortic aneurysms. *N. Engl. J. Med.* **371**, 2101–2108 (2014).
14. Dua, A., Kuy, S., Lee, C. J., Upchurch, G. R. & Desai, S. S. Epidemiology of aortic aneurysm repair in the United States from 2000 to 2010. *J. Vasc. Surg.* **59**, 1512–1517 (2014).
15. De Bruin, J. L. *et al.* Long-term outcome of open or endovascular repair of abdominal aortic aneurysm. *N. Engl. J. Med.* **362**, 1881–9 (2010).
16. Prinssen, M. *et al.* A Randomized Trial Comparing Conventional and Endovascular Repair of Abdominal Aortic Aneurysms. *N. Engl. J. Med.* **351**, 1607–1618 (2004).
17. Stather, P. W. *et al.* Systematic review and meta-analysis of the early and late outcomes of open and endovascular repair of abdominal aortic aneurysm. *Br. J. Surg.* **100**, 863–872 (2013).
18. Patel, R., Sweeting, M. J., Powell, J. T. & Greenhalgh, R. M. Endovascular versus open repair of abdominal aortic aneurysm in 15-years' follow-up of the UK endovascular aneurysm repair trial 1 (EVAR trial 1): a randomised controlled trial. *Lancet* **388**, 1–9 (2016).
19. Bahia, S. S. *et al.* Systematic Review and Meta-analysis of Long-term survival after Elective Infrarenal Abdominal Aortic Aneurysm Repair 1969-2011: 5 Year Survival Remains Poor Despite Advances in Medical Care and Treatment Strategies. *Eur. J. Vasc. Endovasc. Surg.* **50**, 320–330 (2015).
20. Stoeckel, D., Pelton, A. & Duerig, T. Self-expanding nitinol stents: material and design considerations. *Eur. Radiol.* **14**, 292–301 (2004).
21. Santos, I. C., Rodrigues, A., Figueiredo, L., Rocha, L. A. & Tavares, J. M. R. Mechanical properties of stent-graft materials. *Proc. Inst. Mech. Eng. Part L J. Mater. Des. Appl.* **226**, 330–341 (2012).

22. Buck, D. B., van Herwaarden, J. A., Schermerhorn, M. L. & Moll, F. L. Endovascular treatment of abdominal aortic aneurysms. *Nat. Rev. Cardiol.* **11**, 112–23 (2014).
23. Smeds, M. R. *et al.* Infrarenal EVAR: new developments and decision-making in 2016. *Semin. Vasc. Surg.* **0**, 1863–1871 (2016).
24. Lederle, F. A. *et al.* Outcomes following endovascular vs open repair of abdominal aortic aneurysm: a randomized trial. *JAMA* **302**, 1535–42 (2009).
25. EVAR trial participants. Endovascular aneurysm repair versus open repair in patients with abdominal aortic aneurysm (EVAR trial 1): randomised controlled trial. *Lancet* **365**, 2179–2186 (2005).
26. Lederle, F. A. *et al.* Long-Term Comparison of Endovascular and Open Repair of Abdominal Aortic Aneurysm. *N. Engl. J. Med.* **367**, 1988–1997 (2012).
27. Quatromoni, J., Orlova, K. & Foley, P. Advanced Endovascular Approaches in the Management of Challenging Proximal Aortic Neck Anatomy: Traditional Endografts and the Snorkel Technique. *Semin. Intervent. Radiol.* **32**, 289–303 (2015).
28. Droc, I., Raithel, D. & Calinescu, B. Abdominal Aortic Aneurysms – Actual Therapeutic Strategies. doi:10.5772/48596
29. White, G. H., May, J., Waugh, R. C., Chaufour, X. & Yu, W. Type III and type IV endoleak: toward a complete definition of blood flow in the sac after endoluminal AAA repair. *J. Endovasc. Surg.* **5**, 305–309 (1998).
30. White, G. H., Yu, W., May, J., Chaufour, X. & Stephen, M. S. Endoleak as a complication of endoluminal grafting of abdominal aortic aneurysms: classification, incidence, diagnosis, and management. *J. Endovasc. Surg.* **4**, 152–168 (1997).
31. White, G. H., Yu, W. & May, J. Endoleak--a proposed new terminology to describe incomplete aneurysm exclusion by an endoluminal graft. *J. Endovasc. Surg.* **3**, 124–125 (1996).
32. Veith, F. J. *et al.* Nature and significance of endoleaks and endotension: Summary of opinions expressed at an international conference. *J. Vasc. Surg.* **35**, 1029–1035 (2002).
33. Stavropoulos, S. W. & Charagundla, S. R. Imaging techniques for detection and management of endoleaks after endovascular aortic aneurysm repair. *Radiology* **243**, 641–655 (2007).
34. Verhoeven, E. L. G. *et al.* Fenestrated Endovascular Aortic Aneurysm Repair as a First Line Treatment Option to Treat Short Necked, Juxtarenal, and Suprarenal Aneurysms. *Eur. J. Vasc. Endovasc. Surg.* **51**, 775–781 (2016).
35. Kouvelos, G. N., Oikonomou, K., Antoniou, G. A., Verhoeven, E. L. G. & Katsargyris, A. A Systematic Review of Proximal Neck Dilatation After Endovascular Repair for Abdominal Aortic Aneurysm. *J. Endovasc. Ther.* **24**, 59–67 (2016).
36. Endologix. Nellix EndoVascular Aneurysm Sealing System. (2017). Available at: <https://endologix.com/international/products/nellix/>. (Accessed: 14th July 2017)
37. Medtronic Endovascular. Endurant II Delivery & Deployment. (2017). Available at: <http://www.aortic.medtronicendovascular.com/us/EndurantII/DeliveryDeployment/index.htm>. (Accessed: 14th July 2017)
38. Lombard Medical. Lombard Medical, Aorfix. (2017). Available at: <http://www.lombardmedical.com/pwpcontrol.php?pwplID=18003>. (Accessed: 14th July 2017)
39. Mastracci, T. M. Fenestrated endografts for complex abdominal aortic aneurysms. *Perspect. Vasc. Surg. Endovasc. Ther.* **22**, 214–8 (2010).
40. Leotta, D. F. & Starnes, B. W. Custom fenestration templates for endovascular repair of juxtarenal aortic aneurysms. *J. Vasc. Surg.* **61**, 1637–41 (2015).
41. Medtronic. Endurant II and IIs, instructions for use. 7–11 (2016). Available at: http://manuals.medtronic.com/wcm/groups/mdtcom_sg/@emanuals/@era/@cardio/documents/documents/contrib_240218.pdf. (Accessed: 6th August 2017)
42. Kristmundsson, T., Sonesson, B., Dias, N., Malina, M. & Resch, T. Anatomic suitability for endovascular repair of abdominal aortic aneurysms and possible benefits of low profile delivery systems. *Int. Soc. Vasc. Surg.* **22**, 112–115

- (2014).
43. van Keulen, J. W. *et al.* One-year multicenter results of 100 abdominal aortic aneurysm patients treated with the Endurant stent graft. *J. Vasc. Surg.* **54**, 609–615 (2011).
 44. Sternbergh III, C., Money, S., Greenberg, R. & Chuter, T. Influence of endograft oversizing on device migration, endoleak, aneurysm shrinkage, and aortic neck dilation: Results from the Zenith multicenter trial. *J. Vasc. Surg.* **39**, 20–26 (2004).
 45. Meier, H., Haberland, C. & Frenzel, J. Structural and functional properties of NiTi shape memory alloys produced by Selective Laser Melting. in *Innovative Developments in Virtual and Physical Prototyping - Proceedings of the 5th International Conference on Advanced Research and Rapid Prototyping* 291–296 (2012).
 46. Meier, H., Haberland, C., Frenzel, J. & Zarnetta, R. Selective laser melting of NiTi shape memory components. *4th Int. Conf. Adv. Res. Virtual Phys. Prototyping, VRAP 2009; Leir. Port. 6 Oct. 2009 through 10 Oct. 2009; Code 82905* 233–238 (2010).
 47. Dadbakhsh, S. *et al.* Effect of SLM Parameters on Transformation Temperatures of Shape Memory Nickel Titanium Parts. *Adv. Eng. Mater.* **16**, 1140–1146 (2014).
 48. Varadan, V. K., Vinoj, K. J. & Gopalakrishnan, S. Smart material systems and MEMS: design and development methodologies. *John Wiley Sons Ltd* (2006).
 49. Kamila. Introduction, Classification and Applications of Smart Materials: an Overview. *Am. J. Appl. Sci.* **10**, 876–880 (2013).
 50. Fremond, M. & Miyazaki, S. *Shape memory alloys*. **351**, (Springer, 2014).
 51. Khoo, Z. X. *et al.* 3D printing of smart materials: A review on recent progresses in 4D printing. *Virtual Phys. Prototyp.* **10**, 103–122 (2015).
 52. Duerig, T., Pelton, a & Stöckel, D. An overview of nitinol medical applications. *Mater. Sci. Eng. A* **273–275**, 149–160 (1999).
 53. Morgan, N. B. Medical shape memory alloy applications - The market and its products. *Mater. Sci. Eng. A* **378**, 16–23 (2004).
 54. Singh, C., Wong, C. & Wang, X. Medical Textiles as Vascular Implants and Their Success to Mimic Natural Arteries. *J. Funct. Biomater.* **6**, 500–525 (2015).
 55. Shiva, S., Palani, I. A., Mishra, S. K., Paul, C. P. & Kukreja, L. M. Investigations on the influence of composition in the development of Ni–Ti shape memory alloy using laser based additive manufacturing. *Opt. Laser Technol.* **69**, 44–51 (2015).
 56. Elahinia, M. H., Hashemi, M., Tabesh, M. & Bhaduri, S. B. Manufacturing and processing of NiTi implants: A review. *Prog. Mater. Sci.* **57**, 911–946 (2012).
 57. Li, Q., Zeng, Y. & Tang, X. The applications and research progresses of nickel-titanium shape memory alloy in reconstructive surgery. *Australas. Phys. Eng. Sci. Med.* **33**, 129–136 (2010).
 58. Boron, W. F. & Boulpaep, E. L. in *Medical physiology : a cellular and molecular approach* 467–481, 536 (Saunders Elsevier, 2012).
 59. Guan, Y., Wang, L., Lin, J. & King, M. W. Compliance study of endovascular stent grafts incorporated with polyester and polyurethane graft materials in both stented and unstented zones. *Materials (Basel)*. **9**, 658 (2016).
 60. Voûte, M. T. *et al.* Stent graft composition plays a material role in the postimplantation syndrome. *J. Vasc. Surg.* **56**, 1503–9 (2012).
 61. Moulakakis, K. G. *et al.* The impact of endograft type on inflammatory response after endovascular treatment of abdominal aortic aneurysm. *J. Vasc. Surg.* **57**, 668–677 (2013).
 62. Lin, J. *et al.* Fatigue Performance of Fabrics of Stent - Grafts Supported with Z - Stents versus Ringed Stents. *J. Donghua Univ. (Eng. Ed.)* **30**, 367–370 (2013).

63. Stoeckel, D., Bonsignore, C. & Duda, S. A survey of stent designs. *Minim. Invasive Ther. Allied Technol.* **11**, 137–147 (2002).
64. Duda, S. H. *et al.* Physical properties of endovascular stents: an experimental comparison. *J. Vasc. Interv. Radiol.* **11**, 645–54 (2000).
65. Nematzadeh, F. & Sadrnezhaad, S. K. Effects of material properties on mechanical performance of Nitinol stent designed for femoral artery: Finite element analysis. *Sci. Iran.* **19**, 1564–1571 (2012).
66. Georgakarakos, E. *et al.* Geometrical Factors Influencing the Hemodynamic Behavior of the AAA Stent Grafts: Essentials for the Clinician. *Cardiovasc. Intervent. Radiol.* **37**, 1420–1429 (2014).
67. Malas, M. B. *et al.* Absence of proximal neck dilatation and graft migration after endovascular aneurysm repair with balloon-expandable stent-based endografts. *J. Vasc. Surg.* **42**, 639–644 (2005).
68. Monahan, T. S., Chuter, T. A. M., Reilly, L. M., Rapp, J. H. & Hiramoto, J. S. Long-term follow-up of neck expansion after endovascular aortic aneurysm repair. *J. Vasc. Surg.* **52**, 303–7 (2010).
69. Dalainas, I. *et al.* Aortic Neck Dilatation and Endograft Migration Are Correlated With Self-Expanding Endografts. *J. Endovasc. Ther.* **14**, 318–323 (2007).
70. Stanley, B. M. *et al.* Evaluation of Patient Selection Guidelines for Endoluminal AAA Repair with the Zenith Stent-Graft: The Australasian Experience. *J. Endovasc. Ther.* **8**, 457–464 (2001).
71. Jim, J. *et al.* A 5-Year Comparison of EVAR for Large and Small Aortic Necks. *J. Endovasc. Ther.* **17**, 575–584 (2010).
72. Pache, J. *et al.* Intracoronary stenting and angiographic results: strut thickness effect on restenosis outcome (ISAR-STEREO-2) trial. *J. Am. Coll. Cardiol.* **41**, 1283–8 (2003).
73. Kastrati, A. *et al.* Intracoronary stenting and angiographic results: strut thickness effect on restenosis outcome (ISAR-STEREO) trial. *Circulation* **103**, 2816–21 (2001).
74. Powell, A. *et al.* Design and Clinical Considerations for Endovascular Stent Grafts. *Interv. Cardiol. Clin.* **5**, 381–389 (2016).
75. Cao, P. *et al.* Device migration after endoluminal abdominal aortic aneurysm repair: Analysis of 113 cases with a minimum follow-up period of 2 years. *J. Vasc. Surg.* **35**, 229–235 (2002).
76. van Herwaarden, J. A. *et al.* Dynamic magnetic resonance angiography of the aneurysm neck: Conformational changes during the cardiac cycle with possible consequences for endograft sizing and future design. *J. Vasc. Surg.* **44**, 22–28 (2006).
77. Litwinski, R. A. *et al.* The role of aortic neck dilation and elongation in the etiology of stent graft migration after endovascular abdominal aortic aneurysm repair with a passive fixation device. *J. Vasc. Surg.* **44**, 1176–1181 (2006).
78. Morris, L., Stefanov, F., Hynes, N., Diethrich, E. B. & Sultan, S. An Experimental Evaluation of Device/Arterial Wall Compliance Mismatch for Four Stent-Graft Devices and a Multi-layer Flow Modulator Device for the Treatment of Abdominal Aortic Aneurysms. *Eur. J. Vasc. Endovasc. Surg.* **51**, 44–55 (2016).
79. Demanget, N. *et al.* Finite Element Analysis of the Mechanical Performances of 8 Marketed Aortic Stent-Grafts. *J. Endovasc. Ther.* **20**, 523–535 (2013).
80. Duda, S. H. *et al.* Physical Properties of Endovascular Stents: An Experimental Comparison. *J. Vasc. Interv. Radiol.* **11**, 645–54 (2000).
81. Schoretsanitis, N., Georgakarakos, E., Argyriou, C., Ktenidis, K. & Georgiadis, G. S. A critical appraisal of endovascular stent-grafts in the management of abdominal aortic aneurysms. *Radiol. Med.* 1–10 (2017). doi:10.1007/s11547-017-0724-z
82. Rodrigues, A., Figueiredo, L. & Bordado, J. Abrasion behaviour of polymeric textiles for endovascular stent-grafts. in *Tribology International* **63**, 265–274 (2013).
83. Katzen, B. T. & MacLean, A. A. Complications of endovascular repair of abdominal aortic aneurysms: A review. *Cardiovasc. Intervent. Radiol.* **29**, 935–946 (2006).

84. Thubrikar, M. J., Al-Soudi, J. & Robicsek, F. Wall Stress Studies of Abdominal Aortic Aneurysm in a Clinical Model. *Ann. Vasc. Surg.* **15**, 355–366 (2001).
85. Kleinstreuer, C., Li, Z., Basciano, C. A., Seelecke, S. & Farber, M. A. Computational mechanics of Nitinol stent grafts. *J. Biomech.* **41**, 2370–2378 (2008).
86. De Bock, S. *et al.* Virtual evaluation of stent graft deployment: A validated modeling and simulation study. *J. Mech. Behav. Biomed. Mater.* **13**, 129–139 (2012).
87. Gong, X.-Y., Pelton, A. R., Duerig, T. W., Rebelo, N. & Perry, K. Finite element analysis and experimental evaluation of superelastic Nitinol stent. in *SMST 2003: International Conference on Shape Memory and Superelastic Technologies. International Organization on SMST, Pacific Grove, CA* 453–462 (2004).
88. Azaouzi, M., Makradi, A. & Belouettar, S. Deployment of a self-expanding stent inside an artery: A finite element analysis. *Mater. Des.* **41**, 410–420 (2012).
89. Zhao, S., Gu, L. & Froemming, S. Finite Element Analysis of the Implantation of a Self-Expanding Stent: Impact of Lesion Calcification. *Mech. Mater. Eng. Fac. Publ.* (2012).
90. Demanget, N. *et al.* Computational comparison of the bending behavior of aortic stent-grafts. *J. Mech. Behav. Biomed. Mater.* **5**, 272–282 (2012).
91. Mehta, M. Rethink the Neck. *Endovascular Today - supplement* 3–6 (2014). Available at: <http://evtoday.com/2014/09/supplement/rethink-the-neck/>. (Accessed: 9th August 2017)
92. Khamin, N. S. Strength properties of the human aorta and their variation with age. *Polym. Mech.* **13**, 100–104 (1977).
93. Bastos Gonçalves, F. *et al.* The influence of neck thrombus on clinical outcome and aneurysm morphology after endovascular aneurysm repair. *J. Vasc. Surg.* **56**, 36–44 (2012).
94. Jordan, W. D. *et al.* Outcome-based anatomic criteria for defining the hostile aortic neck. *J. Vasc. Surg.* **61**, 1383–1390 (2015).
95. Chinsakchai, K. *et al.* Outcomes of abdominal aortic aneurysm with aortic neck thrombus after endovascular abdominal aortic aneurysm repair. *J. Med. Assoc. Thai.* **97**, 518–24 (2014).
96. Wyss, T. R., Dick, F., Brown, L. C. & Greenhalgh, R. M. The influence of thrombus, calcification, angulation, and tortuosity of attachment sites on the time to the first graft-related complication after endovascular aneurysm repair. *J. Vasc. Surg.* **54**, 965–971 (2011).
97. Stather, P. W. *et al.* Outcomes of endovascular aneurysm repair in patients with hostile neck anatomy. *Eur. J. Vasc. Endovasc. Surg.* **44**, 556–561 (2012).
98. Bastos Goncalves, F. *et al.* Risk factors for proximal neck complications after endovascular aneurysm repair using the enduring stentgraft. *Eur. J. Vasc. Endovasc. Surg.* **49**, 156–162 (2015).
99. Oliveira, N. F. G. *et al.* Clinical outcome and morphologic determinants of mural thrombus in abdominal aortic endografts. *J. Vasc. Surg.* **61**, 1391–1398 (2015).
100. Dadbakhsh, S., Vrancken, B., Kruth, J.-P., Luyten, J. & Van Humbeeck, J. Texture and anisotropy in selective laser melting of NiTi alloy. *Mater. Sci. Eng. A* **650**, 225–232 (2015).
101. Kruth, J.-P., Mercelis, P., Vaerenbergh, J. Van, Froyen, L. & Rombouts, M. Binding mechanisms in selective laser sintering and selective laser melting. *Rapid Prototyp. J.* **11**, 26–36 (2005).
102. Otsuka, K. & Ren, X. Physical metallurgy of Ti-Ni-based shape memory alloys. *Prog. Mater. Sci.* **50**, 511–678 (2005).
103. Nishiyama, Z. *Martensitic Transformation. Martensitic Transformation* (Elsevier, 1978). doi:10.1016/B978-0-12-519850-9.50009-0
104. Groot Jebbink, E., Goverde, P. C. J. M., van Oostayen, J. A., Reijnen, M. M. P. J. & Slump, C. H. Innovation in aortoiliac stenting: an in vitro comparison. in *SPIE Medical Imaging* (eds. Yaniv, Z. R. & Holmes, D. R.) 90361X (International Society for Optics and Photonics, 2014). doi:10.1117/12.2042865
105. Park, K., Lewis, G. & Park, J. B. Ultra-high molecular weight polyethylene (UHMWPE). *Encycl. Biomater. Biomed. Eng.*

- 1, 1690–1696 (2004).
106. Rigberg, D. *et al.* Thin-film nitinol (NiTi): a feasibility study for a novel aortic stent graft material. *J. Vasc. Surg.* **50**, 375–80 (2009).
 107. Shayan, M., Yang, S., Ryu, W. & Chun, Y. A novel low-profile thin-film nitinol/silk endograft for treating small vascular diseases. *J. Biomed. Mater. Res. Part B* **105**, 575–584 (2015).
 108. Shayan, M. & Chun, Y. An overview of thin film nitinol endovascular devices. *Acta Biomater.* **21**, 20–34 (2015).
 109. Chun, Y. J., Levi, D. S., Mohanchandra, K. P., Fishbein, M. C. & Carman, G. P. Novel micro-patterning processes for thin film NiTi vascular devices. *Smart Mater. Struct.* **19**, 105021 (2010).
 110. Levi, D. S. *et al.* Thin film nitinol covered stents: design and animal testing. *ASAIO J.* **54**, 221–6
 111. Kadoglou, N. P. E. *et al.* Differential effects of stent-graft fabrics on arterial stiffness in patients undergoing endovascular aneurysm repair. *J. Endovasc. Ther.* **21**, 850–8 (2014).
 112. Desai, M. *et al.* A sutureless aortic stent-graft based on a nitinol scaffold bonded to a compliant nanocomposite polymer is durable for 10 years in a simulated in vitro model. *J. Endovasc. Ther.* **19**, 415–27 (2012).
 113. Krishna, B. V., Bose, S. & Bandyopadhyay, A. Laser Processing of Net-Shape NiTi Shape Memory Alloy. *Metall. Mater. Trans. A* **38**, 1096–1103 (2007).
 114. Furumoto, T. *et al.* Permeability and strength of a porous metal structure fabricated by additive manufacturing. *J. Mater. Process. Technol.* **219**, 10–16 (2015).
 115. Marattukalam, J. J. *et al.* Microstructure and corrosion behavior of laser processed NiTi alloy. *Mater. Sci. Eng. C* **57**, 309–313 (2015).
 116. Paul, C. P., Mishra, S. K., Tiwari, P. & Kukreja, L. M. Solid-Particle Erosion Behaviour of WC/Ni Composite Clad layers with Different Contents of WC Particles. *Opt. Laser Technol.* **50**, 155–162 (2013).
 117. Paul, C. P. *et al.* Investigating laser rapid manufacturing for Inconel-625 components. *Opt. Laser Technol.* **39**, 800–805 (2007).
 118. Zäh, M. F. & Lutzmann, S. Modelling and simulation of electron beam melting. *Prod. Eng.* **4**, 15–23 (2010).
 119. Kahnert, M., Lutzmann, S. & Zäh, M. Layer formations in electron beam sintering. *Solid Free. Fabr. Symp.* 88–99 (2007).
 120. Liu, L., Li, D. B., Tong, Y. F. & Zhu, Y. F. Fiber laser micromachining of thin NiTi tubes for shape memory vascular stents. *Appl. Phys. A Mater. Sci. Process.* **122**, 638 (2016).
 121. Shishkovskii, I. V., Yadroitsev, I. A. & Smurov, I. Y. Selective laser sintering/melting of nitinol–hydroxyapatite composite for medical applications. *Powder Metall. Met. Ceram.* **50**, 275–283 (2011).
 122. Shirazi, S. F. S. *et al.* A review on powder-based additive manufacturing for tissue engineering: selective laser sintering and inkjet 3D printing. *Sci. Technol. Adv. Mater.* **16**, 33502 (2015).
 123. Memry SAES Group. Manufacturing Capabilities. (2012). Available at: <http://www.memry.com/products-services/production/manufacturing-capabilities>. (Accessed: 11th August 2017)

10.1 APPENDIX 1 – RESEARCH LINE

CLINICAL BACKGROUND

Table 8: classification of endoleak types.^{29–33}

Type I a, b, c	Leak at landing zone: a) Proximal; b) Distal site; c) Iliac occluder.
Type II a, b (most common)	Continuing growth of aneurysm sac through branch vessel. a) One vessel involved; b) Two or more vessels involved.
Type III a, b	Leak through defect of the stent graft. a) Modular break-up; b) Graft defect.
Type IV	Leak through the graft its porous structure.
Type V	Endotension; growth of sac without evidence of a leak.

Often, in patients with vascular diseases, thrombi are encountered on the vessel walls. For AAA patients wall thrombi might be a contra-indication depending on the location. Research has been performed on the influence of thrombi on the outcome of EVAR procedures. Bastos Goncalves et al. reported no effects on short- and mid-term follow up when performing EVAR on AAA with thrombi.⁹³ Whereas Jordan et al., Chinsakchai et al. and Wyss et al. reported a protective effect against endoleaks type Ia for mural thrombi and calcifications in an AAA.^{94–96} Wyss et al. did note the limitations of the data set and the lack of information on the characteristics of thrombus present.⁹⁶ However, Stather et al. found a negative effect by thrombus on short-term results (late type Ia endoleak and total reinterventions required).⁹⁷ In a later study, Bastos Goncalves et al found an increased odds ratio (4.8) in long-term follow-up for adverse events when neck thrombus or calcification of more than 50% is present. Short term follow-up (1-year) showed no increased odds ratio.⁹⁸ A potential explanation might be that soft thrombi are more compliant than the vascular wall, therefore accommodating the stent graft better which results in a better seal. Due to the properties of nitinol thrombi can be ‘over-stented’, if the thrombus changes or disappears altogether the nitinol will expand to its pre-set diameter preventing endoleaks. Though only if the stent has not already reached that nominal diameter. Thrombi are still potential complications factors, for instance it can cause embolization’s distally or endoleaks when its consistency changes over time. An interesting suggestion is the role mural thrombus might play in preventing a ‘barrel-like’ configuration of the stent graft which, as reported by Oliveira et al., might result in more stent graft thrombus.⁹⁹

TECHNICAL BACKGROUND

Nitinol

Nitinol can shift, when in full austenitic phase, to a simple martensitic phase due to outside forces inducing stress in the material. This shift from austenitic to a simple martensitic phase is reversible. This is described as super elasticity of nitinol (i.e. stress induced reversible martensite) it requires the geometry to be as much in austenitic phase as possible. In comparison, the other characteristic of nitinol is shape memory, which is based upon temperature induced memory. Stress induced twined martensite at a temperature under that of a full austenite phase will change to its original austenite roster, thereby resetting the geometry to its initial shape.

For a sufficient super elasticity, the nitinol product needs to be in full austenitic phase, depending on the nitinol composition and annealing (heat) treatment. The body temperature is around 37 degrees Celsius, choosing an austenite finish temperature of less than 37 degrees Celsius will ensure that the nitinol will be in austenitic phase when used in a body. Thereby ensured of super elasticity and shape memory.

During production, small martensitic phase plates are formed that need to be eliminated. This is due to the internal stresses the product experiences while it is produced, in addition to the rapid cooling after the laser has heated the powder. Removing the martensitic plates ensures homogenous material characteristics. Methods to break down these plates are annealing treatments and through slow furnace cooling (let the product cool down in the oven it was created), this aims to create a homogenous crystalline structure in austenitic phase which after cooling reverts to martensitic phase depending on the nitinol composition. These treatments can be applied to Additive Manufacturing (AM) produced nitinol as well. Though complete isotropic mechanical properties are not achieved, due to the product not reaching 100% density during production. The density is decreased during quick furnace cooling which can cause austenite and martensitic phase plates within solidified tracks to segregate, due to rapid cooling on the outside while the inside is still hot. This, in turn, may cause a mixed shape memory response. Annealing is necessary, as can be seen when comparing annealed nitinol with un-annealed nitinol. The difference between both can be found in its ductility the un-annealed nitinol alloys are less ductile (more prone to fracture) than conventional produced nitinol alloys while the annealed versions achieve comparable material characteristics.^{47,51,100–103} For annealing different approaches are available, all use the same principle: through heating the nitinol crystalline structure is 'reset' and given a shape which it will remember after it has cooled. Post-processing is elaborated in the upcoming production method chapter.

Graft

The production of a graft requires precision. Failures such as material fatigue due to production errors causes ruptures to appear in the graft which results in returned risk of aneurysmal rupture. Three techniques are proposed based upon current literature. Dissolving polymer, melting polymer or Thin Film Nitinol (TFN). Groot Jebbink et al. produced a set up to produce a graft using a heated bath with a bowl inside in which the graft material is dissolved and the stent is submersed. The stent with dissolved graft material is kept turning when removed from the bowl for even distribution and put in an oven to dry the graft material. The final product is a covered stent with a flexible graft. A clear biocompatible polyurethane (PU) was used for flow measurements in the experiments of Groot Jebbink et al. The non-clear version is used in stent grafts therefore this set up might also be of interest to produce a graft for the custom-made stent graft.¹⁰⁴ This approach has been performed already by the author and showed a feasible result.

Secondly, the UltraHighMolecularWeightPolyEthylene (UHMWPE) might be suitable as a graft as well. This polymer is biocompatible, highly impact resistant and is wear resistant. Therefore, it is used often in hip arthroplasty.¹⁰⁵ The fibre form of UHMWPE shows excellent fatigue resistance and strength in addition it elicits lower inflammatory responses allowing it to be used in the body. Furthermore, it has a low friction coefficient, a non-stick surface and is self-lubricant which might make it a suitable candidate for use as the graft material. UHMWPE is a thermoplastic and therefore is not dissolved but molten to allow processing, or can be expanded or woven.²¹ The advantage over PU might be that the solidifying process is quicker than the drying process.

The third technique is the TFN technique. This technique uses a sputtering method in a vacuum production space this ensures a micron per micron layer which, after production is finished, is 500 times thinner with the same strength as the current graft material used, and is more flexible. In some cases, a 20% higher flexibility is achieved when compared to conventional grafts. When microscopic holes are created, the flexibility will increase with another 15-30%. Both the low-profile and the increase in flexibility allow future delivery devices to be half the diameter and therefore allow patients with small diameter and/or tortuous vascular systems to be operable.^{106–108}

TFN sounds promising and recent studies demonstrated the feasibility and safety of the stent grafts containing TFN. Though there are problems after implementation, it is described that TFN does not have sufficient and rapid endothelialisation and might cause neo-intimal hyperplasia. Risks such as thrombosis and restenosis are present and endanger long term patency. Microscopic perforations, or treating the TFN with a silk coating results in sufficient and rapid endothelialisation. Other studies found that TFN, due to its circumferential boundary, had similar neo-intimal hyperplasia when compared to conventional grafts.^{106–110} At this point vacuum sputtering is

the only technique to be able to produce TFN, the thickness of the film is in some cases 2 μm . The resolution of the current printers is at best 20 μm , therefore extreme low-profile production with 3D printing is not available at this time. Our goal is to develop a production system for stent grafts to repair AAAs, extreme low-profile devices are not necessary, however, it might make the procedure easier by having a more flexible delivery device. TFN shows promise to be used in the future as a graft in stent grafts for endovascular treatments.¹⁰⁸ The TFN production technique at this point in time, however, is too difficult.

All three graft production techniques are subject of research, as well as the grafts materials used. Nikolaos et al studied different graft fibre types. They showed that using polyester (for instance ePTFE) grafts resulted in high flow and low compliance when compared to the native artery.¹¹¹ Guan et al. studied the PU degradation due to calcification and absorption of lipids resulting in stress cracks. They found that using PU for nitinol stents with their current modularity, causes compliance differences between stented parts and non-stented parts. In contrast, the ePTFE stent graft did not encounter compliance differences between stented parts and non-stented parts. Guan et al. showed PU has 9 times higher compliance in stented areas when compared to the stented areas of polyester stent grafts mimicking the native artery more naturally. Desai et al studied suture-less grafts. This showed potential to be used in stent grafts with the most important outcome being higher compliance.¹¹² This research adds to the feasibility of creating personalized stent grafts using a production method with limited manual labour.

The TFN technique might be promising for graft production if the printer can produce it as well. The stent graft would then be made consisting only of nitinol which might allow the stent and graft to be produced at the same time. This can be useful for the acute cases in immediate need of custom-made stent grafts. However, currently this technique is very difficult to handle. The polyurethane graft has already been applied in commercially available products and it is shown to have superior characteristics with regards to its compliance when compared to ePTFE. In addition, it is dissolvable and might even be made porous. Therefore, PU is a promising material for use in our stent graft. The fact PU needs to be dissolved and thereafter dried means a longer production time than with UHMWPE, which is a molten polymer and only needs to cool to achieve original strength. Both graft materials require further investigation.

PRODUCTION METHOD

There are various options and requirements to produce nitinol stents, these are discussed here.

3D printing

3D printing is a promising technique that might be the production method of choice for personalized stent grafts due to its capability to print more complex shapes than any other manufacturing technique currently available. This production method uses various techniques, of which four produce metal products: binder jetting, laser melting, electron beam melting (see Figure 47) and LENS (laser engineered net shaping). Binder jetting glues metal particles together using a binder, this produces material with limited material characteristics, and therefore is less reliable than the melting processes. LENS uses a laser to create a melting pool and a nozzle through which the powder is sprayed into the melting pool, the absence of a support structure makes it harder to produce objects with this technique than with LM or EBM.^{56,113} Therefore we only consider LM and EBM.

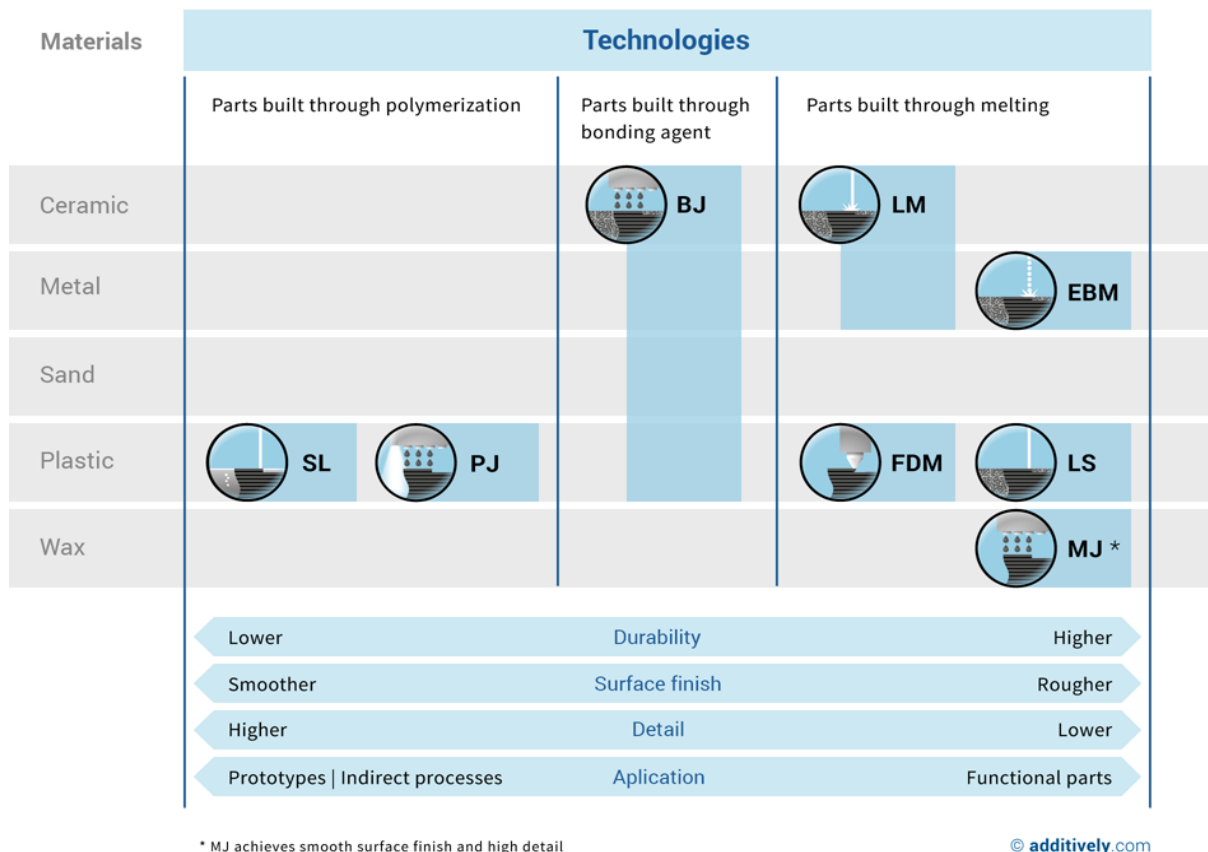


Figure 47: Available 3D printing techniques. (www.additively.com) SL = Stereo lithography, PJ = Photopolymer Jetting, BJ = Binder Jetting, LM = Laser Melting, EBM = Electron Beam Melting, FDM = Fused Deposition Modelling, LS = Laser sintering, MJ = Material Jetting.

LM melts powder particles together creating the product layer by layer. 3D printing allows for multiple parameters to be controlled and varied to alter the final product characteristics. These parameters are: laser power, beam diameter at product level, material feed per layer and scan speed.^{55,56} All directly influence the amount of energy that can be delivered to each powder particle at once. This ‘energy density’ provided by the laser is in direct correlation with the consolidation of the powder mixture. High energy density results in full melting conditions, which is required for our stent, while lower energy density results in a sintering condition (partial melting)^{56,114} Another important parameter is the placement of the laser tracks and the amount of overlap they have with one another. During production of nitinol this may cause variation in grain size relative to tracks that have no overlap. An overlap is necessary to produce ‘full’ density products, otherwise pockets of non-molten powder will be created. This impacts the material characteristics and should be prevented. Low heat transfer, results in smaller grain size which ensues an increase of hardness and a decrease in flexibility. More heat delivered to the powder ensures larger grain sizes which achieves the opposite. In addition, it creates a nobler product this has a corrosion decreasing effect. An increase in grain size decreases the hardness too much and should be prevented to ensure balanced material characteristics. For each powder composition there are numerous sets of possible parameters to achieve the same material characteristics, this allows for flexibility in the production process.¹¹⁵ In addition to the aforementioned parameters; nitinol is a reactive metal, this is due to the titanium in the alloy. Processing this alloy requires security measures to be installed for the removal of toxic fumes created during production. Furthermore a shield gas, often Argon, is used to prevent any oxygen causing a reaction in the melting process, which might cause impurities and impair mechanical properties in the final product.^{55,116,117}

The other technique available is EBM, it uses the same approach as laser melting, however, an electron beam is used instead of a laser. The electron beam achieves greater penetration depth and the energy produced by the

beam achieves a higher absorption rate than that of the laser (i.e. it is more efficient). Though achieving faster production times and a lower need for support structures during production, this technique is not widespread available and has less metals available for use in production. Therefore, at this point, it is a less viable option.^{56,118,119}

Laser cutting

Another fabrication method is laser cutting this creates products in 2 dimensions (a flat sheet of metal alloy) or by rotating a tube of material to cut out the stent shape. And is used mainly for straight tubular shapes such as EVAR and coronary stents. This limitation to straight tubular shapes constrains the possibilities to fully comply to the anatomical variations of the individual patient.¹²⁰ However, advances in the laser industry have made it possible to use multiple axis lasers that can rotate around an object to cut out the desired shape. Though this requires a prefabricated shape of thin walled metal alloy that complies with patient anatomy. This extra step makes the production process more complicated than with 3D printing and is therefore less desirable.

Post processing

After printing or laser cutting post-processing is required, often annealing (i.e. heat treatment or baking) is the method of choice. The powder composition, printer settings and the post-production all influence the mechanical properties of the product.^{121,122}

Nitinol needs an annealing treatment to ensure a high density of the final product, though 100% density is often not reached due to stresses in the product or segregation of material tracks with different phases.

'Memry', a company producing nitinol sheets, wires and tubing describes the annealing process as follows: 'Shape setting is used to form a nitinol wire, tube, strip or sheet into components with specific geometries. Whether the nitinol is designed to provide super elasticity or shape memory, and whether it starts the process cold worked or straightened, the team may need to form the material into a new "memory" shape in subsequent steps. Engineers accomplish this by constraining the material into its new shape in a fixture and then performing a heat treatment. For each shape setting application, the team chooses from the following heat treatment methods, each offering a different mix of control and speed balanced against component requirements and cost:

- Molten Salt Bath;
- Fluidized Bed;
- Air Furnace;
- Heated Die;
- RF Induction;
- Resistance;
- Air Convection Furnace.'¹²³

Which post processing treatment suits our goal best should be investigated.

Braiding wires using a negative mould

Some stents are fabricated using a braiding or weaving technique. This is often used for straight tubular shapes similar to laser cutting, however, the behavioural characteristics of braided or woven stents is different opposed to laser cut stents. These braided or woven stents are more flexible in their longitudinal direction offering better manoeuvrability and more anatomical compliance, though thereby losing some fixational strength.

To produce such stents a negative mould may be used. Some industrial fabrication techniques make use of a negative mould, for instance for pressing out a box of from a sheet of metal or use a mandrel with a cut-out of the specified geometry as the negative template. The principle of a negative mould could also be applied to braiding or weaving of a stent. Using a negative mould requires it to be printed by a 3D printer to be able to capture all the details of the patient's anatomy. With this mould, the wires can be laid across the surface to take the shape of the patient's vascular system. Though it might prove difficult to force wires to fall into the right

paths on the negative mould. Additionally, it requires an extra step in the production process; producing the negative mould. Therefore, this approach is less desirable than 3D printing.

Semi-automatic method

Each patient is unique and therefore each vascular system. To be able to produce a matching stent, data is required. This data is retrieved from the angiographic CT data created by the radiology department. By using a contrast agent injected into the blood stream, the vascular system can be visualized on CT-images. This is the golden standard for measuring the dimensions of the vessels which are used to determine what stents to order and use in the patient. Current vascular measuring systems do not allow detailed dimensional data to be created as an output, therefore an in-house method is being produced to extract the necessary data from the angiographic CT-images.

RESEARCH LINE

In the previous chapters an overview was presented of all the possibilities to produce personalized stent grafts for EVAR procedures. 3D printing is believed to be the method of choice to solve the problems of production time and personalization. A short summary: 3D printing allows for three-dimensional freedom during production without using moulds or weaving methods, amongst others. This freedom gives the opportunity to use patient data allowing to produce patient specific products. The potential reduction in production time and perhaps the reduction in post-operative complications makes 3D printing the most promising production technique. Though 3D printing has potential issues as well, for instance, the material produced might be more brittle than its conventional produced counterpart. The printer has settings that might counter this and to match the needs to produce the right material characteristics for the nitinol stents.¹²²

The goal of this research project is to develop a prototype customized stent graft through 3D printing which can be tested in animals. The team working on this project consist of Meander MC, Mundo 3D (our industrial partner), Peter Besselink (nitinol specialist) and graduate student Tim Boers. In the meantime, multiple M2 students have worked and will work on the project as well. The research has been divided into 3 sub-foci in order of importance:

1. Designing, fabricating, and grafting of a stent graft (eventually including fenestrations).
2. Semi-automated method to extract dimensional data to match stent graft and patient anatomy.
3. Sterilization, packaging, and endovascular delivery of stent graft.

This research line has been arranged in a preferred order, the elaboration on these steps are shown below:

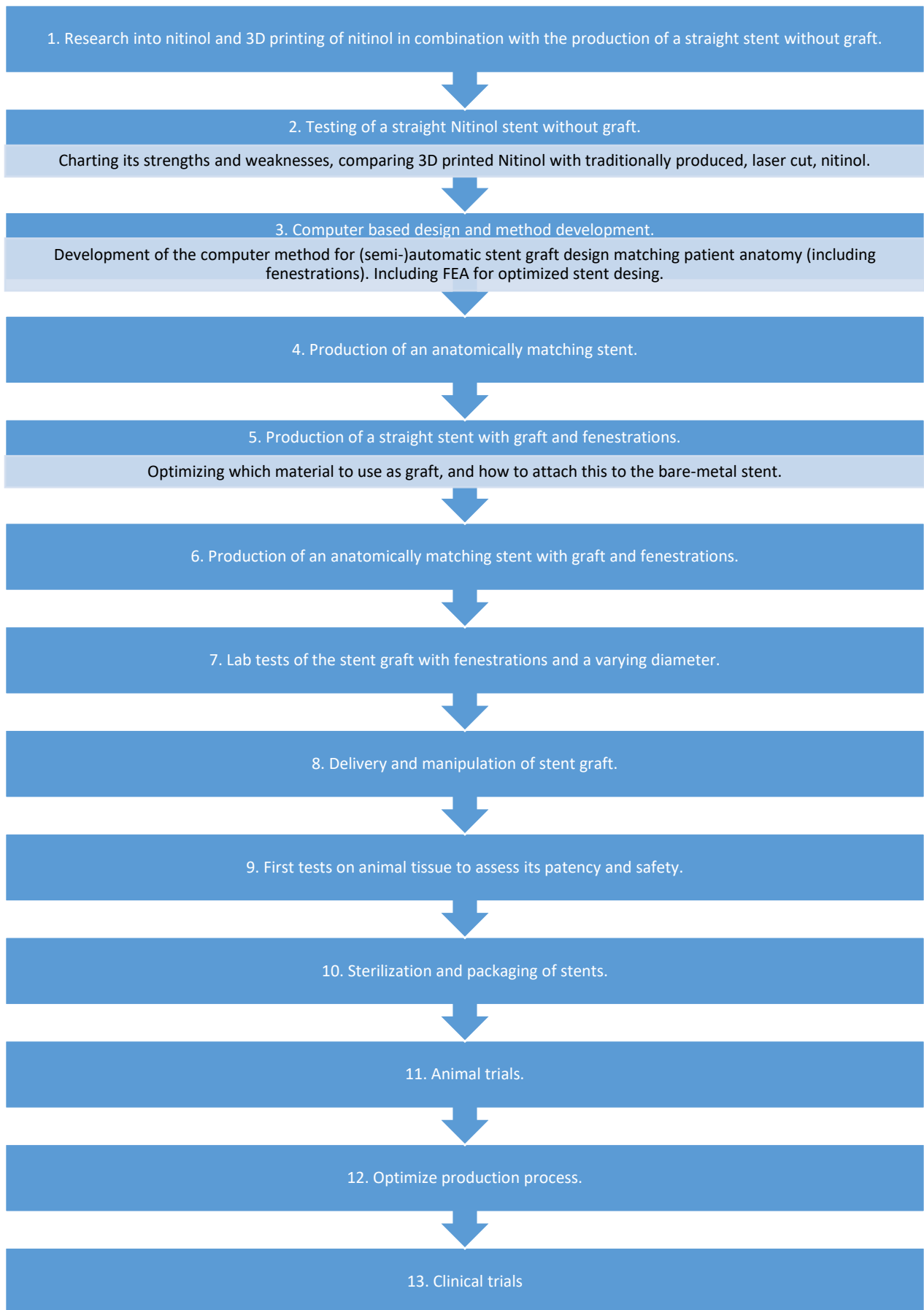


Figure 48: research line.

Elaboration:

1. Without the right powder composition and the possibility of creating a stent-like product, the whole research would be stranded. It is imperative to create a powder composition that shows similar material characteristics when compared to conventional produced, laser-cut, nitinol. To be able to verify those characteristics, standardized tests should be performed during this research project.
2. The above-mentioned tests chart material characteristics of rods and tensile specimens. However, these tests are not performed on stent shape products. To be able to assess the stents in their tubular shape is to know how it will behave in the human body. Testing it for its endurance and potential fatigue in comparison with laser-cut nitinol stents. The insights gained should lead to alterations in the production cycle and after a few iterations should ensure a proper working stent. These tests should also serve as a quality control over a longer period.

If these first two steps show good results, we can assume that nitinol can be printed using an AM machine. Laser cutting has proven itself already and serves as the back-up plan if AM nitinol is not feasible. The next step in the research line comprises of two projects executed at the same time.

3. The computer method should use CTA images of patients to extract data on the morphology of the aneurysm. This should then be used to form a 3D model of the stent. This model should comprise a stent and a graft with fenestrations (for infra-renal aneurysms). In addition, a FEA is performed to develop the most optimal design whilst considering various factors like blood flow, wall stress and fatigue.
4. It is easier to produce a straight stent than it is to produce one with a varying diameter. This is due to the potential stress that the material endures during production, this varying stress could alter the characteristics of the final stent. To be able to assess this potential change in characteristics standardized tests from step 2 must be repeated. If necessary, a change in design or production should be implemented. To be able to offer treatment options to people with large neck angles, full anatomically matching stents should be made. To comply to that requirement the stent should be able to be built with a curve. This might result in more internal stresses during production and therefore alter the final product characteristics. The proposed tests should indicate whether such stent graft designs are possible to produce with SLM.

After step 4 a bare stent with a varying diameter can be produced. These could already be used in for instance the coronary arteries where bare metal stents are used. Though this would probably need somewhat different material characteristics than aortic stents, the basic principle of production is the same.

5. This step is intended for designing the production of a film for the stent as graft. If it is not possible to produce a film without manually sewing it to the stent the potential reduction in production time will be far less. In addition, a process must be designed that allows for fenestrations to be put in, for the time being anatomical correctness is not necessary. This step should produce a straight stent with graft and fenestrations.
6. The addition of a variety in diameter could potentially cause problems in the graft production. This is due to the viscosity of the fluids and gravity; this could lead to an uneven distribution of graft material on the stent. A change in graft material composition or the graft production itself could solve this potential problem.
7. When the previous steps have succeeded, the stent graft should be tested in a lab setting to assess its performance and to identify any problems with the design. If there are any problems the product must be re-designed and if necessary, the production process as well. If this succeeds the next step can be taken.

At this point a stent, with a variety of diameters, with graft and fenestrations can be produced. This can be used for the straight, tapered, and conical neck variations. The next step in the research line again comprises of two projects executed at the same time.

8. For proper use of the stent graft a delivery device must be designed. The delivery device might be based upon the already known EVAR products since this already proven to work. Furthermore, the design should allow for manipulation of the stent graft during placement. This step should not be very difficult since this is being done by all manufacturers producing EVAR products.

When the previous steps are all successful a fully functional stent graft for infra-renal aneurysms should be the result. The next step is to test its performance again in a lab setting and on later animals.

9. It is imperative to know how the stent graft performs considering its patency and safety. First testing in lab setting again, analyse those results, and perhaps change the design and production process. The lab setting should simulate living tissue (ex vivo) as accurate as possible to be able to predict behaviour in vivo.
10. For this product to be used in a clinical setting requires it to be sterile. Therefore, a sterilization procedure and packaging process should be designed that delivers a sterile and packed product ready for use in an EVAR procedure. Manufacturers already produce sterile stent grafts therefore this should not be a problem.
11. At this point animal trials can be started since the product is fully ready to be used as it was intended to. The results of those trials determine its potential for the market and thus for use in humans.

Dependent on the outcome of the trials a market ready product should be developed. The next steps, executed in parallel, expand on the existing production process and making them market ready. In addition, clinical trials are started to assess the performance of the stent graft in humans.

12. Optimize production process.
13. Clinical trials

10.2 APPENDIX 2 – ADDITIONAL RESULTS

The following results are additional information to the Evaluation, Chapter 6. All figures are taken at the end stage, i.e. equilibrium of stent deployment in the aortic neck.

PERSONALIZED VERSUS STRAIGHT STENT

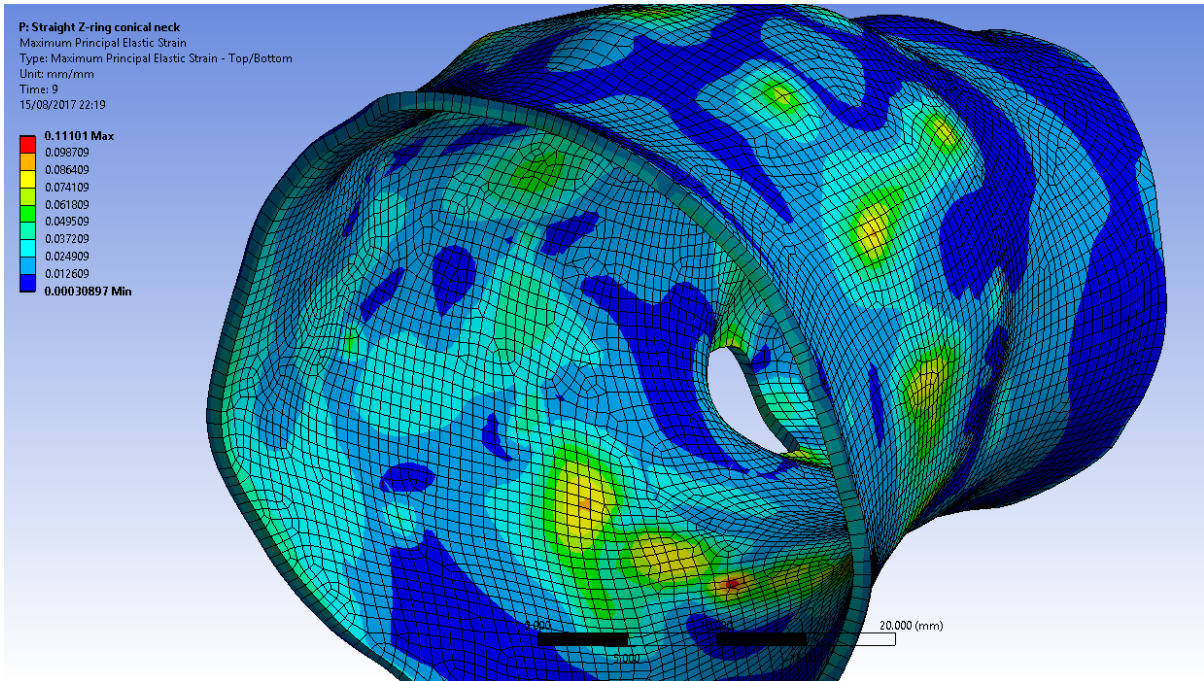


Figure 49: Maximum principal elastic strain in a conical neck under influence of a straight z-shape stent, reaching a maximum of 1.11×10^{-1} mm/mm. The maximum of the encountered strain is found at the locations where the points of the z-shape stent are (yellow / red areas). Corresponding to graph 33.

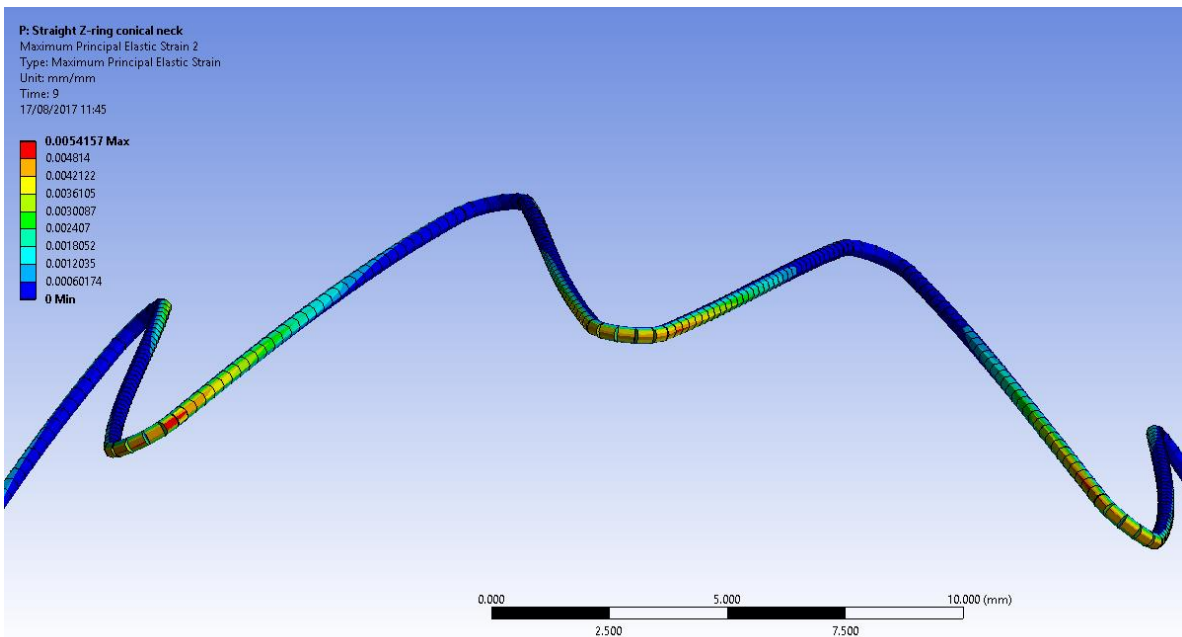


Figure 50: Maximum principal elastic strain in straight z-shape stent under influence of a conical neck, reaching a maximum of 5.42×10^{-3} mm/mm. Note the highest strain is encountered at the peaks on the outside (red/orange areas). Corresponding to graph 34.

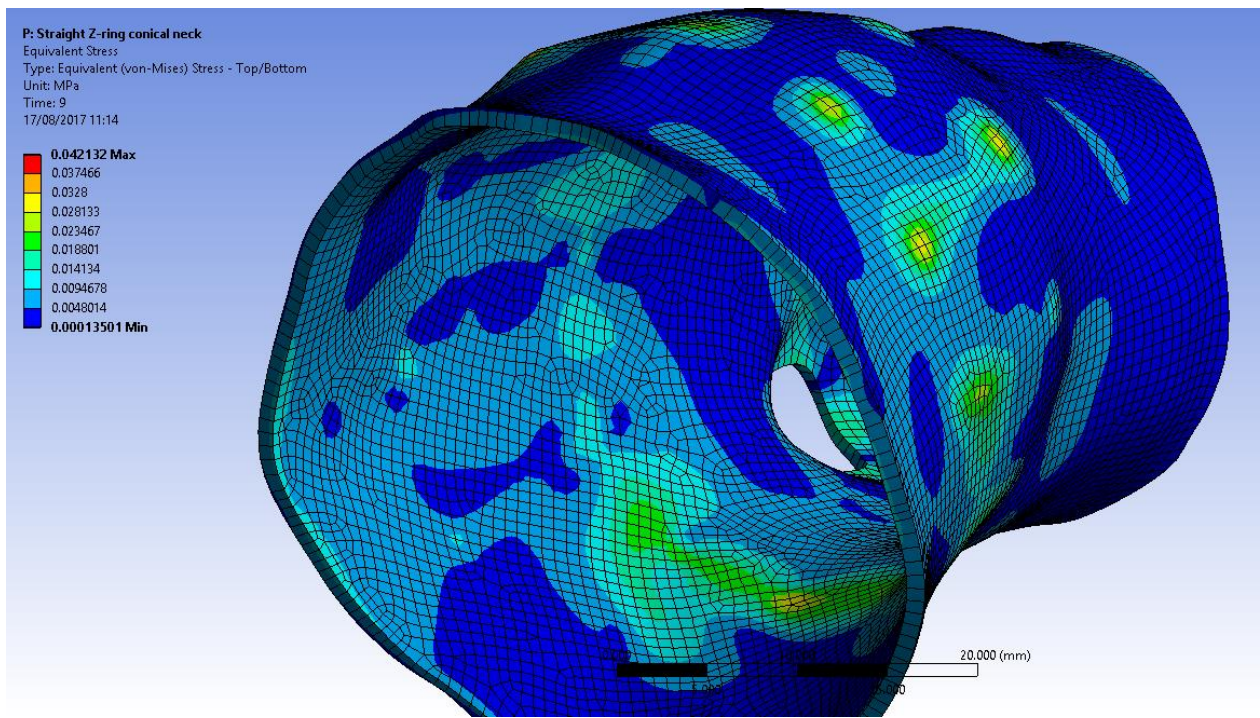


Figure 51: Equivalent (von-Mises) stress in conical neck under influence of a deployed straight z-shape stent, reaching a maximum of 4.21×10^{-2} MPa. Note the highest stresses are encountered at the peaks of the stent (red areas). Corresponding to straight stent graph in Figure 49.

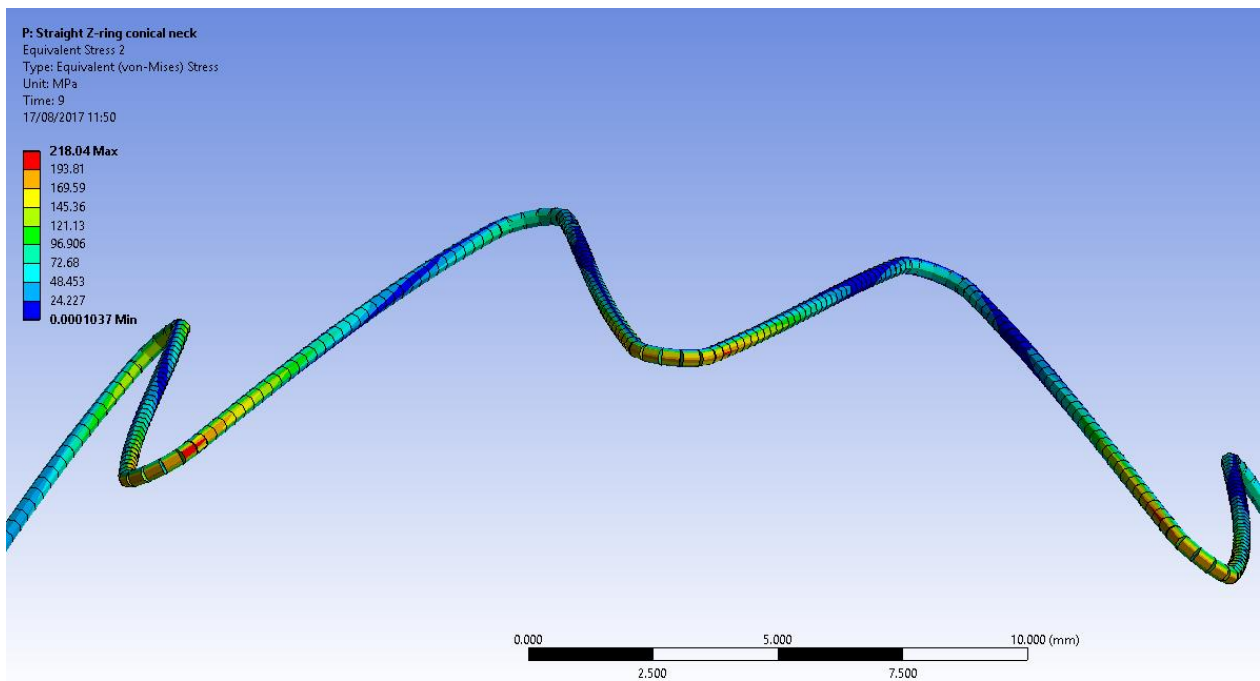


Figure 52: Equivalent (von-Mises) stress in a straight z-shape stent deployed in a conical neck, reaching a maximum of 218 MPa. Note the highest stresses are encountered in the distal peaks of the stent (lower row of peaks in the image) on the in- and outside (red/orange areas, inside not visible here). Corresponding to personalized stent graphs in Figure 50 and 51.

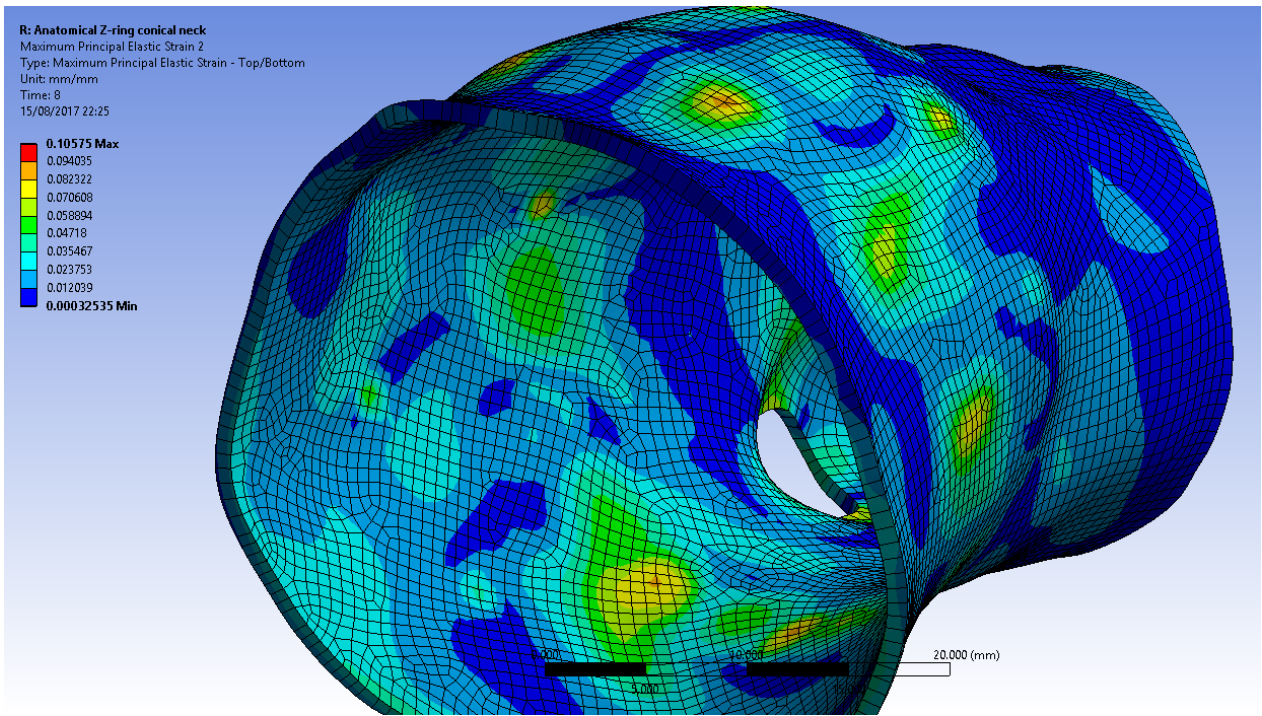


Figure 53: Maximum principal elastic strain in a conical neck under influence of a personalized z-shape stent, reaching a maximum of 1.06×10^{-1} mm/mm. The maximum of the encountered strain is found at the location of the points of the z-shape stent (yellow/red areas). Corresponding to the personalized stent graph in Figure 33.

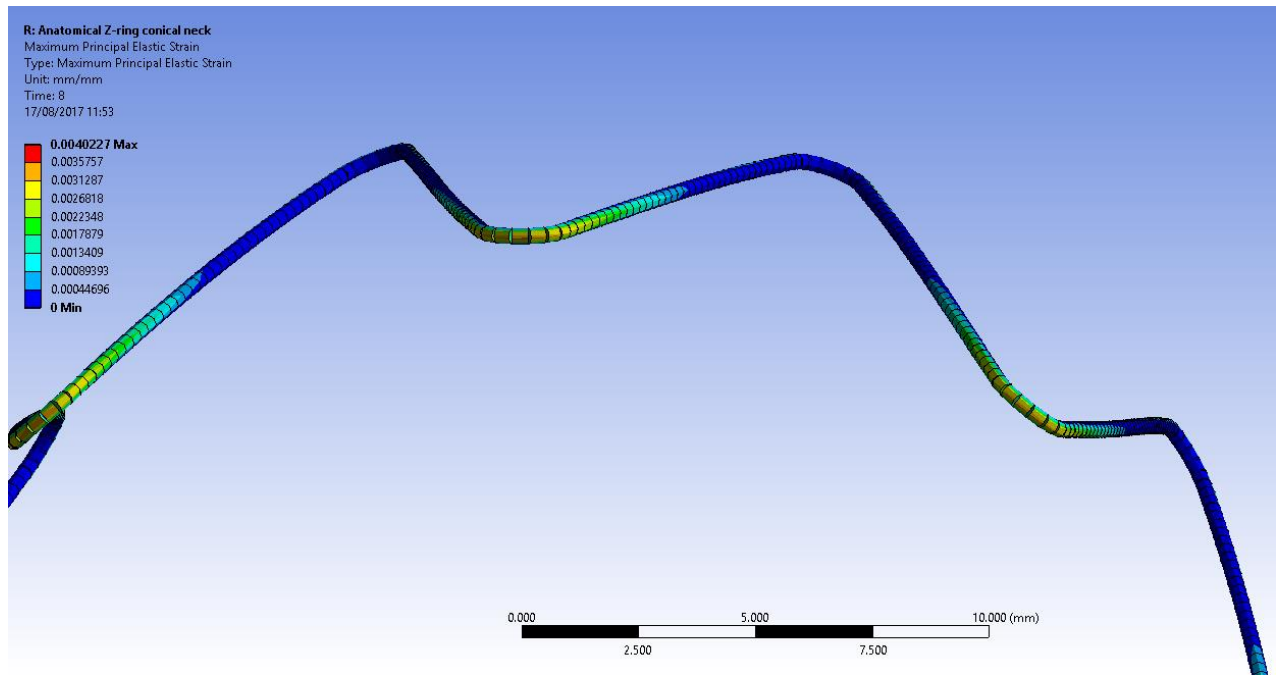


Figure 54: Maximum principal elastic strain in personalized z-shape stent under influence of a conical neck, reaching a maximum of 4.02×10^{-3} mm/mm. Note the maximum encountered strain is found at the upper row (proximal) peaks on the outside (not visible here). Middle to high stress is encountered at the distal peaks (orange / yellow). Corresponding to personalized stent graph in Figure 34.

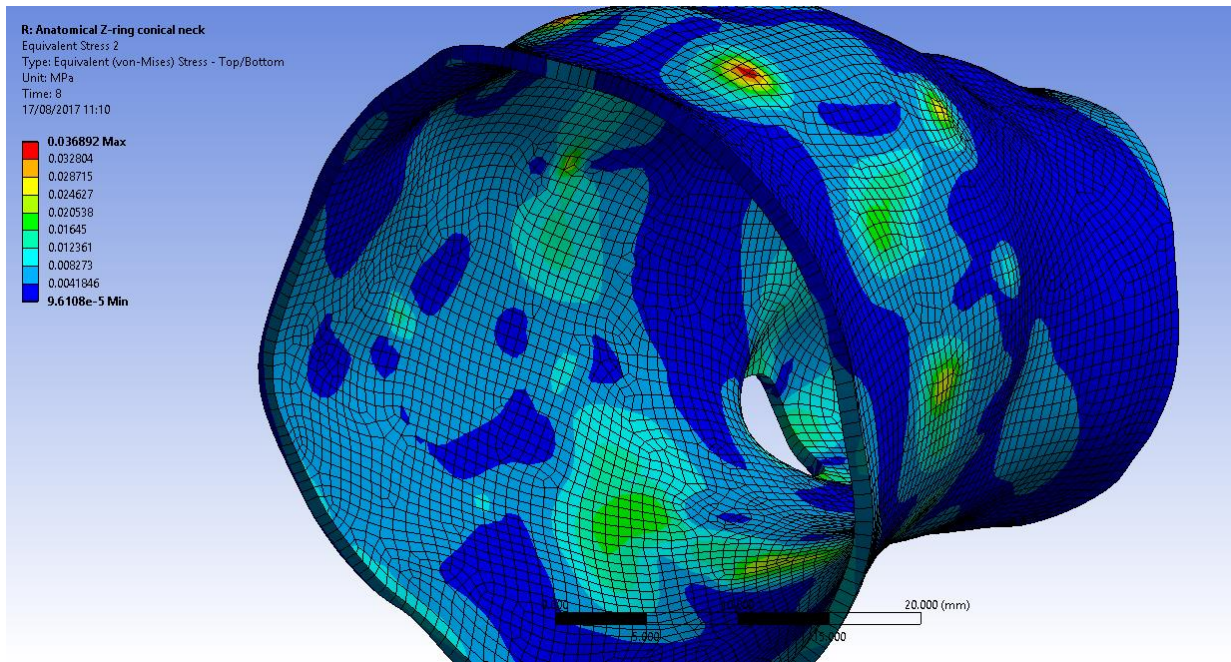


Figure 55: Equivalent (von-Mises) stress in conical neck under influence of a deployed personalized z-shape stent, reaching a maximum of 3.69×10^{-2} MPa. Note the highest stresses are encountered at the peaks of the stent (red areas). Corresponding to personalized stent graph in Figure 49.

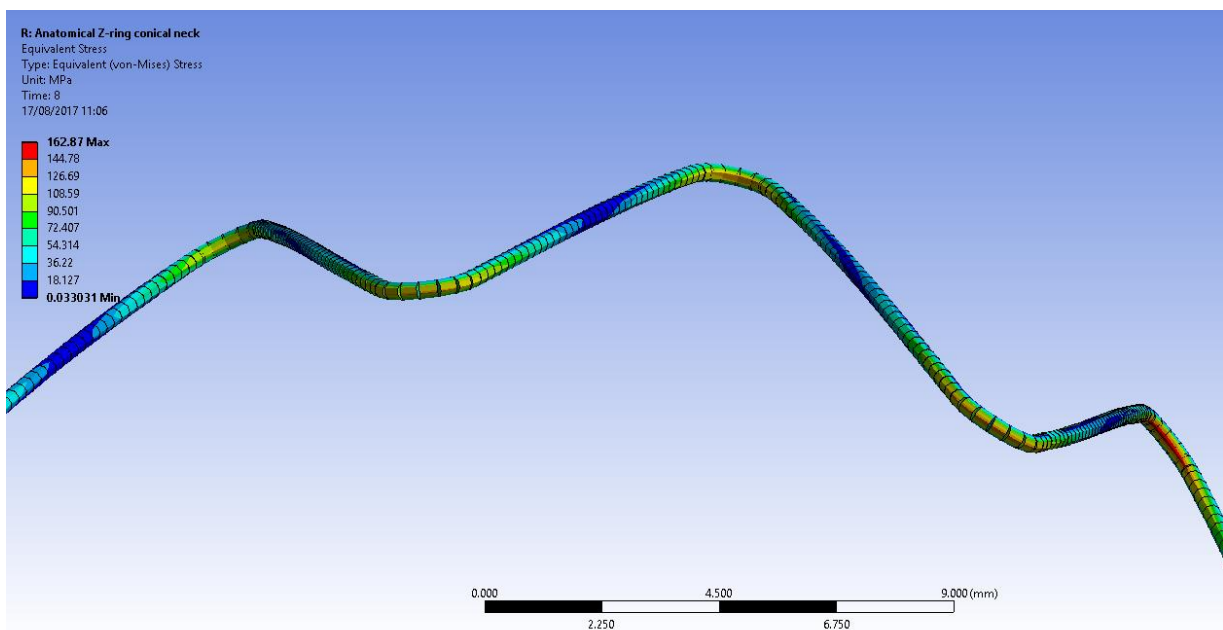


Figure 56: Equivalent (von-Mises) stress in personalized z-shape stent deployed in a conical neck, reaching a maximum of 163 MPa. Note the highest stresses are encountered in the peaks of the stent on the in- and outside (red/orange areas). Corresponding to personalized stent graphs in Figure 50 and 51.

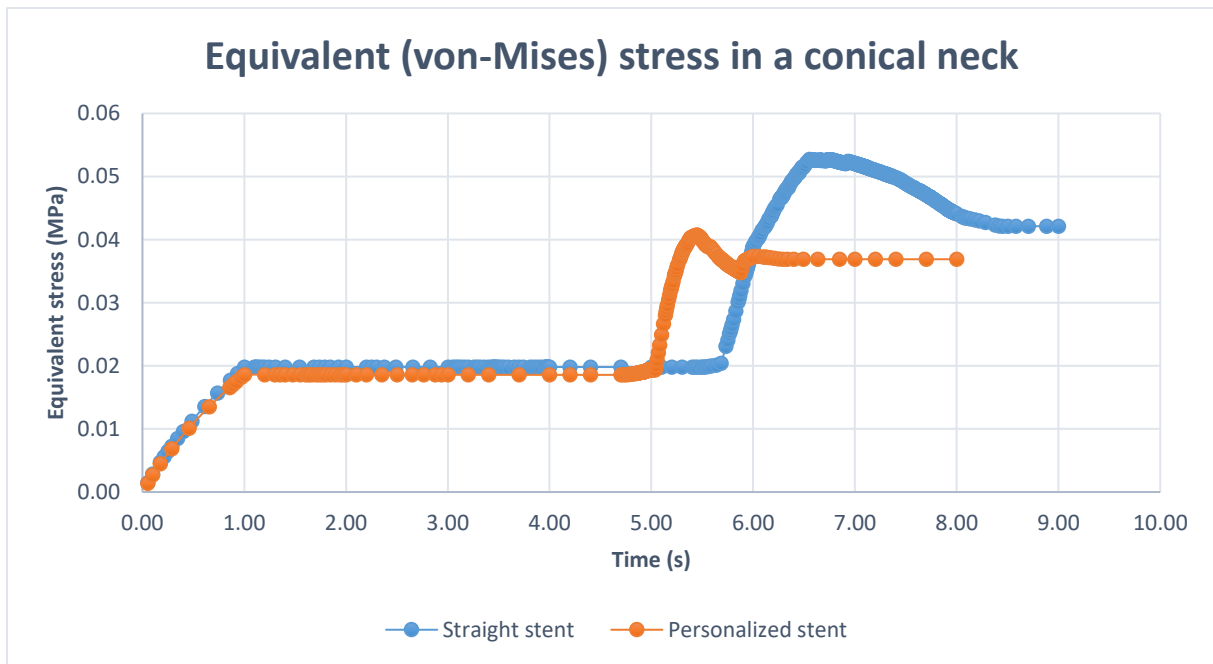


Figure 57: A graph comparing the equivalent stresses (von-Mises) in the conical neck caused by the straight and anatomical z-shape stent. Note the increase in the first second, this is the force mimicking angio-tension. Furthermore, note the overall lower stress levels as well as the peak before equilibrium sets in.

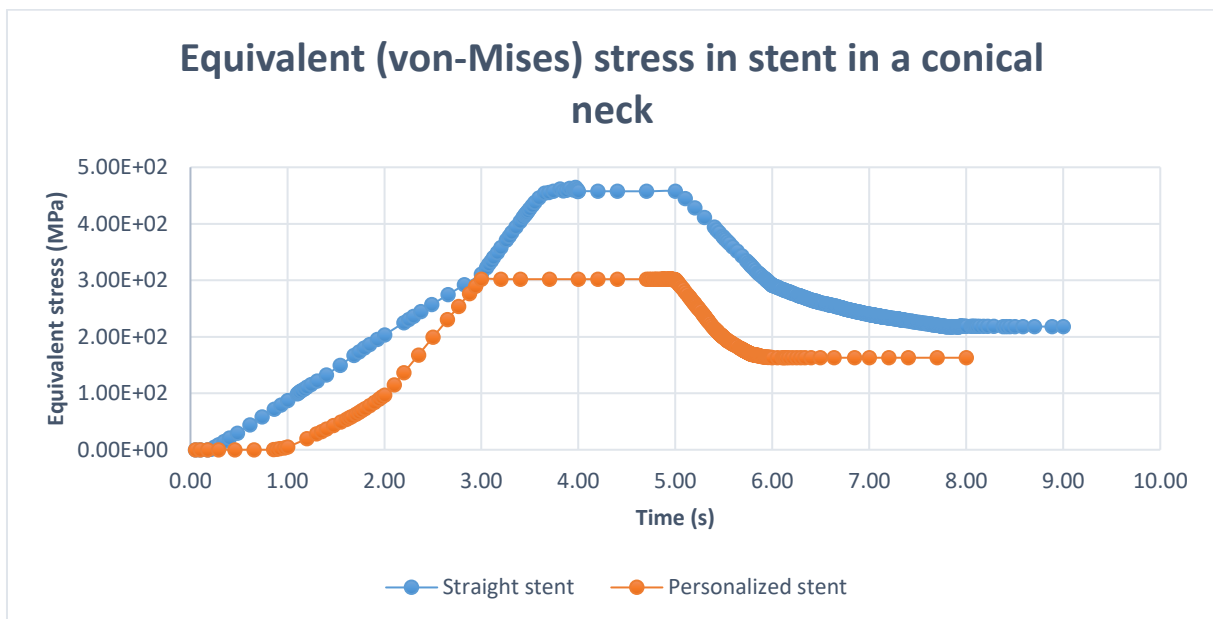


Figure 58: A graph comparing the equivalent stresses (von-Mises) of the straight z-shape stent with that of the anatomical z-shape stent, in a conical neck. Note here the overall reduced stress levels in the stent, as well as the final equilibrium state which is lower in stress for the personalized stent.

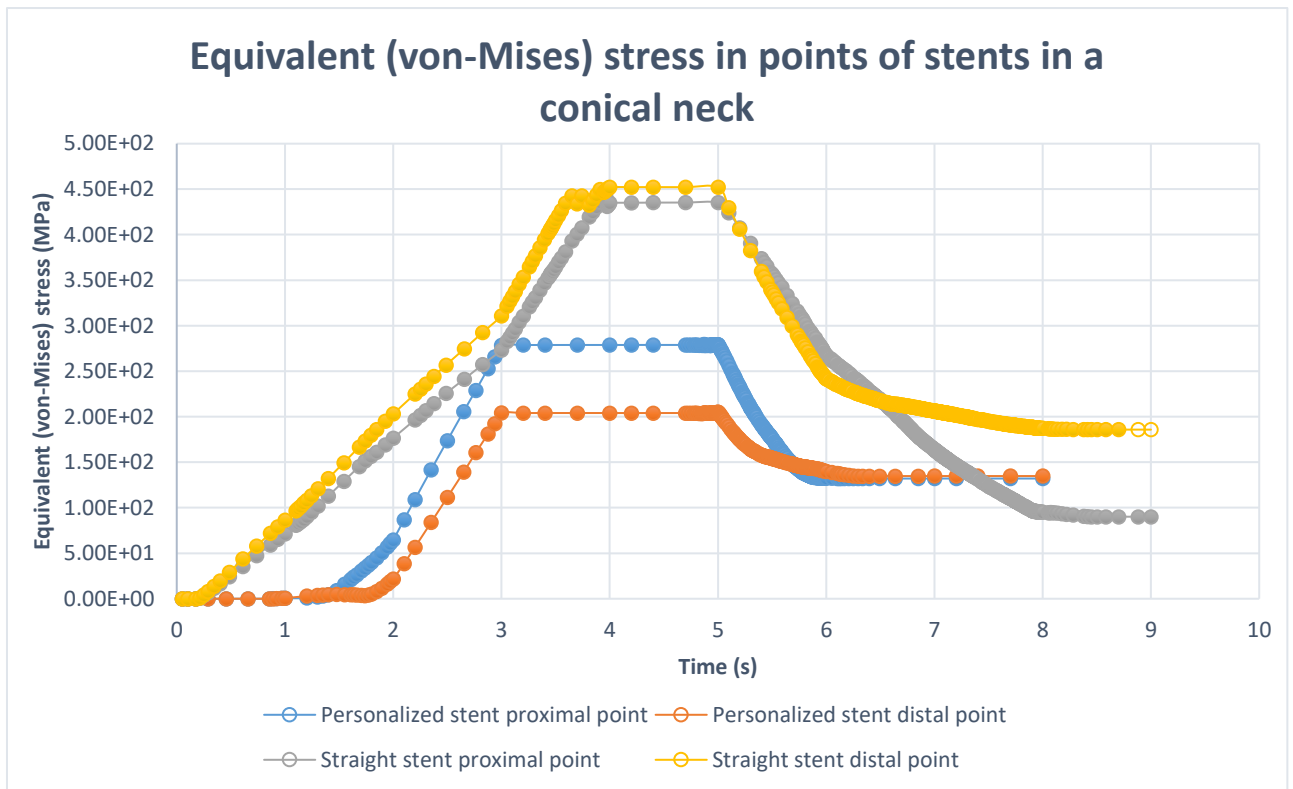


Figure 59: The equivalent (von-Mises) stress measured in one of the proximal points of the straight and personalized stent deployed in a conical neck. Note here the overall lower stresses for the personalized stent, as well as the difference in stress during moving of the aortic neck. Furthermore, the equilibrium stage shows higher stresses for the distal point of the straight stent than for its proximal point.

STRAIGHT Z-SHAPE IN A STRAIGHT TUBE

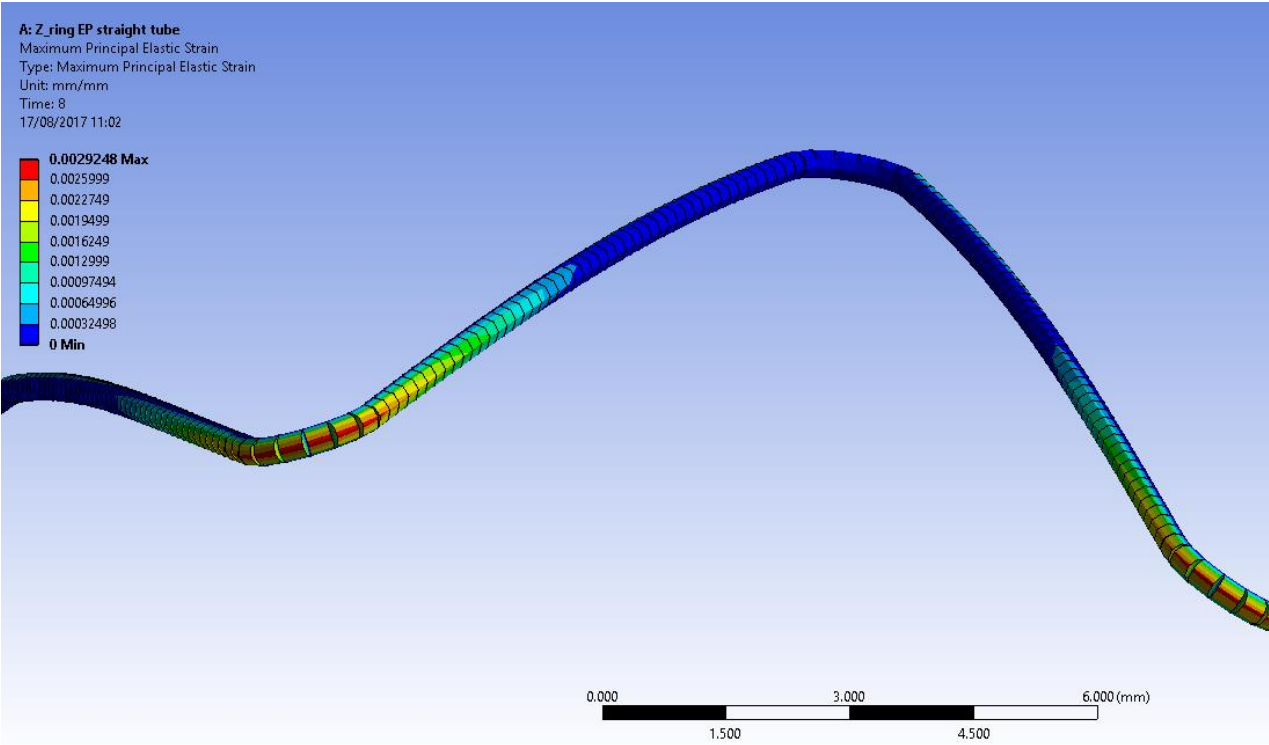


Figure 60: The maximum principal elastic strain in a straight z-shape stent deployed in a straight tube, reaching maximum at 2.92×10^{-3} mm/mm. Note the highest strain is encountered at the outside of the peaks of the stent.

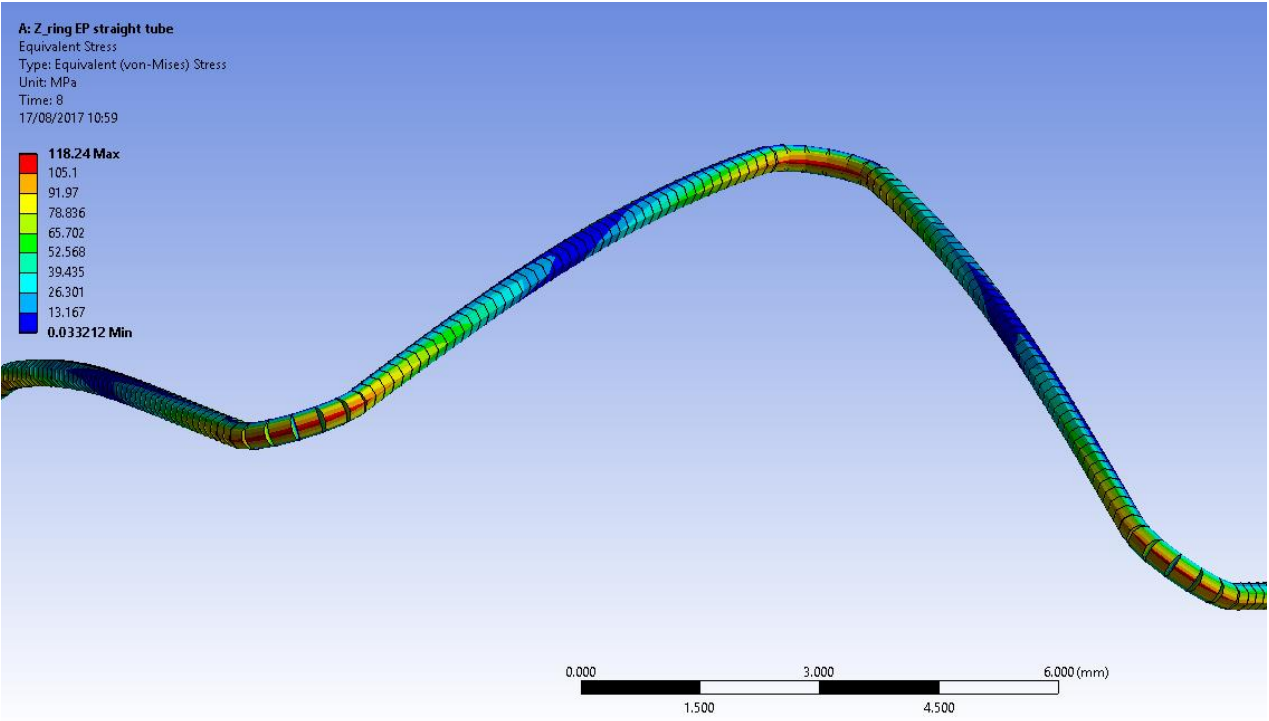


Figure 61: Equivalent (von-Mises) stress in a straight z-shape stent deployed in a straight tube, reaching maximum at 118 MPa. Note the highest stresses are encountered at the peaks of the stent on the in- and outside (red areas).

STRAIGHT Z-RING IN AN ANATOMICAL STRAIGHT NECK

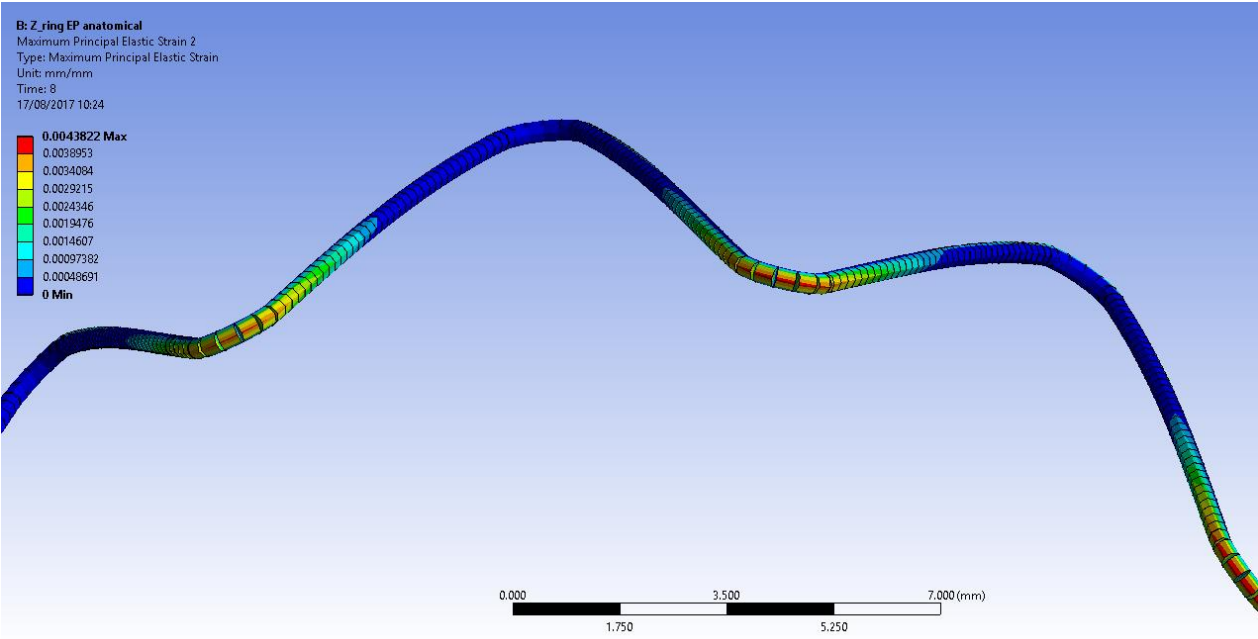


Figure 62: The maximum principal elastic strain in a straight z-shape stent deployed in an anatomical straight aortic neck, reaching maximum at 4.38×10^{-3} mm/mm. Note the highest strain is encountered at the outside of the peaks of the stent.

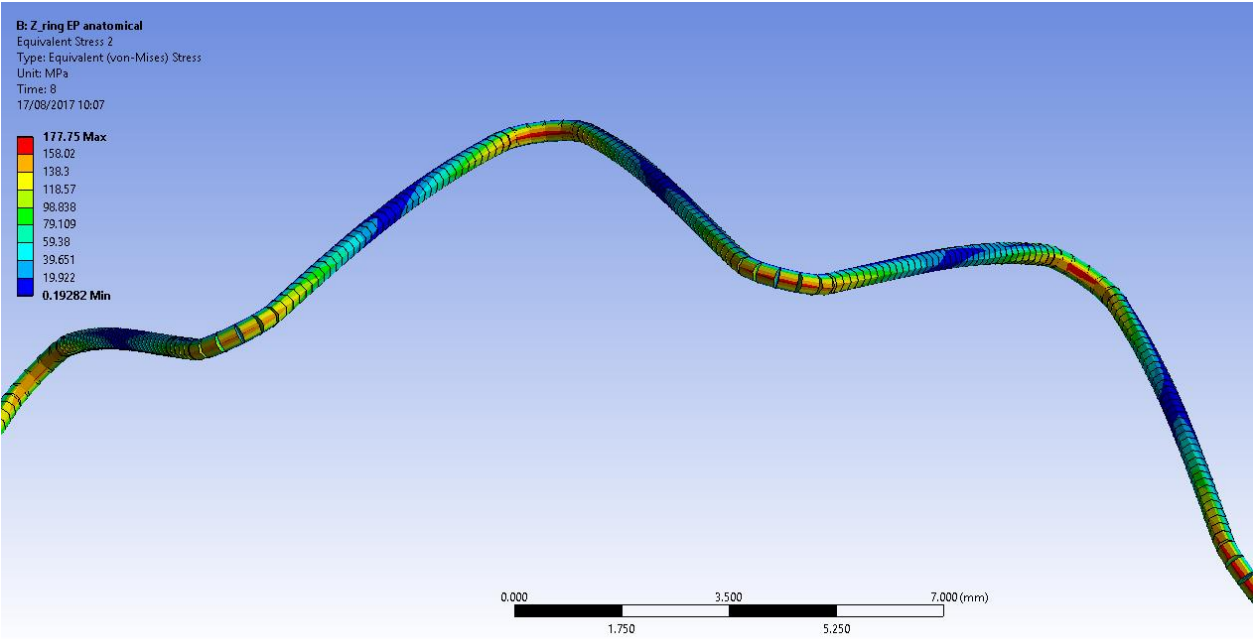


Figure 63: equivalent (von-Mises) stress in straight z-shape stent deployed in an anatomical straight aortic neck, reaching maximum at 173 MPa. Note the highest stresses are found in the peaks of the stent on the in- and outside (red areas). Note mid-strut there is little to no stress (blue area).

10.3 APPENDIX 3 – CLINICAL STUDIES HYBRID OPERATING ROOM

ERGONOMICS STUDY

Ergonomics is often overlooked, however, in the medical sector it is a subject which is increasingly investigated. A new hybrid operating room (HOR) has been opened in the Meander medical centre. This HOR has a lot of screens for use during operations and a fixated C-arm for rotational x-rays during surgery. The addition of this equipment results in reduced space and less room for manoeuvring of equipment and personnel. During pre-planning of the HOR this has been considered, now the effect of this planning should be evaluated. The HOR is used mainly for vascular surgery such as EVAR procedures. These utilize the screens placed in the HOR. To gain a quick insight in the ergonomics of the HOR the vascular surgeon and the interventional radiologist have been followed during vascular procedures.

The Rapid Upper Limb Assessment (RULA) score has been chosen to identify potential problems in the upper body since that part of the body is used the most during vascular surgery and which is most likely to encounter problems that can be flagged as worrisome areas. The arms, wrists, neck, and torso have the focus the legs are considered as well to account for potential support there. In a period of 8 months a total of 14 EVAR procedures have been scored and documented. This has been performed by the author. From this data, the RULA scores have been determined as well as any potential flagged areas which are highlighted from the data set. The RULA scores for EVAR procedures are shown below.

Table 9: Scores per handling.

	PS-A	WAS	PS-B	NTLS	RULA	RULA without lead
Introduction	2.20	2.20	4.47	6.47	4.67	3.87
Proglide – closing device preparation	2.00	2.00	4.22	6.22	4.78	3.78
Catheter wires insertion	2.29	2.29	4.14	6.14	4.57	3.64
Deployment	2.71	2.71	4.93	6.93	5.07	4.29
Expand with balloon	2.31	2.31	4.15	6.15	4.69	3.69
Closing artery	2.07	2.07	4.00	5.87	4.53	3.60

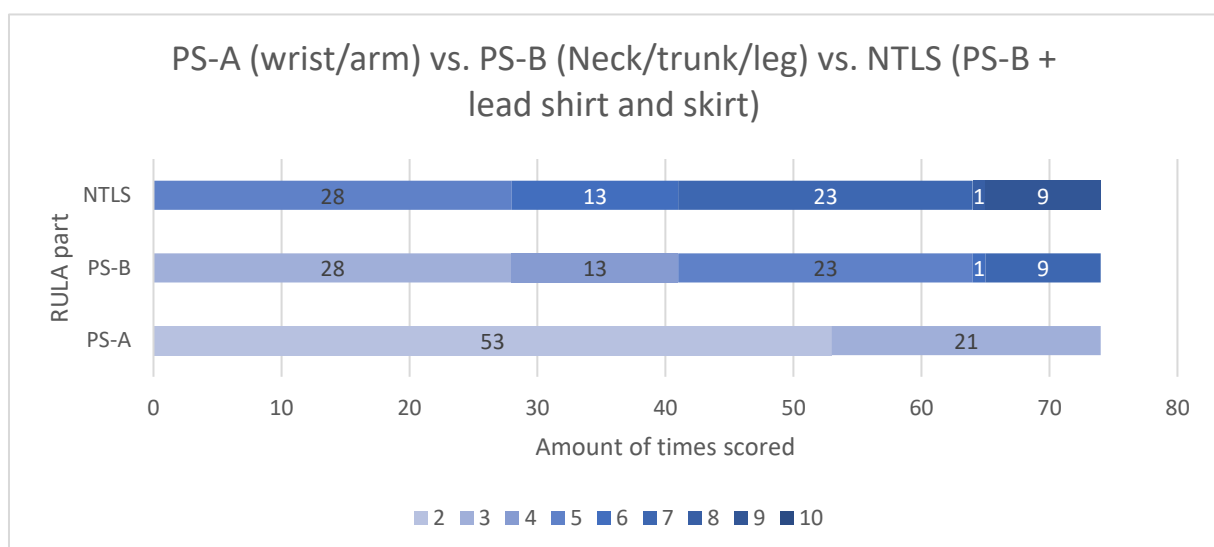


Figure 64: Scores of the 'wrist and arm' versus 'neck, trunk and leg' versus 'neck, trunk and leg including a lead shirt and skirt'. A dark colour indicates a bad ergonomics score (10), a light colour indicates that ergonomics was within allowed limits (2).

These results show that there is necessary improvement in the ergonomics of the neck and torso. These scores structurally higher than the arms and wrists which have little necessity to improve. The high PS-B score resulting directly from the ergonomics of the neck, torso and legs are often caused by misplaced screens, obstruction of screens by personnel or equipment or simply by a bad posture. In addition, during vascular surgery a lead shirt and skirt is worn to protect against radiation from the fixated C-arm. However, the addition of this lead adds static weight to the human body and results in a point increase on the NTLs sub-score and a point increase on the final RULA score.

The addition of the lead shirt and skirt results in a higher RULA score which means an ergonomically worse situation, even in the most positive outcome and with changes to the posture it cannot be prevented that the RULA score will be at least 4 and this is with arms and wrists being estimated rather positively. It can be concluded that, though necessary for prevention of radiation related diseases, the ergonomics of the lead skirt and shirt are abominable. A redesign of the lead shirt and skirt might overcome this problem or at least reduce its impact on ergonomics.

Other recommendations are changing the screens to eye height, and this is for each surgeon different, paying attention to this during surgery set-up can prevent a bad posture. In addition, the size of the screen has some adverse effects, the surgeon must look all over the screen to see the whole image. It is therefore advised that the top of the screen should be at eye height, since looking down is less taxing for the neck than looking up. Furthermore, due to equipment on and around the table screens cannot be positioned ideally, a rearrangement should be made to be able to position the screen for the radiologist at eye height as well. A surgeon or radiologist can therefore not stand ventrally to the table this will cause them to twist their necks to see the screen this reduces the quality of their posture. A diagonally position should be maintained to keep their work lines as straight as possible.

These results have been scored by one researcher, it is strongly suggested to acquire scoring results from independent observers to increase the objectivity of the acquired results.

DISCOVER TRIAL

In this multicentre trial treatment of atherosclerotic disease in the iliac arteries is researched. Treatment consists of angioplasty and often placement of a stent. It is the stent that is subject to investigation due to the availability of covered and non-covered stents for this treatment. The question is posed which stent performs superior to the other. This trial includes patients with occlusive disease of the iliac communal artery with stenosis of at least 3 cm and/or full occlusion of the communal iliac artery. After patient consignment inclusion into the trial occurs after a final angiographic check of the iliac occlusive disease perioperatively. The patient is randomized to receive either a covered or non-covered stent. The patient is blinded to which stent they received. Pressure gradients are measured intra-vascular for detailed results of the procedure. Follow-up consists of 3 months, 6 months, 1 year and 2, year follow-up with an ankle-arm-index, duplex ultrasound, as well as RAND-36 questionnaires.

IFLOW STUDY

iFlow is a rather new program made by Siemens (Germany) to visualize and quantify contrast flow through vessels. Quantification consists of a reference 100% contrast and variable regions where the contrast amount is measured over time. This results in graphs wherein one can use the area under the curve as well as the peak time and time to zero to acquire insight in the flow of the blood in that part of the vessel. This data can be used in combination with clinical outcome to eventually give perioperative an indication on the state of the vessel and whether it needs any further treatment. However, this software has not finished development and some issues remain, such as crossing vessels results in a higher or longer peak of contrast intensity due to the amount of contrast in both vessels is measured instead of one, therefore no realistic representation of the flow in the vessel can be acquired at the point, though the software does give a result. For EVAR procedures this might help gain

insight in the endoleak type II. If flow patterns can be combined with clinical outcome concerning the type II arteries, perioperative a decision can be made whether to coil the artery or not.